REACTOR PHYSICS ASSESSMENT OF THICK SILICON CARBIDE CLAD PWR FUELS

By

David A. Bloore

B.S., Physics (2005)

University of Massachusetts at Amherst

SUBMITTED TO THE DEPARTMENT OF NUCLEAR SCIENCE AND ENGINEERING IN PARTIAL FULFILLMENT OF THE REQUIREMENTS FOR THE DEGREE OF

MASTER OF SCIENCE IN NUCLEAR SCIENCE AND ENGINEERING
AT THE
MASSACHUSETTS INSTITUTE OF TECHNOLOGY

JUNE 2013

Signature of Author: _____
David A. Bloore
Department of Nuclear Science and Engineering
May 6, 2013

Certified by: _____
Mujid S. Kazimi
TEPCO Professor of Nuclear Engineering
Thesis Supervisor

Certified by: _____
Edward E. Pilat
Research Scientist
Thesis Reader

Certified by: _____
Kord Smith
KEPCO Professor of the Practice of Nuclear Engineering
Thesis Reader

Accepted by: _____
Mujid S. Kazimi
TEPCO Professor of Nuclear Engineering
Chairman, Committee on Graduate Students

REACTOR PHYSICS ASSESSMENT OF THICK SILICON CARBIDE CLAD PWR FUELS

by

David A. Bloore

Submitted to the Department of Nuclear Science and Engineering on May 6, 2013 in Partial Fulfillment of the Requirements for the Degree of Master of Science in Nuclear Science and Engineering

ABSTRACT

High temperature tolerance, chemical stability and low neutron affinity make silicon carbide (SiC) a potential fuel cladding material that may improve the economics and safety of light water reactors (LWRs). "Thick" SiC cladding (0.089 cm) is easier (and thus more economical) to manufacture than SiC of conventional Zircaloy (**Zr**) cladding thickness (0.057 cm). Five fuel and clad combinations are analyzed: **Zr** with solid UO_2 pellets, reduced fuel fraction "thick" SiC (**Thick SiC**) with annular UO_2 pellets, Thick SiC with solid UO_2/BeO pellets, reduced coolant fraction annular fuel with "thick" SiC (**Thick SiC RCF**), and Thick SiC with solid PuO_2/ThO_2 pellets.

CASMO-4E and SIMULATE-3 have been utilized to model the above in a 193 assembly, 4-loop Westinghouse pressurized water reactor (PWR). A new program, CSpy, has been written to use CASMO/SIMULATE to conduct optimization searches of burnable poison layouts and core reload patterns. All fuel/clad combinations have been modeled using 84 assembly reloads, and **Thick SiC** clad annular UO_2 has been modeled using both 84 and 64 assembly reloads.

Dual Binary Swap (DBS) optimization via three Objective Functions (OFs) has been applied to each clad/fuel/reload # case to produce a single reload enrichment equilibrium core reload map. The OFs have the goals of: minimal peaking, balancing lower peaking with longer cycle length, or maximal cycle length. Results display the tradeoff between minimized peaking and maximized cycle length for each clad/fuel/reload # case.

The presented **Zr** reference cases and **Thick SiC RCF** cases operate for an 18 month cycle at 3587 MW_{th} using 4.3% and 4.8% enrichment, respectively. A 90% capacity factor was applied to all SiC cladding cases to reflect the challenge to introduction of a new fuel. The **Thick SiC** clad annular UO_2 (84 reload cores) and **Thick SiC** UO_2/BeO exhibit similar reactor physics performance but require higher enrichments than 5%. The **Thick SiC RCF** annular UO_2 fuel cases provide the required cycle length with less than 5% enrichment. The **Thick SiC** clad PuO_2/ThO_2 cores can operate with a Pu% of heavy metal of about 12%, however they may have unacceptable shutdown margins without altering the control rod materials.

Thesis Supervisor: Mujid S. Kazimi
Title: TEPCO Professor of Nuclear Engineering

Acknowledgements

First I would like to thank the United States Navy for ordering me to attend MIT for the purpose of earning a Masters Degree in Nuclear Science and Engineering (NSE). This has been my most challenging and fulfilling assignment.

I would like to thank Ceramic Tubular Products for providing insights into the design and manufacture of silicon carbide for PWR applications.

I would like to thank Studsvik for providing additional SIMULATE licenses to facilitate faster optimization processes by enabling a greater number of parallel instances of SIMULATE to run on the NSE Department clusters. Special thanks to Professor Benoit Forget for allowing me to use his computing cluster.

I would like to thank the faculty of the MIT Nuclear Science and Engineering Department, particularly Professor Mujid S. Kazimi, Dr. Edward E. Pilat, Professor Kord Smith, Professor Benoit Forget, Professor Bilge Yildiz, and Dr. Charles W. Forsberg for many fruitful discussions during this research.

I would like to thank Dr. Koroush Shirvan for his willingness to share his broad knowledge base of industry practice and simulation software with me. I am glad to have known him as a fellow student, and that he has chosen to join the Department as a Research Scientist and continue to be an active member of Professor Kazimi's Advanced Fuels Research Group.

I would like to thank the NSE students in my research group and with which I have taken classes. It has been valuable to debate the merits of different ways of viewing the concepts and methodologies of Nuclear Science and Engineering.

Table of Contents

List of Figures

List of Tables

Nomenclature

B_c	Cycle Burnup
B_d	Discharge Burnup
BOC	Beginning of Cycle
BOL	Beginning of Life
cm	centimeter
CTP	Ceramic Tubular Products
CVD	Chemical Vapor Deposition
DBS	Dual Binary Swap
DNB	Departure from Nucleate Boiling
dpa	Displacements per Atom
EDBS	Exhaustive Dual Binary Swap
EFPD	Effective Full Power Days
EOC	End of Cycle
EOFPL	End of Full Power Life
EOL	End of Life
$F_{\Delta h}$	Maximum Channel Enthalpy Rise
FHR	Fluoride Salt Cooled High-Temperature Reactor
F_q	Maximum Local Power
H/HM	Hydrogen to Heavy Metal Ratio
HFP	Hot Full Power
HIP	Hot Isostatic Pressing
HZP	Hot Zero Power
IFBA	Integral Fuel Burnable Absorber
IHM	Initial Heavy Metal
ITC	Isothermal Temperature Coefficient
kg	kilogram
kgIHM	kilogram Initial Heavy Metal
kW	kiloWatt
LOCA	Loss of Coolant Accident
LWR	Light Water Reactor
MOX	Mixed Oxide Fuel
MTC	Moderator Temperature Coefficient
MWd/kgIHM	Megawatt days per kilogram of initial heavy metal
MWth	Megawatts thermal
NRC	Nuclear Regulatory Commission
NSE	Nuclear Science and Engineering
OF	Objective Function
PCMI	Pellet-Clad Mechanical Interaction
PkExp	Peak Pin Exposure
PWR	Pressurized Water Reactor
RGDBS	Random Greedy Dual Binary Swap
RPV	Reactor Pressure Vessel
SDB	Shutdown Margin at Beginning of Cycle

SDE	Shutdown Margin at End of Cycle
SDM	Shutdown Margin
SiC	Silicon Carbide
SNF	Spent Nuclear Fuel
Thick SiC	Thick SiC Geometry Case
Thick SiC RCF	Thick SiC Reduced Coolant Fraction Geometry Case
Thin SiC	Thin SiC Geometry Case
WABA	Wet Annular Burnable Absorber
Zr	Zircaloy

1 Introduction

1.1 Statement of Purpose

Previous work has examined the potential use of SiC as a fuel cladding material in a PWR environment. However the economic viability of implementing SiC cladding material using the same dimensions as existing **Zr** cladding is not clear. Thicker SiC cladding has been proposed because it is easier to manufacture, and hence improves the economic viability of SiC cladding. The purpose of this thesis is to model and evaluate the neutronic performance of three thick SiC cladded fuels in PWR cores: annular UO_2 fuel pellets, UO_2/BeO fuel, and PuO_2/ThO_2 fuel.

In the case of annular UO_2 and UO_2/BeO fuels it is desired to understand if one or the other is preferable in terms of extending the maximum burnup of the fuel. Furthermore, three annular UO_2 cases are examined: reduced fuel fraction with 64 assembly reloads per cycle, reduced fuel fraction with 84 assembly reloads per cycle, and reduced coolant fraction with 84 assembly reloads per cycle. In the reduced fuel fraction cases, the clad outer radius matches the conventional fuel used today and volume to accommodate the extra thickness of the cladding is taken from the fuel volume. In the case of reduced coolant fraction, the fuel pellets' outer radius matches the conventional pellets used today and the volume to accommodate the extra thickness of the cladding is taken from the coolant volume.

In the case of PuO_2/ThO_2 fuel there are two parameters of primary interest: initial loading of plutonium required in order to meet cycle length, and plutonium remaining in discharged fuel.

1.2 Background

1.2.1 Early experimental reactors

The earliest attempts at creating critical nuclear chain reactions were experimental and so novel at the time that no idea was outside the realm of consideration. The Chicago Pile 1 was a graphite-moderated criticality experiment and had no cooling or shielding whatsoever, and yet this experiment was done in a densely populated area. The third nuclear reactor ever built, LOPO, was a homogeneous aqueous reactor that went critical using water as the moderator and the shield in May of 1944. [1],[2]

The scope of consideration for cladding material was equally broad. For example, in 1944, the B-Reactor at Hanford in the United States used aluminum clad uranium metal fuel to produce plutonium for the Manhattan Project. The British weapons plutonium production also used aluminum cladding, for example at Windscale. British CO_2-cooled MAGNOX reactors used fuel clad in a "non-oxidizing" magnesium alloy.

Austenitic stainless steels and ferritic/martensitic stainless steels have also been used, particularly in fast reactors.

1.2.2 Commercial Reactors

Stainless steel fuel cladding was utilized in the first privately owned, large-scale commercial PWR at Yankee Rowe. **Zr** cladding was adopted by the vast majority of the commercial nuclear power industry after the first few cores due to its reduced neutron absorption and acceptable corrosion resistance. **Zr** cladding service life is primarily limited by corrosion and irradiation embrittlement. While **Zr** is acceptable for normal operations, its performance in accident scenarios has proven problematic—and avoidance of **Zr** failure is a primary goal of nuclear reactor safety engineering and analysis that must be performed to license a reactor.

1.2.3 Chernobyl, TMI, Fukushima

The accident at Three Mile Island (TMI) on March 28th, 1979 is the worst commercial nuclear power generation accident in the history of the United States. Coolant from the primary coolant system leaked resulting in a significant quantity of fuel rods failing. Fuel failure included rupture of the **Zr** cladding and melting of the UO_2 fuel. [NRC site] The nuclear industry in the United States saw new plant construction cease for over thirty years as a result of this partial core melt. It also galvanized anti-nuclear sentiment among significant elements of the voting populace, however the actual release of radionuclides was negligible.

By far the most catastrophic accident in the history of commercial nuclear power occurred on April 26th, 1986 at the then Soviet Chernobyl Nuclear Power Plant in what is now the Ukraine. The reactor at Chernobyl was an RBMK type reactor, which is graphite moderated and light water cooled. Under hot full power conditions this design has a negative moderator temperature coefficient. However, that day the reactor was operated in a low power regime where the moderator temperature coefficient and void coefficient were strongly positive. [ref]

This led to an uncontrollable power transient that almost instantly boiled the coolant inventory and over-pressurized the reactor vessel to the extent that it exploded. The explosion was a steam explosion, not a nuclear explosion. However, the reactor core continued to heat up, lighting the graphite moderator on fire—which carried away in the smoke fission products and other material released from ruptured fuel rods. The confinement design for the RBMK was completely inadequate and significant radionuclide release into the environmental occurred. This nuclear accident infuriated Europe, which was directly downwind of this unprecedented radioactive nuclide release. The world has not forgotten Chernobyl, and the official Russian and IAEA total number of deaths, cancers, and other deleterious health effects from this disaster are at times disputed. The only possible benefit to come from this experience has been that the radiation health physics community now has more data to analyze concerning the effects of exposure to fission products.

The accident at Fukushima Daiichi on March 11th, 2011 was the result of a very high wave tsunami which followed a strong earthquake, and caused the failure all but one of the plant's emergency diesel generators and several switchboards connecting individual reactor buildings to the local power grid. Lacking the power at the pumps needed to circulate the water and cool the reactor, catastrophic fuel heat up and failure occurred, including the **Zr** cladding reaching such high temperatures so as to undergo exothermic hydrogen producing reaction with H_2O. Hydrogen escaped from the path provided for its release and explosions destroyed the top floors of three reactor buildings, and significant amounts of radiation were released into the atmosphere and Pacific Ocean. Germany has claimed that it will permanently phase out nuclear energy in response to this accident, and many other countries now question their commitments to nuclear energy as well. [3]

1.2.4 Silicon Carbide (SiC)

SiC is a ceramic material with a high elastic modulus, high ultimate tensile strength, and low fracture toughness. It's melting point is over 2700°C, and it is chemically stable in liquid H_2O and high temperature steam representative of Loss Of Coolant Accident (LOCA) conditions.

SiC's tolerance of high temperature and chemical stability in aqueous environments is vastly superior to conventional **Zr** fuel cladding, which undergoes a strongly exothermic

hydrogen producing reaction above ~1200°C. SiC is also not susceptible to hydrogen embrittlement.

SiC may also be a candidate cladding material for the Generation IV Fluoride Salt-Cooled High-Temperature Reactor (FHR), since high temperature reactors tend to be limited by degradation of materials performance at high temperature. **Zr** cladding is not stable in 700°C Li_2BeF_4 eutectic molten salt and therefore unacceptable for the FHR—while SiC may enable the use of rod-type fuel assemblies with conventional low-enriched UO_2. This would be an alternative to TRISO particle fuel which must be enriched to ~20%.

SiC clad fuel also dramatically improves the safety of Spent Nuclear Fuel (SNF) wet storage, dry cask storage, and repository disposal. The temperature limit of **Zr** cladding is an engineering constraint that the entire SNF waste management industry currently designs around. SiC cladding would allow for more efficient storage and disposal of SNF by allowing waste management engineers to pack more assemblies into waste packages without overheating the cladding and releasing fission products into the waste package.

The potential safety and economic benefits of SiC fuel cladding may allow for a far-reaching re-evaluation of many aspects of nuclear engineering from fuel performance and reactor physics to fuel cycle and waste management.

However, many questions regarding the *in situ* performance of SiC fuel cladding under irradiation remain unanswered or controversial. How does thermal conductivity degrade with fluence? Does SiC's polymorphism lead to phase instability at high fluence and high displacements per atom (dpa) rates? Are the mechanical and thermal properties and their evolution with fluence particularly sensitive to the manufacturing process and initial microstructure? These questions are beyond the scope of this thesis, yet are critically relevant to nuclear fuel cladding applications of SiC.

1.3 Scope

The results presented in this thesis will focus on designing nuclear reactor cores to operate within the desired limiting parameters of particular interest to electrical power generation utilities and the United States Nuclear Regulatory Commission (NRC). Peaking factors, soluble boron concentration, neutron leakage, reactivity coefficients, and shutdown margin calculations have been performed for all cores and are the primary metrics by which they be evaluated.

Assembly burnable pin layouts and core reload maps have been produced via optimization algorithms. In each batch only a single enrichment assembly is used. This methodology has produced a **Zr** clad reference case competitive with more heterogeneous core designs sold by major vendors.

A total of 18 cores have been designed; one core per OF has been designed for each of six fuel and cladding combinations. An OF is the means by which to quantify the relative value of a given system configuration in an optimization algorithm. The three OFs have been chosen to elucidate the dynamic range of performance achievable by each fuel and clad combination—using extremes of design criteria valuations from peaking only optimization to cycle length only optimization.

A software suite, CSpy, has been written to facilitate this design work. The development of this software is essential to studies of this type since it integrates and organizes many different functions such as initial sensitivity studies using lattice depletions, optimization at both the assembly and full-core levels, and automated generation of plots, tables, and full reports summarizing core physics performance.

2 PWR Core Parameters and Parameter Limitations

2.1 Geometry

Since the fuel-clad gap in SiC clad fuel does not close as rapidly as in the case of **Zr** clad fuel, fuel temperatures will be higher in SiC fuel. To compensate for this, the fuel pellets must be altered. One option is to make the pellet annular with an inner hole of about 10% volume—an option based on FRAPCON results by D. Carpenter. [4] Another option is to add a high conductivity constituent in the fuel, which in this study was chosen to be BeO.

In order to preserve the thermal hydraulics of conventional 17x17 PWR assemblies, **Thick SiC** clad fuel is modeled in most cases as having the same cladding outer radius as conventional fuel. [5] Thus, the outer radius of the fuel has been decreased (while maintaining an equivalent fuel/clad gap), but the thermal hydraulics of the core remain unaltered.

In the case of **Thick SiC 2**, the thermal hydraulics are altered by increasing the cladding outer radius and keeping the pellet outer radius constant. The likely thermal hydraulic compensation for this reduction in coolant volume will be an increase in coolant velocity in order to preserve the total coolant mass flow rate through the core. The larger surface area will reduce the heat flux at the outer surface of the cladding, which together with the higher mass flux in the core will improve the margin to departure from nucleate boiling (DNB). The downside to this change is the increase in the required pumping power. Another downside to this change could be that the reduction in the space between the rods could result in coolant flow blockage and increased flow velocity will increase the vibrational amplitude and result in increased risk of Grid To Rod Fretting and other fuel failures. Detailed thermal-hydraulic analysis of **Thick SiC 2** is considered beyond the scope of this thesis and left as future work.

Table 1 describes the fuel rod geometry for each case. All dimensions are in **cm**. The asterisk for **Thick SiC** indicates that the fuel inner radius is case dependent—0.1290 cm in the case of annular UO_2, and 0.0 cm in the UO_2/BeO and PuO_2/ThO_2 cases.

Table 1: Fuel Pin Dimensions in Centimeters

	Zircaloy	**Thin SiC**	**Thick SiC**	**Thick SiC 2**
Clad Outer Radius (R_{co})	0.4750	0.4750	0.4750	0.5069
Clad Inner Radius (R_{ci})	0.4180	0.4180	0.3861	0.4180

Fuel Outer Radius (R_{fo})	0.4096	0.4096	0.3777	0.4096
Fuel Inner Radius (R_{ci})	0.0000	0.1290	*	0.1290
Clad Thickness (δ_c)	0.0570	0.0570	0.0889	0.0889
Gap Thickness (δ_g)	0.0084	0.0084	0.0084	0.0084
% Vol. of PWR Fuel	100.00	90.08	*	90.08

Thick SiC rods contain the following fraction of fuel present in **Thin SiC** rods:

$$\frac{\pi(0.3777^2 - 0.1290^2)}{\pi(0.4096^2 - 0.1290^2)} = 83.382\ \%$$

$L = 365.76$	Heated length
$P = 1.26$	Rod-to-rod pitch
$l = 21.50$	Assembly pitch

2.2 Material Densities

Material densities utilized in this work are shown below in Table 2.

Table 2: Material Densities

Material	Density (g/cc)	Comments
Zircaloy-4	6.55	
Triplex SiC	2.85	Manufacturer's Spec
UO_2	10.47	95.5% TD
BeO	2.85	
PuO_2	10.925	95.5% TD
ThO_2	9.158	95.5% TD

The BeO content of the proposed UO_2/BeO fuel is specified as 10% by volume. Calculations in Appendix A provide values for use in specifying the isotopic composition of the homogeneous UO_2/BeO fuel in CAMSO. UO_2/BeO is modeled as having no ^{234}U content, while CASMO's default ^{234}U content is used for UO_2 fuel (both annular and solid).

Fuel density in the PuO_2/ThO_2 core is a function of the weight percent of plutonium metal. Calculations for PuO_2/ThO_2 fuel density and isotopics' weight percent are also presented in Appendix A.

Previous work used a triplex SiC density of 2.39 g/cc. [6] However, we found no reference as to why this value was used. The sensitivity of core design parameters to SiC density has not been investigated in detail, however it is only reasonable to imagine that underestimation of cladding density and thus neutron absorption may produce non-conservative results, particularly for enrichment requirements to meet cycle length. The Triplex SiC cladding density specified in Table 2 was provided by Ceramic Tubular Products (CTP). [private comm Herb, date]

Recent literature from Oak Ridge National Laboratory (ORNL) lists SiC monolith density as 3.215-3.219 g/cc depending on polytype. [7] 3.20 g/cc and 3.21 g/cc have been reported for SiC produced by chemical vapor deposition (CVD) and hot isostatic pressing (HIP), respectively. [8] Density of SiC fiber has been reported to vary from 2.55-3.1 g/cc. [9]

Cladding volume per rod in **Thick SiC** fuel is considerably larger than in **Zr** or **Thin SiC** rods. Fuel clad in **Thick SiC 2** has even more cladding volume per rod. The calculations in Table 2 assume a fuel rod heated length of 365.76 cm, and a fuel density of 10.47 g/cc (for UO_2):

Table 3: Fuel Rod Masses for Different Clads

Quantities Per Rod	**Zircaloy**	**Thin SiC**	**Thick SiC**	**Thick SiC 2**
Clad Vol (cc)	58.49	58.49	87.96	94.49
Fuel Vol (cc)	192.8	173.7	144.8	173.7
Clad Mass (g)	383.1	166.7	250.7	269.3
Fuel Mass (g)	2018	1818	1516	1818
Clad + Fuel Mass (g)	2401.1	1984.7	1766.7	2087.7

The increase in fuel cladding volume for **Thick SiC** decreases the fuel volume and increases the neutron absorption by the cladding. **Thick SiC 2** has the same fuel volume as the **Thin SiC**, however it has the highest cladding volume of all cases presented here.

2.3 Fuel Mass (Core Total)

The total mass of the fuel and the Initial Heavy Metal (IHM) loadings vary considerably among the conventional case and the new conceptual designs as illustrated in Table 3. For the PuO_2/ThO_2 fueled core the fuel mass is dependent on the Pu wt% and will vary from design to design, whereas the variation of fuel mass as a function of enrichment of UO_2 is insignificant.

Table 4: Core Clad, Fuel, and IHM Masses in kg

	Zircaloy	Thn SiC UO_2 Annular	Thk SiC UO_2 Annular	Thk SiC UO_2/ BeO	Thk SiC PuO_2/ ThO_2	ThkSiC2 UO_2 Annular
Clad Mass (kg)	19522	8494	12775	12775	12775	13721
Fuel Mass (kg)	102850	92652	77255	81092	78095	92652
IHM Mass (kg)	90661	81667	68095	69379	68662	81667
Fuel+Clad (kg)	122380	101146	90030	93867	90869	106373

2.4 Enrichment: Main Length, Axial Blankets, and Overall

In order to improve neutron economy and axial power shape, the axial ends of the fuel rods had lower enrichments than the bulk of the fuel. The following enrichment zones were used. When Integral Fuel Burnable Absorber (IFBA) is used, it is present only in the main heated length of the fuel.

Table 5: Axial Enrichment Zones for All Core Designs

Segment	Length	84 Zr4 UO_2 (w/o)	64 SiC UO_2 (w/o)	84 SiC UO_2 (w/o)	84 SiC2 UO_2 (w/o)	84 SiC UO_2/ BeO	84 SiC PuO_2/ ThO_2
Top Outer	6"	2.00	3.20	3.60	2.60	3.39	6.82
Top Inner	6"	4.50	6.90	5.60	5.00	5.49	12.51
Main Length	10'	4.50	6.90	5.60	5.00	5.49	12.51
Bottom Inner	6"	4.50	6.90	5.60	5.00	5.49	12.51
Bottom Outer	6"	2.00	3.20	3.60	2.60	3.39	6.82
Average		4.292	6.592	5.433	4.800	5.325	12.037

The percentage reported in Table 5 for plutonium content in the fuel is the plutonium weight percent of IHM, excluding all oxygen bound in the fuel matrix.

The enrichment needs for the nominal Zr4 and the 84 SiC2 case shown in Table 5 do not exceed the current enrichment limit (5%) for PWRs in the US, significantly simplifying and reducing the cost of implementation of these designs.

No attempt was made to further flatten axial power shapes by slightly reducing enrichment in the bottom two axial blanket zones. This may be considered in future work.

The isotopic compositions for the outer blanket regions were chosen to provide the correct cycle length, and to be roughly half the enrichment or plutonium content of the main length. Since axial power peaking is not particularly sensitive to the enrichment or plutonium composition of this outer blanket region, this method has produced results sufficient to provide evidence that designs with the above desired materials are viable.

More refinements in enrichment and plutonium specification will allow for finer control of cycle length via adjustment of the composition of the fuel's main length while also allowing precise specification of the outer blanket composition. In such a case the outer blanket composition could be specified as a function of the main length composition. This approach is left to future investigators, in addition to analysis of the impact of axial power on DNB calculations.

2.5 Plutonium Vector

The plutonium vector used in this work is typical of discharged fuel from current PWR practice and is as indicated in the following Table 6:

Table 6: Plutonium Vector

Isotope	Wt%
^{238}Pu	3.18
^{239}Pu	56.35
^{240}Pu	26.62
^{241}Pu	8.02
^{242}Pu	5.83

Americium and other higher actinides are not present in the fuel modeled in this thesis. These conditions would represent loading of fuel that had been recently reprocessed and fabricated in a manner sufficiently rapid so that decay of ^{241}Pu produces only negligible quantities of ^{241}Am.

The plutonium vector utilized is characteristic of LWR SNF that has been discharged at approximately 50 MWd/kg (based on CASMO output of a typical PWR assembly). This plutonium vector is not favorable for utilization as fissile material in thermal spectrum reactors; the fissile content is less than 65 wt%. The even mass number Pu isotopes fission more readily as the neutron spectrum hardens, or as ^{238}Pu and ^{240}Pu transmute via neutron absorption, reducing the reactivity penalty for non-fissile content.

Other sources of plutonium will provide different isotopic compositions. Low burnup LWR SNF (previous modi operandorum were 30 MWd/kg) would be significantly higher in ^{239}Pu. Plutonium extracted from fast reactor fuel would also be significantly higher in ^{239}Pu. These high-fissile content plutonium vectors are more reactive and capable of achieving higher burnup than low-fissile content plutonium. In thermal spectrum reactors the initial vector will gradually accumulate higher proportions of even numbered Pu isotopes.

In practice, core designers may specify a desired plutonium vector for delivery from the reprocessor to the fuel fabricator. In the event that the reprocessor is unable to deliver fuel utilizing the desired plutonium vector, the core must be redesigned according to the specific plutonium vector supplied in the fuel as delivered from the fuel fabricator.

2.6 Clad Isotopic Composition

For triplex silicon carbide clad, an isotopic composition of 70 wt% Si, 30 wt% C is used. This is approximately stoichiometric, with the carbon composition rounded up very slightly to reflect the presence of residual carbon from the manufacturing process. The manufacturer Ceramic Tubular Industries has specified that these conditions are accurate and applicable to their product.

Previous work used a value of 62 wt% Si, 37 wt% C, and 1 wt% O. A reference as to where these values come from has not been found. However, SiC monolith manufacture can be accomplished via deposition over a graphite rod and SiC fiber manufacture entails the use of a graphite lubricant. These facts may have led to the assumption of high carbon content used in previous modeling of the neutronic performance of SiC cladding.

Previous work used SiC instrumentation and control rod guide tubes of conventional thickness. The inner radius of these tubes might not be easily changeable (without redesign of the control rods), therefore it may be required to use **Thin SiC** or even **Zr** for them because using a thicker clad would change an assembly's thermal hydraulics. In this analysis **Zr** has remained as the material of the guide tubes since the guide tube thickness is smaller than that of fuel cladding (in all cases).

2.7 Burnable Poison

IFBA is a thin layer of ZrB_2 painted onto the outer curved surface of fuel pellets. It is now the most common burnable poison used in Westinghouse PWRs and the only burnable poison utilized in this analysis.

All cores designed in this work use 156 1.0x IFBA rods per assembly, with the exception of the PuO_2/ThO_2 core which uses 156 1.5x IFBA rods per assembly. Further optimization may require using different numbers of burnable poison rods to achieve desired reactor physics parameters.

Table 7: IFBA Composition

IFBA Type	$mg^{10}B/cm$	$mg^{10}B/inch$
1.0x	0.618	1.570
1.5x	0.927	2.355

2.8 State Parameters

The following state parameters are used:

Table 8: State Parameters

Parameter	Value	Units
Power Density	109.9	kW/L
Reactor Pressure	155.1	bar
Core Inlet Temp	558.6	K

These conditions are representative of Westinghouse 4-loop PWRs, and in particular are modeled after Seabrook's Stretch Power Uprate of 2004. [10]

2.9 Fuel Temperature Relations

A relation defining nodal average fuel temperature in terms of nodal relative power fraction and nodal burnup is required in order to faithfully model core physics performance. These correlations must be specified by the user in SIMULATE. Yanin Sukjai and Dr. Koroush Shirvan have performed a FRAPCON analysis and provided a curve fit for the results to be used in this work.

The form of the temperature relation for nodal average fuel temperature is given below.

$$T_{AVE} = T_{MOD} + c_0 + [c_1 + b]P + c_2P^2$$

This primary form is further modified by burnup dependent modification of the linear term (***b***).

Table 9 presents the coefficients of the correlations used below.

Table 9: SIMULATE Temperature Relation Coefficients

	Zircaloy	**Thn SiC UO_2 Annular**	**Thk SiC UO_2 Annular**	**ThkSiC2 UO_2 Annular**	**Thk SiC UO_2/ BeO**	**Thk SiC PuO_2/ ThO_2**
c_0	0.0	0.0	0.0	0.0	0.0	0.0
c_1	316.25	470.5	335.18	335.18	361.81	397.28
c_2	-12.33	-27.359	-19.31	-19.31	-3.414	-31.17
Source	Shirvan & Sukjai	Carpenter	Shirvan & Sukjai	Shirvan & Sukjai	Shirvan & Sukjai	Shirvan & Sukjai

In addition to the above table, a table of values for ***b*** as a function of burnup exists in SIMULATE for each fuel and cladding combination. Values of ***b*** were used for all temperature correlations produced by Dr. Shirvan and Yanin Sukjai.

The temperature correlation used for **ThickSiC2** case is the same as for **ThickSiC**. Future work may consider using an updated temperature correlation, however the assumption of this work is that the temperature correlations for the two cases will not be significantly different.

2.10 Specific Power

Specific power is the ratio of a core's rated thermal power to its IHM mass. It is typically expressed as kW/kgIHM. Multiplication of this power by the time interval of one day is equivalent to the energy produced in one day per kgIHM—i.e. the daily burnup. Since the core thermal power and cycle length are the same for all cases considered herein—yet the core IHM loadings vary, it is reasonably expected that designs with less IHM will be associated with higher specific power and higher burnup. The higher specific power reduces SNF production. The higher specific power also implies that the fuel cost may be reduced as less Uranium is utilized. However, for total fuel cycle cost analysis, the enrichment level has to also be considered.

Table 10 shows the specific power for each core designed in this thesis.

Table 10: Specific Powers For Fuel/Clad Combinations

	Zircaloy	Thn SiC UO_2 Annular	Thk SiC UO_2 Annular	Thk SiC UO_2/ BeO	Thk SiC PuO_2/ ThO_2	ThkSiC2 UO_2 Annular
Thermal Power (MW_{th})	3587	3587	3587	3587	3587	3587
IHM Mass (kg)	90661	81667	68095	69379	68662	81667
Specific Power (kW/kg)	39.57	43.92	52.68	51.70	52.24	43.92

Thick SiC Annular UO_2 and **Thick SiC** PuO_2/ThO_2 have the highest specific powers. Thick SiC UO_2/BeO is less than the previous two, but not significantly different. **Thick SiC 2** has the same specific power as **Thin SiC**, and all cases considered have higher specific powers than the **Zr** clad case.

2.11 Cycle Length

The target cycle length for all cores designed in this study is 469 Effective Full Power Days (EFPD) at a power level of 3587 MW_{th} with a 90% capacity factor between refuelings. This capacity factor is more likely to be representative of implementation of new technology, in this case SiC cladding, than the conventional 95% capacity factor. The **Zr** reference cores were also designed with a capacity factor of 90% to allow for direct comparison of the SiC cores to the reference cores.

Burnup increases appreciably for cores that have a smaller IHM loading. This effect is unavoidable, since burnup is energy produced per unit mass IHM. By demanding the same (or higher) quantity of energy from a core before a reload while reducing the fuel mass burnup must increase.

Table 11 shows Linear Reactivity Model (LRM) burnup predictions for equilibrium cores loading 84 fresh assemblies per reload. [11] The values presented are core averaged for End of Full Power Life (EOFPL), and discharge burnup is the batch average for the discharged assemblies. These values are calculated from the IHM mass and specific power—and are not results from full-core modeling. All burnup units are in MWd/kgIHM, and each core will be referred to by the fuel type except for **Zr** clad UO_2 and **Thin SiC** clad UO_2.

Table 11: 84 Assembly per Reload Core Burnups, LRM Calculation

	EFPD	Zircaloy	Thn SiC	ThkSiC UO_2 Annular	ThkSiC2 UO_2 Annular	ThkSiC UO_2/ BeO	ThkSiC PuO_2/ ThO_2
Cycle	469	18.5	20.5	24.6	20.5	24.2	24.4
EOFPL	773	30.5	33.8	40.6	33.8	39.8	40.2
Discharge	1078	42.5	47.2	56.6	47.2	55.5	56.1

Table 12 shows Linear Reactivity Model (LRM) burnup predictions for cores loading 64 fresh assemblies per reload:

Table 12: 64 Assembly per Reload Core Burnups, LRM Calculation

	EFPD	Zircaloy	Thn SiC	ThkSiC UO_2 Annular	ThkSiC2 UO_2 Annular	ThkSiC UO_2/ BeO	ThkSiC PuO_2/ ThO_2
Cycle	469	18.5	20.5	24.6	20.5	24.2	24.4
EOFPL	938	37.0	41.1	49.2	41.1	48.3	48.8
Discharge	1407	55.5	61.6	73.4	61.6	72.5	73.3

A detailed procedure for the calculation of these values is presented in Appendix A.

2.12 Core Performance Evaluation Criteria

2.12.1 Design-Limiting Performance Parameters

Peaking factors, soluble boron concentration, moderator temperature coefficient (MTC), peak pin burnup, and shutdown margin (SDM) are the primary design considerations. Typical targets are shown below:

Table 13: Design-Limiting Performance Factors

Parameter	Target Value
$F_{\Delta h}$	< 1.55
F_q	< 2.00
Maximum boron concentration (ppm)	< 1700
MTC (pcm/°F) @ HFP	< 0.0
Peak pin burnup (SiC)	< 100 MWd/KgU

Peak pin burnup (Zr)	< 62 MWd/KgU
SDM	> 1.3% or 1300 pcm

Values for these parameters with the exception of shutdown margin have been calculated for all cores. Minor violations of these guidelines are present in the current designs, however the current designs do provide a clear picture of the capability to effectively utilize the desired clad/fuel combinations. Further optimization is expected to provide superior conformity with the complete set of above guidelines.

Further, the results achieved in this work utilize only a single enrichment for a given reload. While CSpy does allow for multiple assembly types to be utilized in a single reload pattern, this feature has not been utilized in order to reduce the number of parameters that must be investigated throughout the course of optimization. Multiple assembly types used in a single reload batch may allow for core performance superior to the designs presented in this work. However, since this study is meant to show the comparative performance of each design, a single assembly type is advantageous in decoupling specific core reload loading pattern designs from the physics of each specific design that result in differences in performance.

2.12.2 Maximum Channel Enthalpy Rise ($F_{\Delta h}$)

$F_{\Delta h}$ is the ratio of the maximum value of axially integrated power for a single fuel rod to the core-average pin power (the core's total power divided by the total number of fuel rods). It is one of the primary criteria of interest for the NRC when evaluating license approval for design, construction, and operation of commercial reactors. The NRC does not directly limit $F_{\Delta h}$ but requires it to be such as to preclude DNB in normal operation or in Anticipated Operational Occurrences. [12]. The higher the value of $F_{\Delta h}$, the more likely an unanticipated power transient is to cause DNB; for a fixed coolant mass flow rate increasing $F_{\Delta h}$ reduces margin to DNB. The value of 1.55 is a typical value found in commercial reactors.

2.12.3 Maximum Local Power (F_q)

F_q is the ratio of the peak to core average linear power. This value is particularly relevant in the determination of the minimum critical heat flux ratio for a PWR.

The SIMULATE output parameter that reports F_q is "4PIN." This differs from "3PIN" in that "3PIN" reports the peak node-averaged relative power fraction—whereas "4PIN" reports the

actual intra-node peak value of relative power fraction. In SIMULATE, a node is modeled as quarter of an assembly in the core and so "4PIN" is therefore more conservative, and thus the parameter reported in this thesis. It is worth noting however that others may opt to report "3PIN" or similar such spatially-averaged peak values of relative power fraction which do not correspond to the true peak value.

2.12.4 Soluble Boron

Boric acid is injected into the primary coolant loop of PWRs to control long term changes in reactivity. Its concentration is easily controlled, and since it is soluble in the coolant it provides a reactivity control effect that is homogeneous—unlike control rods which can significantly alter the power distribution in a reactor's core.

Soluble boron concentration is not limited by the NRC, however soluble boron concentrations more than 2000 ppm are generally considered undesirable since boric acid is corrosive in the PWR primary loop environment. If the soluble boron concentration is high enough, the MTC can become positive (which is unacceptable in a LWR). In today's operational reactors, the desired concentration of boric acid is even lower (~1200 ppm) as it will reduce the risk for inducing axial offset anomalies. [13]

2.12.5 Moderator Temperature Coefficient (MTC)

The MTC is the change in the core's reactivity resulting from a permutation in moderator temperature of one degree (typically K or °F).

This value is of particular interest in plant power level maneuvering and in preventing uncontrollable over-power transients. A negative hot-full-power (HFP) MTC causes a reactor power level to drop in response to an increase in moderator temperature. This builds into the reactor a level of inherent safety in handling power and temperature transients. The NRC requires the MTC at rated power to be non-positive.

A highly negative MTC can be a hindrance however in the event of reactor shutdown and anticipated decrease in coolant temperature transients such as steam generator tube rupture, since the core's reactivity will increase as the temperature drops (due to the increase in number density of the coolant which is also the fuel's moderator). This can sometimes require an increase in shutdown margin.

The isothermal temperature coefficient (ITC) is the change in the core's reactivity resulting from a permutation in both moderator and fuel temperature of one degree (typically K or °F).

2.12.6 Peak Pin Burnup

Peak fuel pin burnup is a major criterion of interest from a fuel performance point of view. Material limitations in terms of dpa, plenum pressure, corrosion, and Pellet-Clad Mechanical Interaction (PCMI) all play a role in determining the level of material damage a clad can sustain without suffering an unacceptable increase in the probability of cladding failure.

Radiation damage to **Zr** causes degradation of its mechanical properties. Thermal stress, vibration, fatigue, fretting wear, oxidation, and hydrogen embrittlement are all factors that increase the probability of cladding failure. All of these effects are damaging to **Zr**'s mechanical properties even in the absence of radiation, however radiation increases the severity of these effects—and the effect of radiation accumulates with continued exposure.

For **Zr** cladding, the NRC currently limits peak rod burnup to 62 MWd/kg.

2.12.7 Shutdown Margin (SDM)

There is a large difference in reactivity between HFP and hot zero power (HZP). The density of the moderator increases as power is reduced, therefore the reactivity worth of the control rod system must be sufficient to overcome this difference.

A conservative calculation includes the assumed failure of the control rod with the highest reactivity worth, and an assumed level of insertion of control rods. The calculation of SDM proceeds as follows:

Table 14: Shutdown Margin Calculation Terms

Symbol	Reactivity Difference
Δk_1	HFP to Control Rods 30% In
Δk_2	HFP to HZP
Δk_3	HFP to All Rods In (ARI)
Δk_4	HFP to Most Effective Rod In

$$\text{SDM} = (\Delta k_1 + \Delta k_2) + 0.9(\Delta k_3 + \Delta k_4)$$

Equations for the above parameters are included in Appendix A.

2.12.8 Additional Criteria

Various additional criteria are considered in evaluating the value of a particular core design. Leakage, fast fluence to the reactor pressure vessel (RPV), boron worth, fast to thermal neutronic flux ratio, breeding ratios and other parameters may be considered. Fuel performance consequences must be evaluated such as peak centerline temperature and End Of Life (EOL) plenum pressure.

Leakage is a measure of neutron economy, and reducing leakage tends to increase cycle length or alternatively reduce the enrichment required. Leakage also results in neutron absorption by materials outside the core, including PWR baffles, heat shields, and RPVs. Transmutation of structural materials via neutron absorption tends to lead to degradation of mechanical properties via formation of elements not present in the as manufactured alloy, helium production, and hydrogen production. [14] Fast neutron dose to the RPV also embrittles it by elevating the nil ductility transition temperature, degrading the RPV performance during accidents involving thermal shock and hindering the extending of the plant's operating lifetime.

3 Methodology of Fuel Management

Two primary tools were used to conduct this analysis: Studsvik Core Management software, and CSpy. It should be noted that a few particular phenomena are not accurately captured by the Studsvik Core Management software since it was designed to be a commercial production code for utilities working only with UO_2 and UO_2/PuO_2 mixed oxide (MOX) fuels.

3.1 Studsvik Core Management Software

CASMO-4E and SIMULATE-3 are the primary computational tools utilized in this thesis.

3.1.1 CASMO-4E

CASMO is an industry standard assembly level depletion code for *in silico* analysis and modeling of LWR reactor physics performance. The version used to collect the data in this report is CASMO-4E.

It uses a 2D method of characteristics algorithm to solve the neutron transport equation for single assemblies or groups of assemblies.

The primary results of interest from CASMO assembly calculations are reactivity and intra-assembly pin peaking as a function of burnup. CASMO also produces cross section data which can then be used in SIMULATE, to simulate the operation of a full core in 3D. Myriad other parameters are produced by CASMO including fuel elemental and isotopic composition, and fast (>0.625 eV) and thermal (<0.625 eV) group neutron fluxes.

The following is a map of k_∞ as a function of burnup. It contains data from 78 CASMO runs. Each "series" ranges in enrichment from 5% to 7.5%, in 0.1% increments. Unpoisoned, 1x IFBA, and 1.5x IFBA cases are presented.

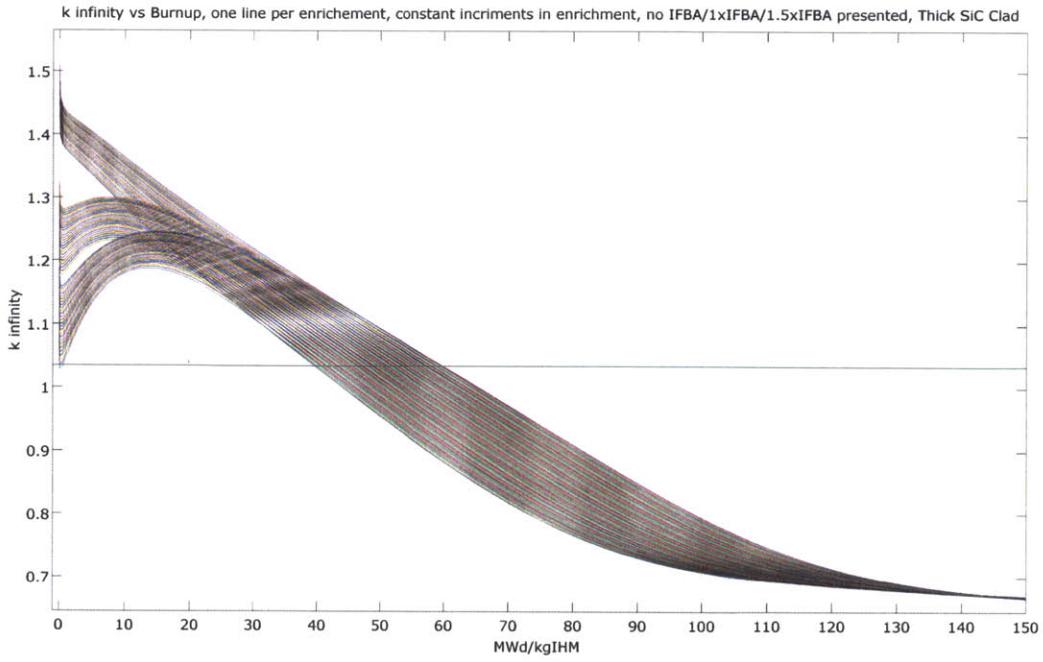

Figure 1: Thick SiC Clad Annular UO_2: CASMO k_∞ vs Burnup with Varied IFBA Content

3.1.2 SIMULATE-3

SIMULATE-3 is an industry standard tool for simulation of core performance. It uses a three dimensional two-group nodal method capable of pin-power reconstruction. SIMULATE-3 has been benchmarked against various other numerical methods and also experimental data.

3.2 CSpy

CSpy is a software suite written to efficiently utilize CASMO and SIMULATE to analyze potential fuel and cladding configurations on the assembly level and as implemented in a 193 assembly Westinghouse 4-loop PWR core. CSpy generates input files for CASMO according to a range of parameters of interest that may be varied in a specified manner so as to conduct sensitivity studies and optimization. CSpy also generates CASMO input files for the purpose of constructing a cross section library for use in full-core simulations by SIMULATE. SIMULATE input files are also generated by CSpy for 193 assembly cores using either 64 or 84 reloads per cycle. CASMO and SIMULATE output files are parsed by CSpy which uses output results in optimization schema, writing CSpy's own succinct report files, and plotting of results.

3.3 Design Process

The core design process is an iterative one, since the range of input parameters includes several factors and the design criteria satisfied by one iteration might not be satisfied by the next. Nevertheless, the process itself consists of a specific set of steps:

1. Choose the cladding material.
2. Choose the cladding geometry.
3. Choose the fuel compound(s). If plutonium is present in the as loaded fuel then the plutonium vector must be specified.
4. Choose the fuel geometry. If the fuel is annular, what criteria determine the inner radius?
5. Choose the composition of other materials, such as the control rod guide tubes and instrumentation tubes, control rods, and stainless steel support structures.
6. Choose the core reflector geometry.
7. Choose the number of reloads per cycle.
8. Choose a concentration of IFBA: 1.0x, or 1.5x.
9. Choose a burnable poison pin layout. Optimize burnable poison layout to minimize intra-assembly peaking.
10. Choose a core reload pattern.
11. Determine an average fuel temperature correlation as a function of nodal relative power fraction and burnup.
12. Optimize the core reload pattern according to the desired design criteria.

Several steps could be added to this process in the future. For example, the cycle length could be chosen to be other than the cycle length of 469 EFPD used in this study. Power uprated cores could be designed using a different volumetric power density. Different numbers of assemblies could be used, for example if one wished to design a core for a 157 assembly AP1000. Assemblies with different control rod positions could be used, or assemblies other than standard 17 x 17 PWR assemblies. Different burnable poisons could be used, such as gadolinium, Wet Annular Burnable Absorber (WABA), erbium, or hafnium. Combinations of burnable absorbers could be investigated.

Fuel performance parameters can be entered into the design process, either as threshold limits to disqualify prospective designs or as parameters that enter the optimization algorithm's OF.

Even within the narrow guidelines defining the core design work in this work, the potential search space for a core design is massive. There exist multiple levels of optimization, each one dependent on a great abundance of preceding parameter selections. Similarly, the design work possible depends on the computing power available and the flexibility afforded by the basic tools used in the analysis.

The end result of the design process in this case is an "equilibrium core." The properties of the equilibrium core are the theoretical core performance results if an operational cycle and reload pattern are repeated until core performance artifacts from the initial configuration are negligible. For example, a cycle that begins using fresh assemblies for each location (but varying enrichment) will behave differently compared to a cycle that begins using assemblies that have been depleted during a previous cycle.

4 Optimization Schema

Optimization schema have been implemented to produce burnable poison pin layouts and quarter core, rotationally symmetric reload maps. Optimization schema in general are comprised of two mechanisms: a means by which to permute system parameters, and a means by which to evaluate new permutations. Both mechanisms must have unambiguous, explicit, quantitative or procedural definitions.

4.1 Objective Functions (OFs)

The optimization designer must ask, "what exactly do I wish to optimize?" Equivalently, the designer may ask, "what are the properties of an optimal system?" Trade-offs between parameters influencing overall system behavior and value must be considered.

An OF must be defined in order to compare new optimizer results with the best results to date. The OF of an optimization algorithm can be as simple as a single parameter—or exceedingly complex in an attempt to address non-linearities and idiosyncratic behavior near saddle points.

Once an OF has been defined in terms of quantitative system performance parameters, the OF result from a new system permutation can be compared with historical results. Comparison and acceptance criteria may be as simple as selecting the system configuration with the higher OF result. Any mathematical comparator may be utilized, and equality of certain parameters may be acceptable (particularly if the number of significant figures input into the OF are limited). The historical best OF result may be used as the reference for comparison and acceptance of new permutations, or more sophisticated comparisons against multiple historical OF results and other parameters may also be used.

In this work the ideal assembly burnable poison layout has maximal burnup when reactivity reaches an arbitrary endpoint (when reactivity letdown reaches 1.035 or 0.95 or another arbitrary value) and minimal peaking (pin power, pin exposure).

In this work the ideal nuclear reactor core has maximal cycle length, and minimal peaking ($F_{\Delta h}$, F_q, peak pin exposure). Shutdown margin, soluble boron, and leakage must be within specified limits. Specific details of OFs used in this work will be explained in detail in the sections introducing their context.

4.2 Permutation Algorithms

There exist many algorithms by which to permute system properties in search of an optimal configuration. Before beginning to construct any such algorithmic process, a set of quantitative and/or logical conditions must completely define the system. In the case of burnable poison layouts or core reload maps a vector whose elements represent each pin or assembly is sufficient. Element values represent the possible occupants, and the number of element values is not necessarily related to the number of elements in the vector. For example, in the burnable poison layouts presented in this work every pin is either poisoned or unpoisoned. Completely defining the burnable poison layout then is a vector with one element for each fuel pin in an octant where each pin is either a 1 (unpoisoned) or a 2 (poisoned). (Poison type and loading are preselected.) The numbers are arbitrary labels in this case. The following is a vector defining the burnable poison pin layout for a 17 x 17 Westinghouse assembly using octant symmetry.

VECTOR=[1, 1, 1, 2, 2, 1, 1, 1, 2, 1, 1, 1, 1, 2, 2, 1, 1, 1, 1, 1, 1, 1, 1, 1, 2, 1, 2, 2, 2, 2, 2, 1, 2, 2, 1, 2, 1, 2, 1]

Permutation of this vector can occur by a variety of processes, so long as the number of 1's and 2's are conserved. In the case of burnable poison layouts, some elements lie on the diagonal of the octant and count for a different number of burnable poison pins than those in the interior of the octant. Phenomena of this nature must be carefully accounted for, the number of burnable poison pins is to be conserved by the permutation process.

A binary swap is the interchange of two elements. This is the simplest permutation possible. There is however no upward limit to the complexity of possible permutations.

4.2.1 Genetic Algorithm

The "Genetic Algorithm" starts with the creation of a group of independent and unique configurations of a given system. Applied to nuclear reactor core reload map optimization the starting point would be a group of different maps.

The algorithm would then create a "generation" of new maps by combining pieces of existing maps. These maps would then be tested and their value computed via an OF. A group of new maps is then chosen from the best valued maps to form the basis for the next generation. [15]

4.2.2 Simulated Annealing

Simulated Annealing is an optimization algorithm that allows acceptance of system configurations that produce OF results worse than the reference OF value. By allowing this to occur, the algorithm is less constrained by local extrema. As the number of iterations of a Simulated Annealing algorithm increases, generally the tolerance of worse OF results decreases. This tolerance is compared to the temperature in an annealing process, where the temperature initially is high (to allow the greatest possibility of escaping local extrema) and is gradually reduced (to hone in on the value of the closest extremum). [16]

4.2.3 Dual Binary Swap (DBS)

The primary algorithm used to produce new configurations and while attempting to avoid local extrema in the search space is the DBS. The DBS is the execution of two binary swaps at the same time. Any map or layout element involved in one of the swaps may not be involved in the other; for each DBS four elements are moved. The DBS has been implemented as a random walk to generate core reload maps. Figure 2 below illustrates an example of the DBS process.

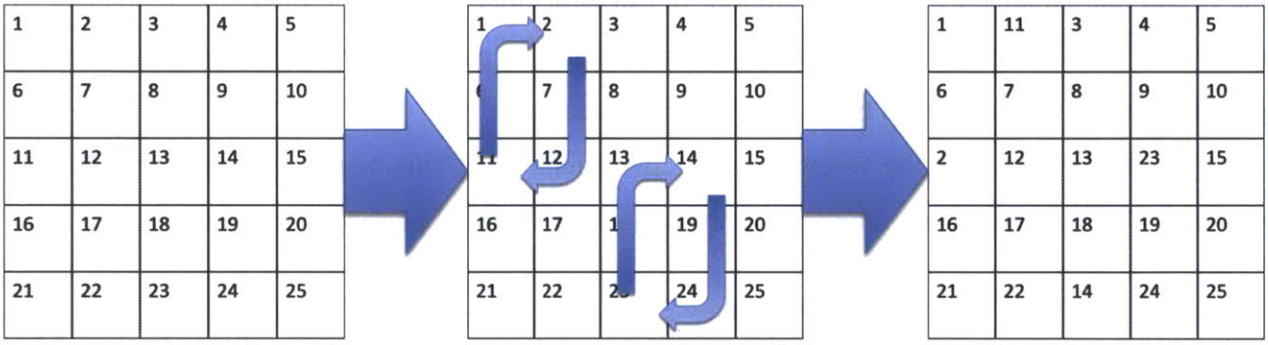

Figure 2: DBS Process: Before (left), Swap (center), After (right)

4.2.4 Exhaustive Dual Binary Swap (EDBS)

An EDBS is a collection of all DBSs possible given a specified initial condition. An Exhaustive Dual Binary Swap (EDBS) algorithm has been implemented to produce burnable poison layouts.

4.2.5 Random Greedy Dual Binary Swap (RGDBS)

While the EDBS performs an exhaustive sweep of the possible permutations of a system via DBS and compares the best result from that analysis to the historical best result, an RGDBS

explores the permutation space of a given configuration until any improvement whatsoever is found.

This is a fundamentally different process since it cannot be guaranteed that the best possible new permutation is chosen at each step. The RGDBS is a stochastic process, and a significantly greater variation in end states produced from a given initial condition is possible if there exists a high density of local extrema in the search space.

4.3 CASMO Burnable Poison Layout Optimization

The EDBS has been implemented for the optimization of burnable poison pin layouts using lifetime peak intra-assembly power peaking as the OF. Several iterations of the EDBS process are required before further EDBSs no longer produce improvement. In the case of burnable poison pin layouts, EDBS has consistently reached the same maximum lifetime intra-assembly peaking factor for a given enrichment and number of burnable poison pins. For example, if 5.0% UO_2 and 156 1.0x IFBA rods were specified, the final result was invariant with respect to the initial burnable poison pin layout. For 156 burnable poison pins per assembly, a single EDBS iteration consists of 11,898 individual layouts that must be run in CASMO and the results must be parsed to find the best resulting layout. This was typically accomplished in about 10 hours by running multiple instances of CASMO in parallel via CSpy. The optimal maximum intra-assembly peaking factor was achieved by many different layouts, on the order of hundreds of layouts. A maximum of three iterations of EDBS were required to reach an end-state intra-assembly peaking value in all cases investigated throughout the course of this work.

It was also found that burnable poison layouts were transferrable to fuels and enrichments other than those for which they were originally intended. Some layouts were found to be optimal for multiple fuel types at the same enrichment, and for multiple values of enrichment for each fuel. For example, the burnable poison layout for 6.7% enriched Thick SiC clad annular UO_2 was also optimal (as tested by EDBS) for several neighboring enrichments. The burnable poison map utilized in all 1.0x IFBA cases was exactly the same through the first generation of SIMULATE reload map optimization. Optimization via EDBS of a map that has been applied to a fuel or geometry different from its original parameters tended to produce no improvement or an improvement of intra-assembly peaking by 0.001.

2D and 3D histograms of occurrences of cycle burnup vs peaking, and peaking vs enrichment plots have been constructed describing the CASMO burnable poison layout optimization process.

Figure 3 below shows an EDBS result for 4.5% enriched **Zr** clad UO_2. These results are from the re-optimization effort described below in Section 5.1. It is particularly noteworthy that over 5% of the DBSs in the exhaustive sweep produced the optimal value of maximum lifetime intra-assembly peaking. Even more noteworthy is that over 7% of the DBSs were 0.001 higher than the optimal value. Over 12% of the results are at or near the optimal OF result.

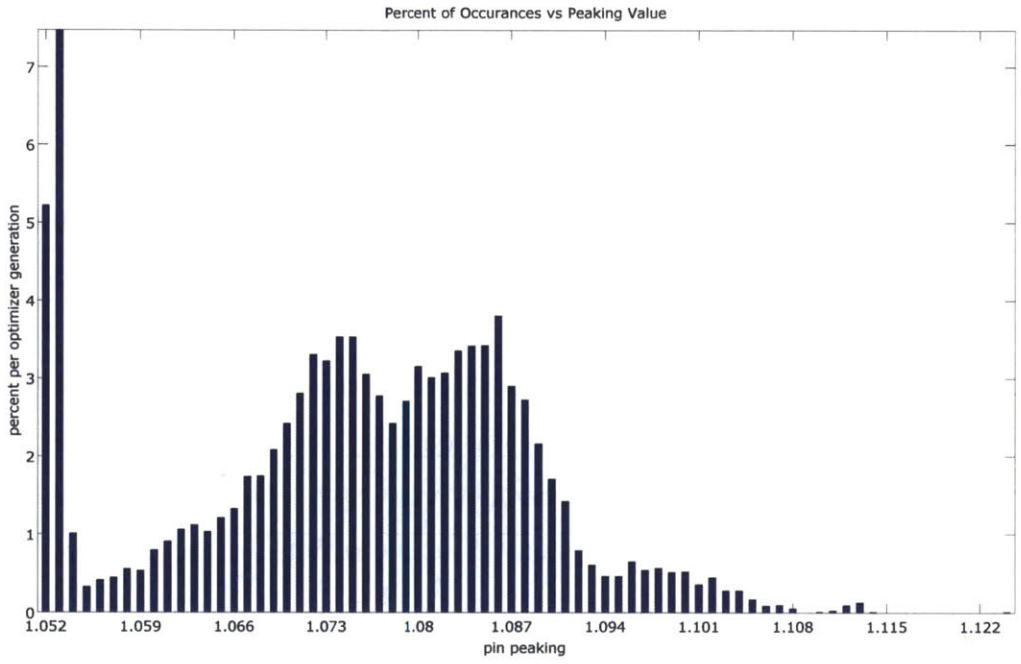

Figure 3: EDBS, % Occurrences vs. Peaking Value

Figure 4 shows the number of occurrences for each pairing of: the point at which the reactivity curve of an assembly crosses 1.035 (B_1), and maximum lifetime intra-assembly peaking.

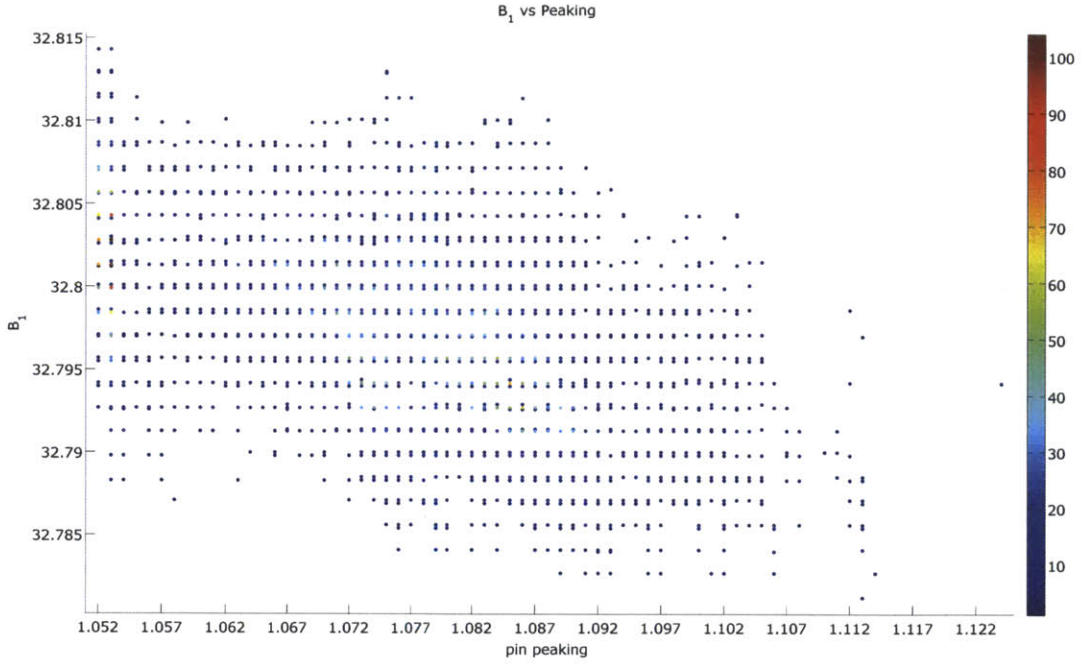

Figure 4: EDBS, B_1 vs Peaking, Occurrences by Color (2D)

Figure 5 shows the same data as Figure 4, however by using a 3D plot the data is easier to interpret.

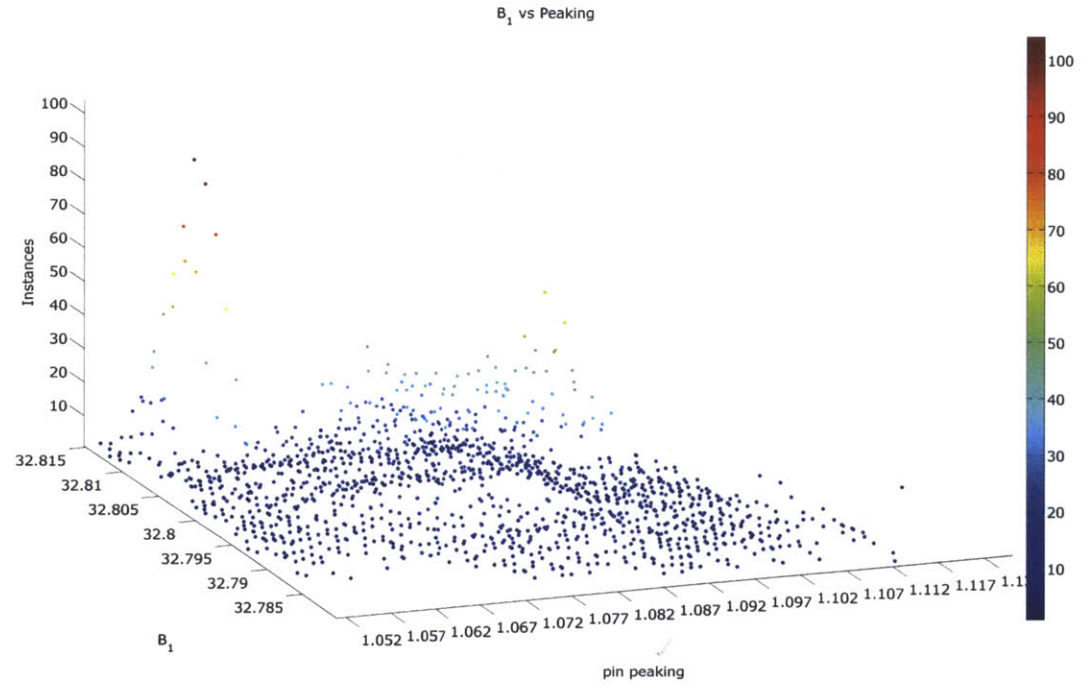

Figure 5: EDBS, B_1 vs Peaking, Occurrences by Color (3D)

Considerable variation exists in the results of an EDBS, and the regions of high occurrence show the most probable results using stochastic DBSs.

4.3.1 CASMO Burnable Poison Layout Optimization OFs

The OF utilized for burnable poison layout optimization was lifetime peak intra-assembly pin power peaking factor.

More sophisticated OFs may include: lifetime peak intra-assembly power peaking, lifetime averaged intra-assembly peaking, and B_1.

Heuristics could be applied to reject layouts containing time steps in which the peak power pin occurs in peripheral locations. It has been observed that SIMULATE results using the exact same core reload pattern can be significantly altered by changing the burnable poison layout of the assemblies used. OFs for burnable poison maps could therefore also include parameters from full-core implementation. Iteration between CASMO and SIMULATE could involve OFs that interact with each other.

4.4 SIMULATE Core Reload Map Optimization

Implementation of EDBS for core reload maps in SIMULATE involves over an order of magnitude more combinations of DBSs to run and parse and to date has not been implemented. Optimization of SIMULATE core reload maps instead relies on the RGDBS, in which a new map is constructed by a randomly generated DBS and if the new result is superior to the previous best result then the new map is accepted as the new best result.

SIMULATE is capable of performing core physics calculations at various levels of precision, reducing calculation time while reducing accuracy. This effect was utilized to accelerate optimization. The first layer of optimization using SIMULATE was using a single axial node to model core performance, i.e solving only a 2-dimensionoal problem. These calculations were exceedingly fast (~10 seconds per complete equilibrium core calculation). The second layer of optimization of a core reload pattern used 12 axial nodes, and thus represented the 3 dimensions. The final layer of optimization used 24 axial nodes—the same number used in the full calculation of all parameters presented herein. Typically, when transitioning from one axial node count to the next the performance parameters would change; the single axial node calculations tended to over-predict cycle length and under-predict peaking. 12 axial node

calculation results would also differ from 24 axial nodes, however this time over-predicting both peaking and cycle length.

The starting point for the first core reload maps was a conventional checkerboard pattern with very high peaking. When starting a new core design for a new fuel and clad combination, either an existing map could be adapted and re-optimized for the new configuration or a pattern could be found using the checkerboard baseline starting point.

A heuristic is applied to the map generation algorithm that rejects any map containing one or more fresh fuel assemblies on the periphery of the core. Additional heuristics for SIMULATE core reload map generation have been proposed but not implemented, including requiring that most twice burnt fuel be loaded on the periphery. In the case of 84 reloads per cycle there would not be enough twice burnt fuel to completely fill the peripheral assembly locations and some once burnt assemblies would also be present.

4.4.1 Peaking Factor OFs

4.4.1.1 OF 0.1

The first OF utilized was $F_{\Delta h}$.

$$F_{\Delta h_{New}} < F_{\Delta h_{Best}}$$

Without any other constraint, implementation of this OF resulted in the optimization algorithm placing fresh fuel at the periphery of the core. While $F_{\Delta h}$ was reduced, the cycle length was significantly diminished. Leakage was also increased.

The heuristic rejecting DBSs that placed fresh fuel on the periphery significantly improved results. Core reload maps thus generated looked similar to "ring of fire" cores in which the highest concentration of fresh fuel assemblies was near the periphery. The core interiors were mostly checkerboard-like patterns.

This simple OF was used to ensure that all considered fuel and clad combinations were capable of satisfying the core physics parameter limitations. While this end was achieved, several resultant cores had a high, rapidly decreasing Beginning of Cycle (BOC) F_q indicative of over poisoning.

4.4.1.2 OF 0.2

Experience running optimization with this OF led to the observation that tens of thousands of DBS permutations may be checked between finding new improvements. A new OF was implemented in order to reduce this average interval between finding new improvements, speculating that increasing overall activity may be preferable to a more stagnant situation. The new OF also only considered $F_{\Delta h}$.

$$F_{\Delta h_{New}} \leq F_{\Delta h_{Best}}$$

4.4.1.3 OF 0.4

This was producing results that were not significantly different from the previous algorithm. It was then decided to optimize considering both $F_{\Delta h}$ and cycle peak soluble boron. The logic for this system was to accept new maps with a lower $F_{\Delta h}$ and accept maps with an equal $F_{\Delta h}$ but lower cycle peak soluble boron.

$$\{F_{\Delta h_{New}} < F_{\Delta h_{Best}}\} \text{ or } \{F_{\Delta h_{New}} = F_{\Delta h_{Best}} \text{ and } [B]_{New} < [B]_{Best}\}$$

This OF was observed to increase core leakage and often negatively affected cycle burnup, however this effect on cycle burnup was inconsistent.

4.4.1.4 OF 0.5

Given that OF 0.2 increased leakage and often reduced cycle length, it was logical to try the reverse—accepting new maps if they had higher cycle peak soluble boron.

$$\{F_{\Delta h_{New}} < F_{\Delta h_{Best}}\} \text{ or } \{F_{\Delta h_{New}} = F_{\Delta h_{Best}} \text{ and } [B]_{New} > [B]_{Best}\}$$

This OF was observed to decrease core leakage and its effect on cycle length was also inconsistent.

4.4.1.5 OF 0.6

While the above OFs were useful investigations, the first set of optimizations had produced several cores whose BOC F_q was significantly higher than at any other period in the cycle. This high initial F_q would also drop off quickly, indicating a potentially over-poisoned condition. It was therefore attempted to reduce BOC F_q via reshuffling of the core reload map.

$$\{F_{\Delta h_{New}} < F_{\Delta h_{Best}}\} \text{ or } \{F_{\Delta h_{New}} = F_{\Delta h_{Best}} \text{ and } F_{q_{New}} \leq F_{q_{Best}}\}$$

This OF was observed to reduce F_q.

4.4.1.6 OF 0.7

As in OF 0.6, OF 0.7 is also an attempt to reduce F_q. The only difference between 0.6 and 0.7 is that 0.7 does not accept maps with both an equal $F_{\Delta h}$ and F_q.

$$\{F_{\Delta h_{New}} < F_{\Delta h_{Best}}\} \text{ or } \{F_{\Delta h_{New}} = F_{\Delta h_{Best}} \text{ and } F_{q_{New}} < F_{q_{Best}}\}$$

This OF was also observed to reduce F_q and not observed to be significantly different from OF 0.6.

4.4.2 Exposure to Peaking Ratio OFs

The peaking factor OFs accomplished their intended purpose of showing that acceptable peaking factors can be achieved for the fuel and clad combinations presented herein. However, it was noticed that cycle length was affected negatively upon application of OF 0.7. Therefore it was speculated that an OF involving cycle burnup and peaking factors may extend cycle length without compromising peaking factor minimization.

4.4.2.1 OF 1.0

OF 1.0 was constructed to allow for small changes in output results to lead to the acceptance of new maps with the following trends.

1. If cycle burnup ($\boldsymbol{B_c}$) increases and everything else stays the same then the new map should be accepted.
2. If $F_{\Delta h}$ decreases and everything else stays the same then the new map should be accepted.
3. If F_q decreases and everything else stays the same then the new map should be accepted.

These three criteria lead to the construction of OF 1.0.

$$OBJ_{1.0} = \frac{B_c}{F_{\Delta h} F_q}$$

It was noticed that if the product of $F_{\Delta h}$ and F_q remain constant while cycle burnup increases then the new map will also be accepted.

As implemented, this OF was able to reduce the BOC F_q that was so problematic with earlier OFs. It appeared to be less susceptible to becoming trapped in local extrema, and gradually extended cycle length while essentially maintaining the low peaking achieved using the 0.x series of OFs.

Many of the new maps would be accepted with a completely new combination of B_c, $F_{\Delta h}$ and F_q. Generally, lower values of peaking might cut cycle length—but then cycle length would again be extended.

4.4.2.2 OF 1.1

OF 1.0, despite its effectiveness in extending cycle length in practice, heavily weights the peaking factors in its determination of a given reload maps objective value. The following OF is the first variation of OF 1.0 attempting to extend cycle length while retaining an appropriate level of peaking factor minimization.

$$OBJ_{1.1} = \frac{EXP}{\sqrt[n]{F_{\Delta h} F_q}}$$

By setting $n > 1$ and reducing the importance of the peaking factors this OF acts somewhat differently, however the overall results are similar to OF 1.0.

4.4.3 Threshold Dependent OFs

Since cycle length is the primary parameter of interest when considering the economic value of nuclear fuel to the utility, it was decided to explore optimization that was constrained within the safety limits of core physics parameters.

4.4.3.1 OF 2.0

What if peaking were allowed to take any value $F_{\Delta h} < 1.55$ and $F_q < 2.00$, and the OF was solely the cycle length?

$$B_{c_{New}} > B_{c_{Best}}$$

4.4.4 Other OFs

A vast quantity of parameters may be considered in the design of OFs for the purpose of reactor core optimization. Peaking factors and cycle length may be common factors to take into account, however the dynamics of core physics can be exposed in a variety of ways by optimizing according to combinations of parameters.

For example, leakage could be investigated using rational OFs as above. Cycle length divided by leakage could be an OF that may be relevant to a designer attempting to reduce RPV fluence.

4.4.4.1 Peak Pin Burnup

Peak pin burnup is another parameter that may be incorporated into an OF. A rational OF with peak pin burnup in the denominator (perhaps raised to a power less than 1) may assist in optimization motivated from a fuel performance point of view.

4.4.4.2 Combinations of OFs and Thresholds

Future OFs may include flow charts where different regimes of optimization are entered when specific parameters are reached. For example, before applying OF 2.0, either OF 0.7 or OF 1.0 could be applied to reduce peaking to within the threshold limits of OF 2.0. However, what would be the effect of changing the transition from 0.7 to 2.0 from the threshold of 2.0 to a lower limit (either defined in absolute terms or by a number of optimization trials)?

5 Results for UO_2 Fueled Cores

Six fuel and clad combinations have been evaluated. The first is a reference case, using conventional **Zr** clad, solid UO_2 fuel pellets and 84 reloads per cycle. It is the benchmark against which all other results will be compared since this core most closely resembles current industry practice.

Four additional fuel and clad combinations have been evaluated using **Thick SiC** cladding. Two reload numbers per cycle have been evaluated utilizing annular **Thick SiC** clad UO_2 fuel pellets: 64 reloads per cycle and 84 reloads per cycle. All remaining combinations have been evaluated using 84 reloads per cycle. The urania/beryllia and plutonia/thoria fuels are both mixed homogeneously, as opposed to being modeled as duplex pellets.

Lastly, **Thick SiC RCF** has been evaluated using annular UO_2 fuel pellets. This clad represents a departure from conventional 17x17 PWR thermal hydraulics and is included to assess the effect of taking the extra cladding volume from the coolant fraction as opposed to the fuel fraction (as in all other cases).

For each fuel and cladding combination there are three core designs—one design produced via the action of each optimization OF: 0.7, 1.0, and 2.0. These results range from a peaking-minimization only approach to a cycle length only approach (utilizing peaking acceptability thresholds). The middle ground between these two extremes is OF 1.0, which considers cycle length and peaking.

One fact to consider in interpreting the results produced via OF 0.7 is that the temperature correlation used by SIMULATE was updated after the optimization algorithm was run. Therefore the performance of those cores is slightly degraded. An addendum may include an updated set of OF 0.7 optimized cores.

5.1 Zr Clad UO_2 84 Reload Cores

The reference core for this work is solid UO_2 fuel clad in **Zr**, utilizing 84 reloads per cycle. This core is intended to resemble commercial cores, although it is acknowledged that the use of a single assembly type is a departure from commercial designs. Nevertheless, in order to compare cladding material and fuel combinations the reference core was designed using the same methodology as other cores.

Figure 6 shows the peaking factors and soluble boron letdown curves of the **Zr** clad reference cases. The peaking factors are considerably higher for the case produced via OF 2.0.

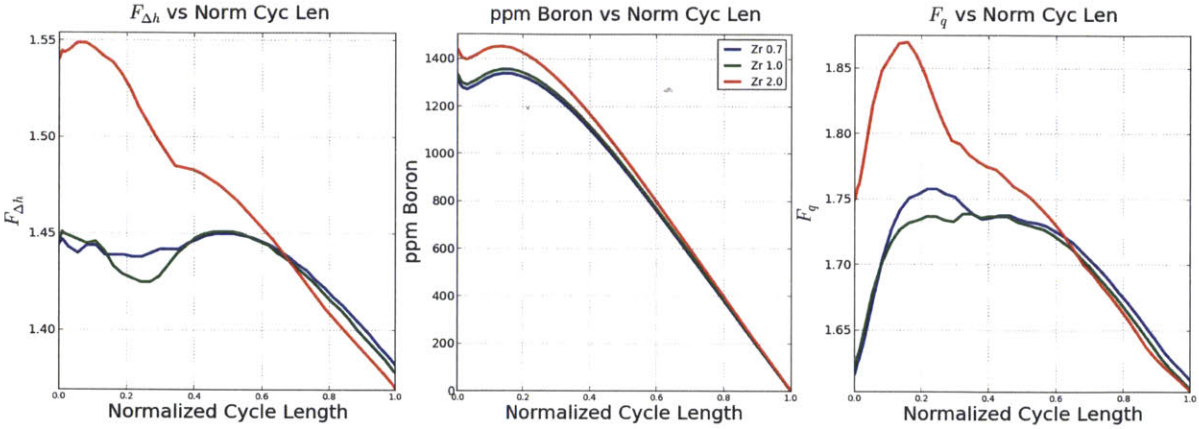

Figure 6: Zr Clad UO_2 84 Reload Cores, Peaking Factors and Soluble Boron

Figure 7 shows reactivity coefficient results for the **Zr** clad reference cases.

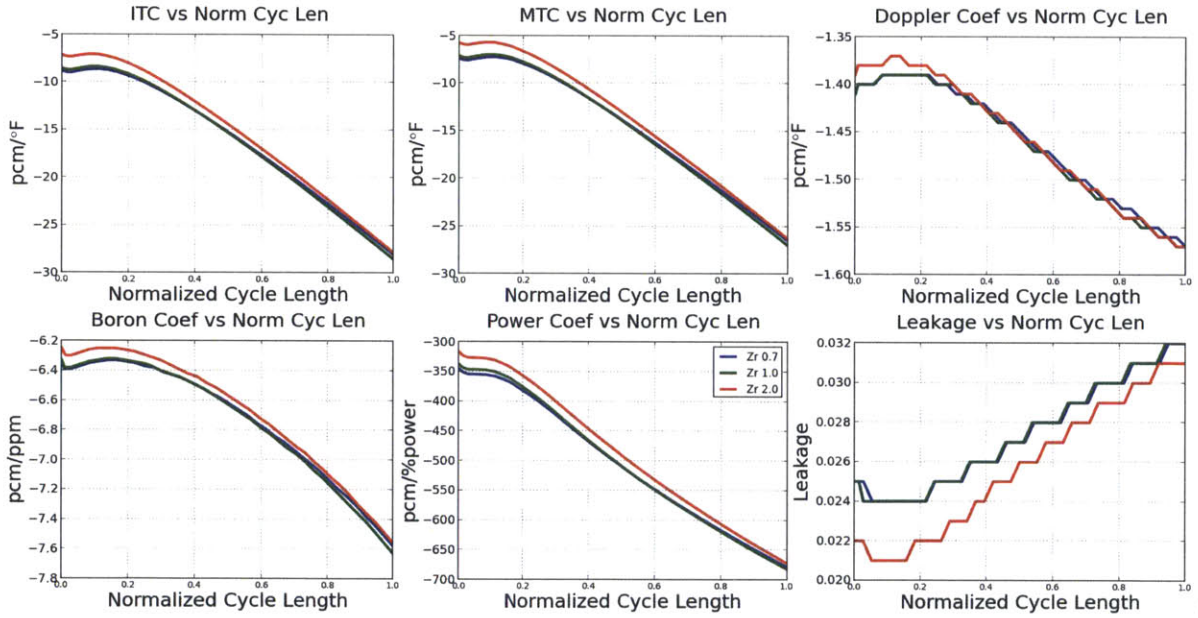

Figure 7: Zr Clad UO_2 84 Reload Cores, Coefficient Calculations

Figure 8 shows the core reload maps utilized in the **Zr** clad reference cases.

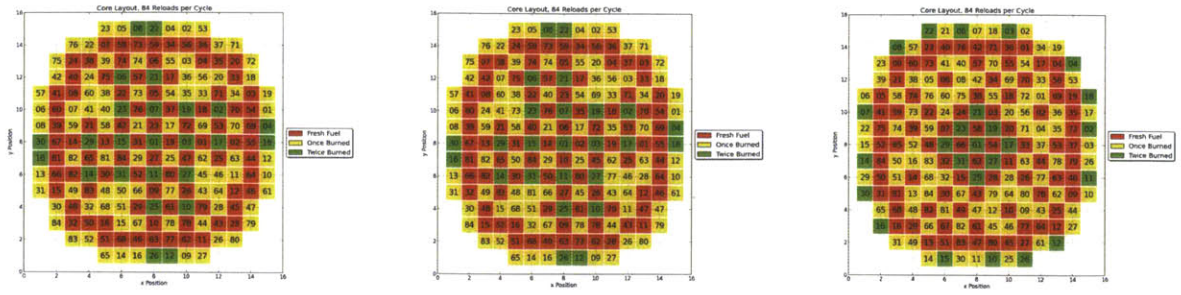

Figure 8: Zr Clad UO_2 84 Reload Cores, Reload Maps. (Left - 0.7 / Center - 1.0 / Right - 2.0)

Table 15 summarizes core geometry, material densities, and mass for the **Zr** clad reference cases. The hydrogen atom to heavy metal atom (H/HM) ratio is reported below as "**H/HM**."

Table 15: Zr Clad UO_2 84 Reload Geometry, Material Density, and Mass

R_{co}	R_{ci}	R_{fo}	R_{fi}	ρ_f	ρ_c	H/HM	m_{HM} (kg)
0.4750	0.4180	0.4096	0	10.47	6.55	3.35	90661

Table 16 summarizes physics performance values for the **Zr** clad reference cases. In Table 16, "SDB" and "SDE" refer to shutdown margin at BOC and End of Cycle (EOC), respectively. Also in Table 16, "PkExp" refers to peak pin exposure.

Table 16: Zr Clad UO_2 84 Reload Physics Summary

Obj Fcn	w/o	EFPD	B_c	B_d	BOR	$F_{\Delta h}$	F_q	PkExp	SDB	SDE
0.7	4.29	466.5	18.46	42.78	1340	1.450	1.758	71.6	-2090	-1610
1.0	4.29	470.8	18.63	42.21	1358	1.451	1.739	71.1	-2074	-1601
2.0	4.29	481.3	19.04	41.68	1454	1.549	1.870	67.5	-2055	-1645

During the design of these cores many generations of optimization were executed. The burnable poison layouts used in the CAMSO lattice calculations for **Zr** were adopted without modification from the initial optimization work on burnable poison layouts developed for **Thick SiC** annular UO_2 fuel. EDBS determined that 3.8% enriched fuel clad in **Zr** already had a fully optimized burnable poison layout. Therefore, optimization of the SIMULATE reload map began.

The optimization occurred at many levels of resolution, starting with a single axial node, then 12 axial nodes, then all 24 axial nodes of the standard case. SIMULATE optimization produced a result that proved difficult to improve upon. This result was an end-point arrived at after more than ten re-initializations of the optimization process from the initial checkerboard

pattern (returning to the initial checkerboard to start optimization again hoping to avoid undesirable local minima).

Once the correct fuel main length enrichment was found, CASMO burnable poison layout optimization was re-conducted on the layout applied to the main length enrichment. Intra-assembly peaking in the 2D infinite lattice case dropped from 1.053 to 1.052. In the interest of further depressing the core peaking factors, the CASMO library used by SIMULATE was updated with the new map—just for the main length enrichment.

The result of this modification was a strong de-optimization of the core physics parameters. Both peaking factors developed a spike early in the cycle that was not present prior to this modification. Cycle length was also diminished. The critical observation is that burnable poison configurations can strongly affect core reload pattern performance. To state this phenomenon in another way, core reload pattern performance can be sensitive to burnable poison layouts.

Switching back to the original burnable poison layout, further optimization of the SIMULATE reload map also reduced cycle length while reducing $F_{\Delta h}$. This experience contributed to the motivation to explore alternate OFs for more complete and dynamic optimization.

The difference in EFPD observed between the OF 0.7 and the OF 2.0 cases is 3.4%. More detailed discussion of the differences in results from the use of different OFs will be presented in Chapter 7.

The **Zr** cases have the lowest cycle burnup, discharge burnup, peaking factors, and peak pin burnup of all cases presented herein.

Comparison of the **Zr** reference cores produced in this work to the 84 reload **Zr** case in previous work by Dobisesky is presented in Table 17. LRM has been used to match EFPD values across all designs. $\mathbf{B_c}$, $\mathbf{B_d}$, and w/o% have been adjusted as well. Details of these calculations are presented in Appendix A. The remaining values have not been altered and may or may not reflect actual performance. Further modeling would be required to produce directly comparable cores using the methodology developed herein.

Table 17: Comparison of Zr Reference Cores to Previous Work

Obj Fcn	w/o	EFPD	B_c	B_d	BOR	$F_{\Delta h}$	F_q	PkExp	SDB	SDE
0.7	4.50	492	19.47	45.11	1340	1.450	1.758	71.6	-2090	-1610

1.0	4.46	492	19.47	44.10	1358	1.451	1.739	71.1	-2074	-1601
2.0	4.37	492	19.47	42.61	1454	1.549	1.870	67.5	-2055	-1645
Dobisesky	4.52	492	19.45	44.7	1477	1.53	1.80	66.8	-2737	-1928

The superior performance of the **Zr** cases of this work clearly demonstrate the efficacy of the methodology developed herein. Dobisesky's **Zr** case uses three different types of assemblies for each batch. The peaking factors of Dobisesky's **Zr** case are not much less than those of the OF 2.0 **Zr** case, and are not likely to change much pending design of the **Zr** cores of this work for a longer cycle. The extra enrichment of Dobisesky's **Zr** case does not yield a significant extension of cycle length.

5.2 Thick SiC Clad Annular UO_2 64 Reload Cores

Figure 9 shows the peaking factors and soluble boron letdown curves of the 64 reload **Thick SiC** clad annular UO_2 cases.

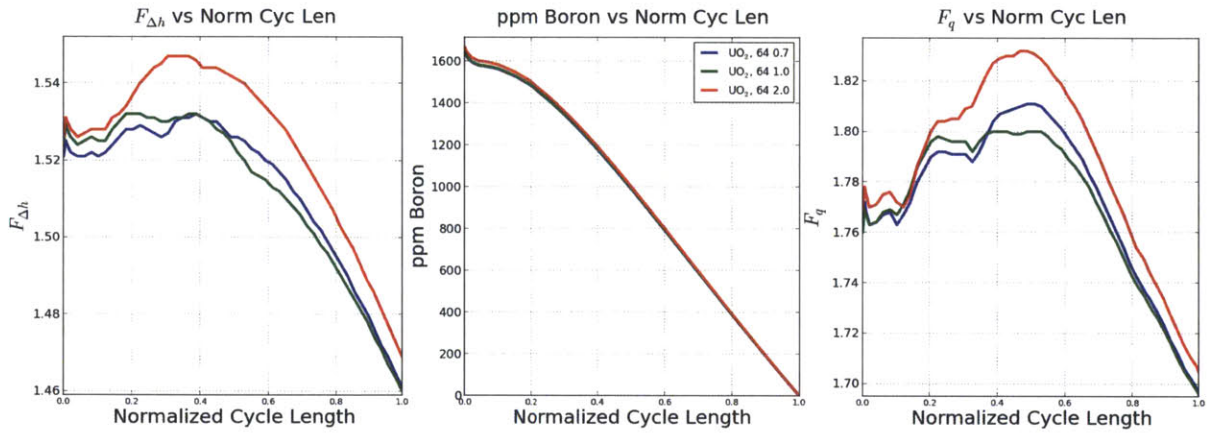

Figure 9: Thick SiC Clad Annular UO_2 64 Reload Cores, Peaking Factors and Soluble Boron

Figure 10 shows reactivity coefficient results for the 64 reload **Thick SiC** clad annular UO_2 cases.

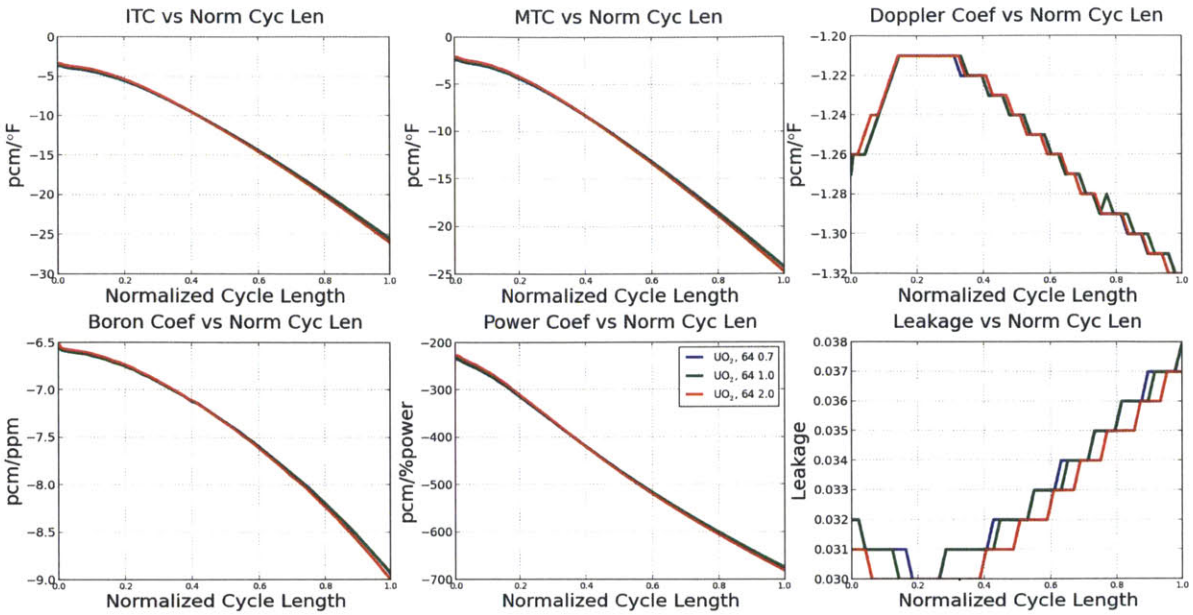

Figure 10: Thick SiC Clad Annular UO_2 64 Reload Cores, Coefficient Calculations

Figure 11 shows the core reload maps utilized in the 64 reload **Thick SiC** clad annular UO_2 cases.

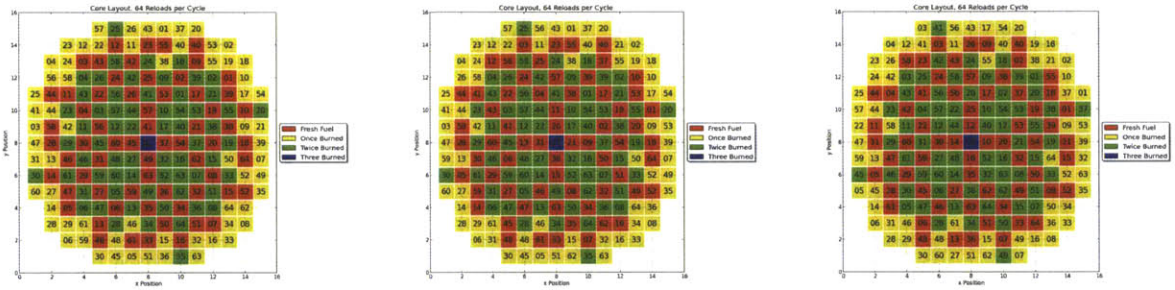

Figure 11: Thick SiC Clad Annular UO_2 64 Reload Cores, Reload Maps. (Left - 0.7 / Center - 1.0 / Right - 2.0)

Table 18 summarizes core geometry, material densities, and mass for the 64 reload **Thick SiC** clad annular UO_2 cases.

Table 18: Thick SiC Clad Annular UO_2 64 Reload Geometry, Material Density, and Mass

R_{co}	R_{ci}	R_{fo}	R_{fi}	ρ_f	ρ_c	H/HM	m_{HM} (kg)
0.475	0.3861	0.3777	0.129	10.47	2.85	4.47	68094

Table 19 summarizes physics performance values for the 64 reload **Thick SiC** clad annular UO_2 cases.

Table 19: Thick SiC Clad Annular UO_2 64 Reload Physics Summary

Obj Fcn	w/o	EFPD	B_c	B_d	BOR	$F_{\Delta h}$	F_q	PkExp	SDB	SDE
0.7	6.59	466.3	24.57	74.06	1641	1.532	1.811	102.6	-2897	-2458
1.0	6.59	466.5	24.57	74.07	1643	1.532	1.800	101.8	-2900	-2458
2.0	6.59	468.0	24.65	74.20	1664	1.547	1.832	98.7	-2895	-2449

The 64 reload **Thick SiC** clad annular UO_2 fueled core designs represent the least adaptable situation. Peaking cannot be suppressed to anywhere near the reference case levels. The high peaking results from the high enrichment and high burnup which increases the reactivity differences between the assemblies of different batches. Peak pin burnup is beyond the guideline outlined in Section 2.12.1.

Negligible variation in results are observed for each OF. Cycle length ranges from 466.3 to 468.0 EFPD—a variation of less than 0.4%. In this fuel/clad combination both cycle burnup and discharge burnup increased with optimization via OF 2.0—contrary to the trend observed with all other fuel/clad combinations where cycle burnup increases and discharge burnup decreases with optimization via OF 2.0.

These results demonstrate the viability of 3 batch **Thick SiC** clad annular UO_2 fueled cores.

Comparison of the 64 reload **Thick SiC** clad annular UO_2 cores produced in this work to the 64 reload **Thin SiC** clad annular UO_2 case in previous work by Dobisesky is presented in Table 20. The presented **Thick SiC** and **Thin SiC** cases exhibit similar performance in terms of peaking factors and soluble boron. Enrichment requirements are higher in **Thick SiC**, and peak pin exposure is lower in **Thin SiC**. However, the methodology used in the previous work by Dobisesky is significantly different and it may be reasonable to speculate that superior performance may be obtained via the application of the methodology developed herein.

Comparison of the 64 reload **Thick SiC** clad annular UO_2 cores produced in this work to the 64 reload **Thin SiC** clad annular UO_2 case in previous work by Dobisesky is presented in Table 20. LRM has been used to match EFPD values across all designs.

Table 20: Comparison of 64 Reload Thick SiC Annular UO_2 to Thin SiC of Previous Work

Obj Fcn	w/o	EFPD	B_c	B_d	BOR	$F_{\Delta h}$	F_q	PkExp	SDB	SDE
0.7	6.93	492	25.92	78.12	1641	1.532	1.811	102.6	-2897	-2458

1.0	6.93	492	25.92	78.13	1643	1.532	1.800	101.8	-2900	-2458
2.0	6.90	492	25.92	78.01	1664	1.547	1.832	98.7	-2895	-2449
Dobisesky	5.74	495	21.70	65.5	1654	1.55	1.81	81.3	-2889	-1776

The significantly lower fuel fraction of the 64 reload **Thick SiC** clad annular UO_2 cores requires higher cycle burnup and higher enrichment. The higher H/HM ratio of the 64 reload **Thick SiC** clad annular UO_2 cores may mitigate this slightly, but not enough to bring the enrichment down to values near previous work for **Thin SiC**.

5.3 Thick SiC Clad Annular UO_2 84 Reload Cores

Figure 12 shows the peaking factors and soluble boron letdown curves of the 84 reload **Thick SiC** clad annular UO_2 cases. The peaking factors are considerably higher for the case produced via OF 2.0.

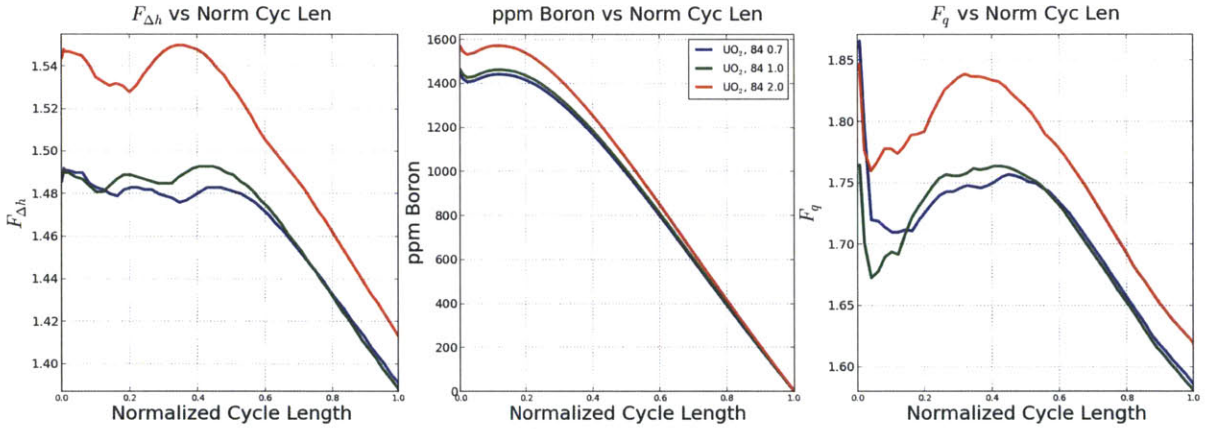

Figure 12: Thick SiC Clad Annular UO_2 84 Reload Cores, Peaking Factors and Soluble Boron

Figure 13 shows reactivity coefficient results for the 84 reload **Thick SiC** clad annular UO_2 cases.

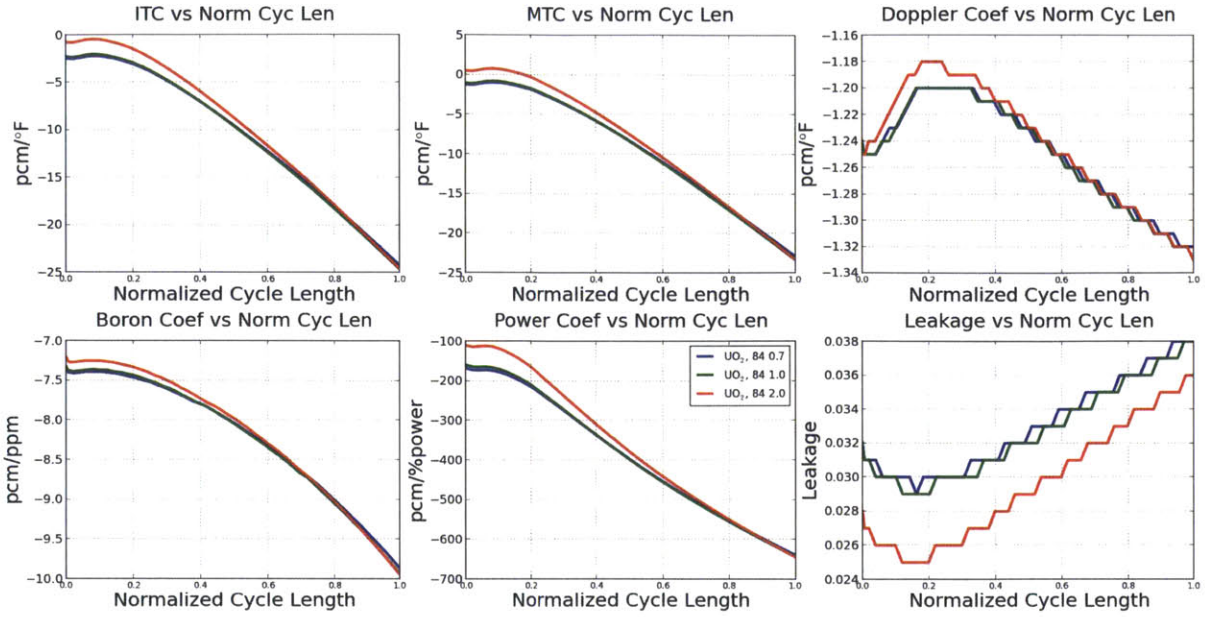

Figure 13: Thick SiC Clad Annular UO_2 84 Reload Cores, Coefficient Calculations

Figure 14 shows the core reload maps utilized in the 84 reload **Thick SiC** clad annular UO_2 cases.

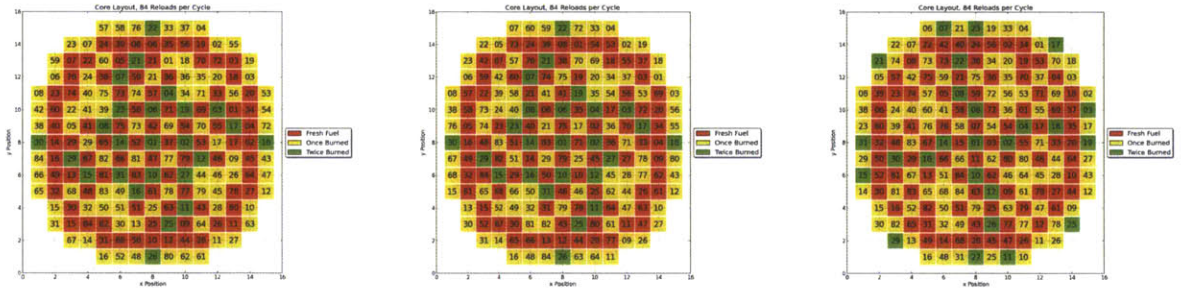

Figure 14: Thick SiC Clad Annular UO_2 84 Reload Cores, Reload Maps. (Left - 0.7 / Center - 1.0 / Right - 2.0)

Table 21 summarizes core geometry, material densities, and mass for the 84 reload Thick SiC clad annular UO_2 cases.

Table 21: Thick SiC Clad Annular UO_2 84 Reload Geometry, Material Density, and Mass

R_{co}	R_{ci}	R_{fo}	R_{fi}	ρ_f	ρ_c	H/HM	m_{HM} (kg)
0.475	0.3861	0.3777	0.129	10.47	2.85	4.47	68096

Table 22 summarizes physics performance values for the 84 reload **Thick SiC** clad annular UO_2 cases.

Table 22: Thick SiC Clad Annular UO_2 84 Reload Physics Summary

Obj Fcn	w/o	EFPD	B_c	B_d	BOR	$F_{\Delta h}$	F_q	PkExp	SDB	SDE
0.7	5.43	466.3	24.56	55.65	1444	1.492	1.866	90.9	-2637	-2434
1.0	5.43	469.3	24.72	55.35	1464	1.493	1.765	88.7	-2711	-2416
2.0	5.43	476.7	25.11	54.69	1573	1.550	1.847	80.6	-2713	-2575

There is a significant problem with the OF 2.0 optimized 84 reload **Thick SiC** clad annular UO_2 case—it has a positive MTC for the first ~20% of the cycle. The **Thick SiC** clad annular UO_2 cases all have a high soluble boron worth and small negative MTC, so that an increase of soluble boron concentration of less than 10% is enough to push the MTC positive. This difficulty could be probably be alleviated via the use of 1.5x IFBA as opposed to 1.0xIFBA.

These observations imply that H/HM for the **Thick SiC** clad annular UO_2 cases may be too high, particularly given the loss of self-shielding due to pellet annularization. Being too high on the moderation curve would explain the positive MTC and high soluble boron worth for the OF 2.0 case.

Comparison of the 84 reload **Thick SiC** clad annular UO_2 cores produced in this work to the 64 reload **Thin SiC** clad annular UO_2 case in previous work by Dobisesky is presented in Table 23. The presented **Thick SiC** and **Thin SiC** cases again exhibit similar performance in terms of peaking factors and soluble boron. Also, enrichment requirements are again higher in **Thick SiC**, and peak pin exposure is lower in **Thin SiC**. Again, it may be reasonable to speculate that superior **Thin SiC** performance may be obtained via the application of the methodology developed herein.

Comparison of the 84 reload **Thick SiC** clad annular UO_2 cores produced in this work to the 84 reload **Thin SiC** clad annular UO_2 case in previous work by Dobisesky is presented in Table 23. LRM has been used to match EFPD values across all designs.

Table 23: Comparison of 84 Reload Thick SiC Annular UO_2 to Thin SiC of Previous Work

Obj Fcn	w/o	EFPD	B_c	B_d	BOR	$F_{\Delta h}$	F_q	PkExp	SDB	SDE
0.7	5.71	492	25.92	58.72	1444	1.492	1.866	90.9	-2637	-2434
1.0	5.67	492	25.92	58.03	1464	1.493	1.765	88.7	-2711	-2416
2.0	5.59	492	25.92	56.45	1573	1.550	1.847	80.6	-2713	-2575
Dobisesky	4.79	492	21.56	49.6	1509	1.50	1.76	74.7	-2784	-2203

The significantly lower fuel fraction of the 84 reload **Thick SiC** clad annular UO_2 cores also necessitates higher cycle burnup and higher enrichment. The higher H/HM ratio of the 84 reload **Thick SiC** clad annular UO_2 cores also helps mitigate this slightly, but again—not enough to bring enrichment down to values near previous work for **Thin SiC**.

5.4 Thick SiC RCF Clad Annular UO_2 84 Reload Cores

Figure 15 shows the peaking factors and soluble boron letdown curves of the 84 reload **Thick SiC RCF** clad annular UO_2 cases. The peaking factors are considerably higher for the case produced via OF 2.0.

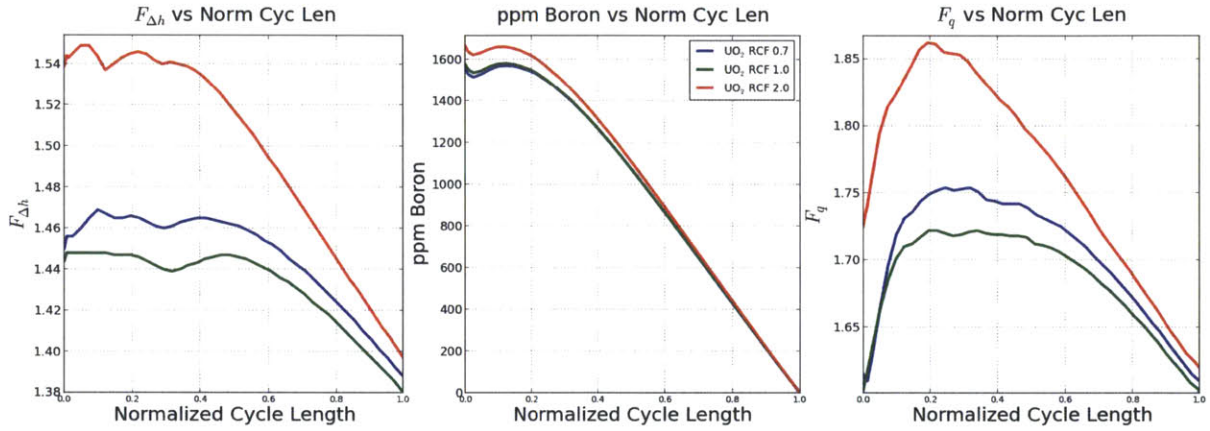

Figure 15: Thick SiC RCF Clad Annular UO_2 84 Reload Cores, Peaking Factors and Soluble Boron

Figure 16 shows reactivity coefficient results for the 84 reload **Thick SiC RCF** clad annular UO_2 cases.

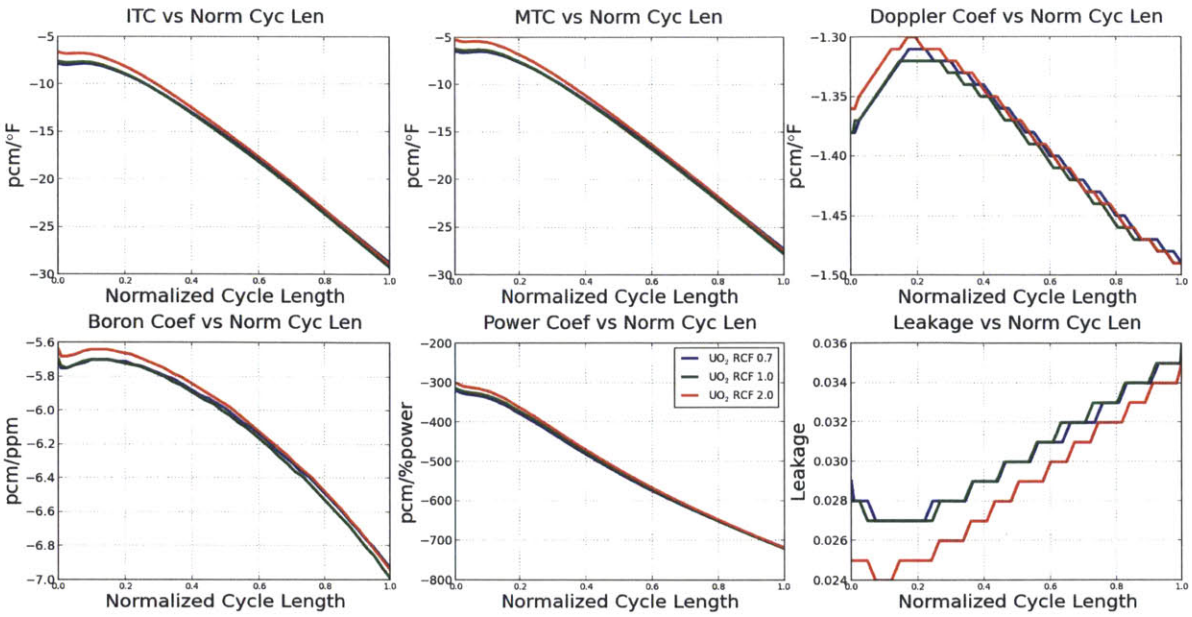

Figure 16: Thick SiC RCF Clad Annular UO_2 84 Reload Cores, Coefficient Calculations

Figure 17 shows the core reload maps utilized in the 84 reload **Thick SiC RCF** clad annular UO_2 cases.

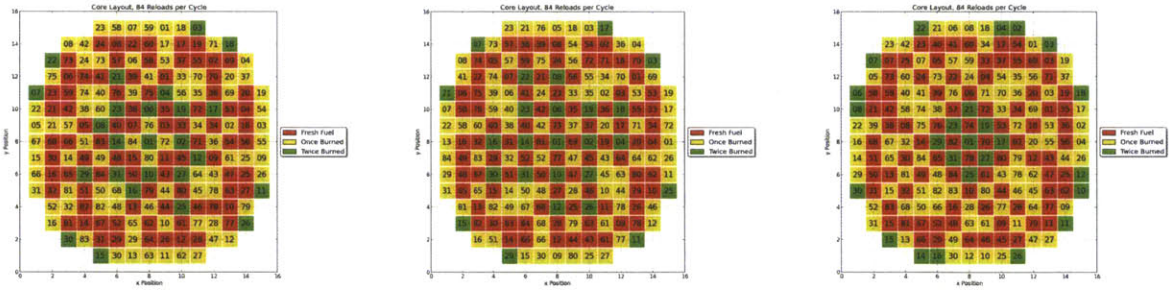

Figure 17: Thick SiC RCF Clad Annular UO_2 84 Reload Cores, Reload Maps. (Left - 0.7 / Center - 1.0 / Right - 2.0)

Table 24 summarizes core geometry, material densities, and mass for the 84 reload Thick SiC RCF clad annular UO_2 cases.

Table 24: Thick SiC RCF Clad Annular UO_2 84 Reload Geometry, Material Density, and Mass

R_{co}	R_{ci}	R_{fo}	R_{fi}	ρ_f	ρ_c	H/HM	m_{HM} (kg)
0.5069	0.4180	0.4096	0.129	10.47	2.85	3.31	81668

Table 25 summarizes physics performance values for the 84 reload **Thick SiC RCF** clad annular UO_2 cases.

Table 25: Thick SiC RCF Clad Annular UO_2 84 Reload Physics Summary

Obj Fcn	w/o	EFPD	B_c	B_d	BOR	$F_{\Delta h}$	F_q	PkExp	SDB	SDE
0.7	4.80	465.8	20.46	45.55	1571	1.469	1.754	79.5	-2275	-1433
1.0	4.80	468.7	20.59	45.64	1582	1.448	1.722	76.8	-2173	-1379
2.0	4.80	474.3	20.83	45.64	1665	1.549	1.862	72.0	-2038	-1414

The most significant and useful observation relating to the 84 reload **Thick SiC RCF** clad annular UO_2 cases is that they require no more than 5.00% enrichment—which is the current limit of licensed operational fuel fabrication facilities. Therefore, the licensing and implementation considerations for this set of core designs are fundamentally different from all of the rest. It is however not without qualification, since a full thermal-hydraulic analysis and other elements of a feasibility study must be conducted in order to confirm the viability of cores of this type. Regardless, this result establishes a meaningful basis for further work.

The physics performances of these SiC cores are actually very similar to those of the **Zr** clad reference case. Chapter 7 contains comparative plots to illustrate this similarity which will be discusses there in more detail. Here however, the physics behind the similarity warrant further discussion.

In the above 84 reload **Thick SiC** clad annular UO_2 cases reactivity was simply too high because of the significant alteration of the H/HM ratio and large loss of self-shielding. In the **Thick SiC RCF** clad cases hydrogen is removed concurrently with removal of fuel—resulting in an H/HM ratio similar to a conventionally fueled LWR. The annular region in the **Thick SiC RCF** clad cases constitutes a smaller fraction of the area inside the clad than in the **Thick SiC** clad cases—resulting in less loss of self-shielding than in the **Thick SiC RCF** clad annular UO_2 fueled cases.

The 84 reload **Thick SiC RCF** clad annular UO_2 cases exhibit the best physics performance of the **SiC** cores due to their similarity to the conventional **Zr** cases—in particular their ability to power a 469 EFPD cycle at 3587 MW_{th} using 5.0% or less.

Comparison of the 84 reload **Thick SiC RCF** clad annular UO_2 cores produced in this work to the 84 reload **Thin SiC** clad annular UO_2 case in previous work by Dobisesky is presented in Table 26. LRM has been used to match EFPD values across all designs.

Table 26: Comparison of 84 Reload Thick SiC RCF Annular UO_2 to Thin SiC of Previous Work

Obj Fcn	w/o	EFPD	B_c	B_d	BOR	$F_{\Delta h}$	F_q	PkExp	SDB	SDE
0.7	5.03	492	21.61	48.11	1571	1.469	1.754	79.5	-2275	-1433
1.0	5.00	492	21.61	47.90	1582	1.448	1.722	76.8	-2173	-1379
2.0	4.95	492	21.61	47.35	1665	1.549	1.862	72.0	-2038	-1414
Dobisesky	4.79	492	21.56	49.6	1509	1.50	1.76	74.7	-2784	-2203

The reactivity of the 84 reload **Thick SiC RCF** clad annular UO_2 cores is reduced by the lower H/HM ratio and thus requires a higher enrichment than the 84 reload **Thin SiC** clad annular UO_2 case of previous work.

5.5 Thick SiC Clad UO_2/BeO 84 Reload Cores

Figure 18 shows the peaking factors and soluble boron letdown curves of the 84 reload **Thick SiC** clad UO_2/BeO cases. The peaking factors are considerably higher for the case produced via OF 2.0.

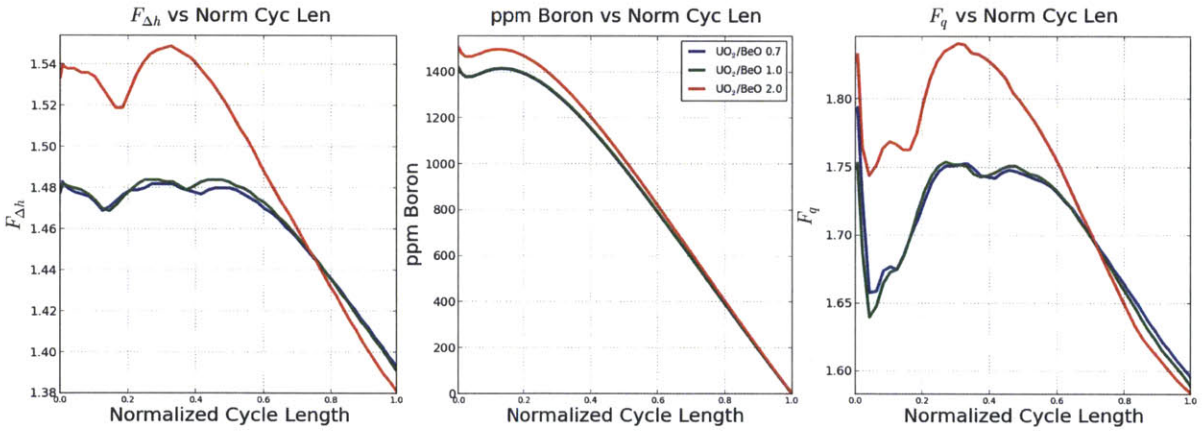

Figure 18: Thick SiC Clad UO_2/BeO 84 Reload Cores, Peaking Factors and Soluble Boron

Figure 19 shows reactivity coefficient results for the 84 reload **Thick SiC** clad UO_2/BeO cases.

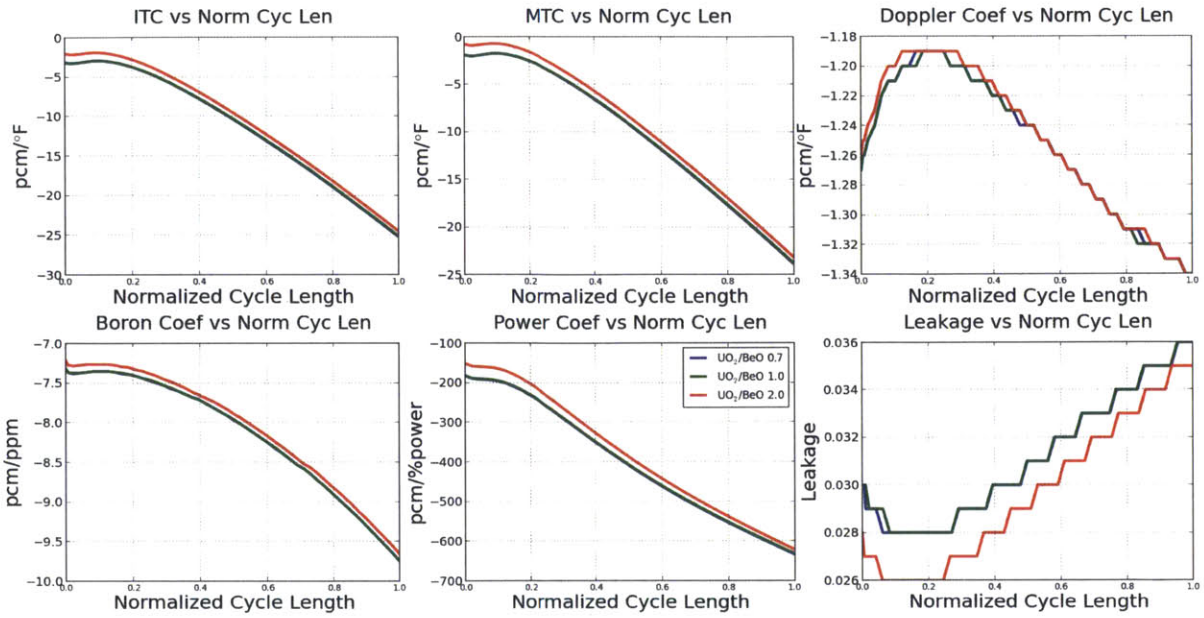

Figure 19: Thick SiC Clad UO_2/BeO 84 Reload Cores, Coefficient Calculations

Figure 20 shows the core reload maps utilized in the 84 reload **Thick SiC** clad UO_2/BeO cases.

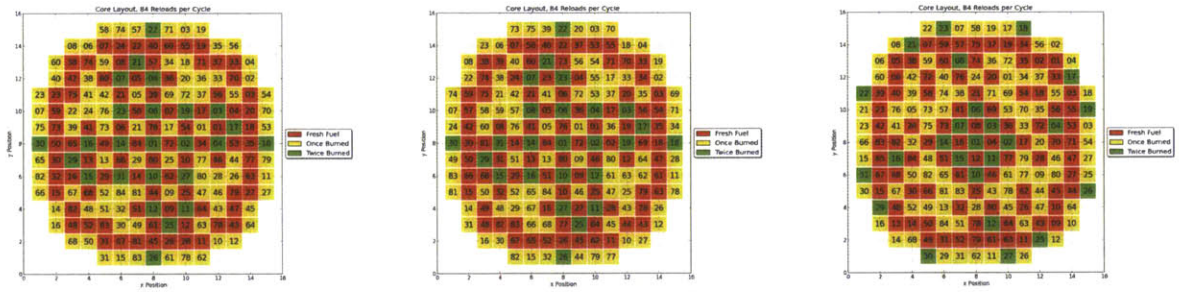

Figure 20: Thick SiC Clad UO_2/BeO 84 Reload Cores, Reload Maps. (Left - 0.7 / Center - 1.0 / Right - 2.0)

Table 27 summarizes core geometry, material densities, and mass for the 84 reload Thick SiC clad UO_2/BeO cases.

Table 27: Thick SiC Clad UO_2/BeO 84 Reload Geometry, Material Density, and Mass

R_{co}	R_{ci}	R_{fo}	R_{fi}	ρ_f	ρ_c	H/HM	m_{HM} (kg)
0.475	0.3861	0.3777	0	9.71	2.85	4.38	69380

Table 28 summarizes physics performance values for the 84 reload **Thick SiC** clad UO_2/BeO cases.

Table 28: Thick SiC Clad UO_2/BeO 84 Reload Physics Summary

Obj Fcn	w/o	EFPD	B_c	B_d	BOR	$F_{\Delta h}$	F_q	PkExp	SDB	SDE

0.7	5.32	465.9	24.09	54.53	1417	1.483	1.794	85.4	-2214	-2034
1.0	5.32	466.6	24.12	54.31	1419	1.484	1.754	87.5	-2242	-2020
2.0	5.32	475.0	24.56	53.62	1506	1.549	1.841	79.7	-2418	-2227

The initial loading of heavy metal in the 84 reload **Thick SiC** clad UO_2/BeO cores is greater than in the 84 reload **Thick SiC** clad annular UO_2 cores. Therefore the H/HM ratio is lower for the UO_2/BeO cores, which reduces reactivity.

In addition to this, the **Thick SiC** clad UO_2/BeO cores use solid fuel pellets, while the **Thick SiC** clad annular UO_2 cores use annular pellets. This results in an effectively reduced self-shielding effect per ^{238}U atom in the **Thick SiC** clad UO_2/BeO cores—but an overall increase in ^{238}U absorption that reduces the reactivity of the **Thick SiC** clad UO_2/BeO cores.

The combined effect of these reactivity reductions is that the **Thick SiC** clad UO_2/BeO cores are farther away from the over-moderation seen in the 84 reload **Thick SiC** clad annular UO_2 OF 2.0 core. To state it another way, the **Thick SiC** clad UO_2/BeO cores are essentially at a lower point on the moderation curve than the 84 reload **Thick SiC** clad annular UO_2 cores.

6 Results for Thorium Hosted Plutonium

6.1 Thick SiC Clad PuO_2/ThO_2 84 Reload Cores

Figure 21 shows the peaking factors and soluble boron letdown curves of the 84 reload **Thick SiC** clad PuO_2/ThO_2 cases. The peaking factors are considerably higher for the case produced via OF 2.0.

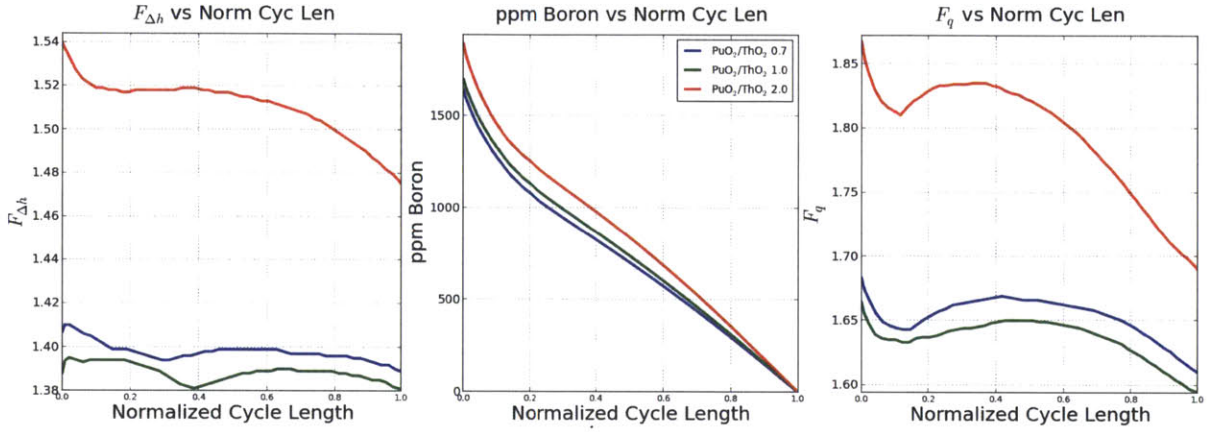

Figure 21: Thick SiC Clad PuO_2/ThO_2 84 Reload Cores, Peaking Factors and Soluble Boron

Figure 22 shows reactivity coefficient results for the 84 reload **Thick SiC** clad PuO_2/ThO_2 cases.

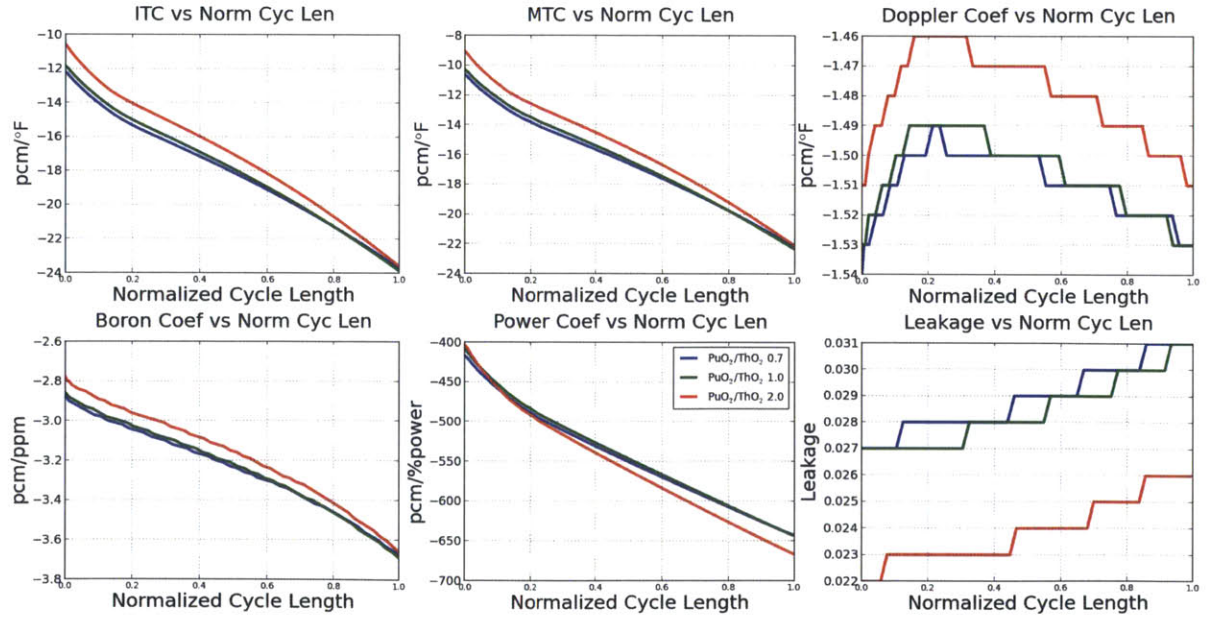

Figure 22: Thick SiC Clad PuO_2/ThO_2 84 Reload Cores, Coefficient Calculations

Figure 23 shows the core reload maps utilized in the 84 reload **Thick SiC** clad PuO_2/ThO_2 cases.

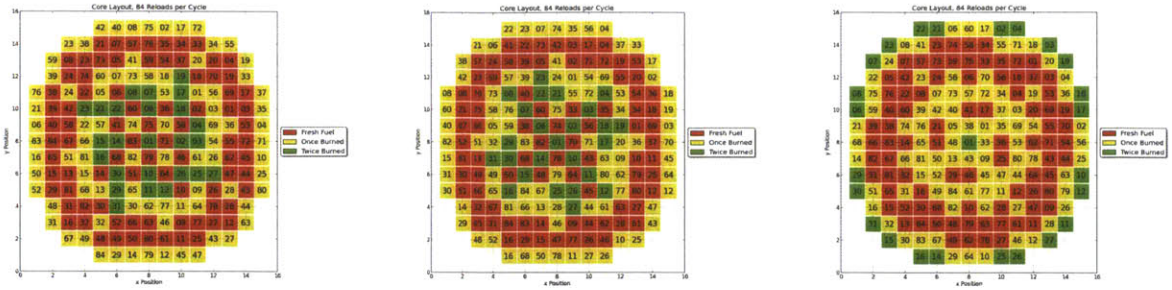

Figure 23: Thick SiC Clad PuO_2/ThO_2 84 Reload Cores, Reload Maps. (Left - 0.7 / Center - 1.0 / Right - 2.0)

Table 29 summarizes core geometry, material densities, and mass for the 84 reload Thick SiC clad PuO_2/ThO_2 cases.

Table 29: Thick SiC Clad PuO_2/ThO_2 84 Reload Geometry, Material Density, and Mass

R_{co}	R_{ci}	R_{fo}	R_{fi}	ρ_f	ρ_c	H/HM	m_{HM} (kg)
0.475	0.3861	0.3777	0	9.35	2.85	4.34	68662

Table 30 summarizes physics performance values for the 84 reload **Thick SiC** clad PuO_2/ThO_2 cases.

Table 30: Thick SiC Clad PuO_2/ThO_2 84 Reload Physics Summary

Obj Fcn	w/o	EFPD	B_c	B_d	BOR	$F_{\Delta h}$	F_q	PkExp	SDB	SDE
0.7	12.04	458.0	23.93	54.08	1640	1.410	1.683	101.8	-779	-209
1.0	12.04	471.4	24.63	53.89	1697	1.395	1.664	102.2	-781	-235
2.0	12.04	492.6	25.73	57.69	1890	1.539	1.867	97.9	-614	43

The 84 reload **Thick SiC** clad PuO_2/ThO_2 cases exhibit the greatest variation in cycle length from the application of different OFs. The reactivity differences between fresh and burned assemblies are less here than in any other fuel and clad combination presented herein.

The soluble boron worth is very low in these cases, and the shutdown margins are unacceptable—indicating low control rod worth. The shutdown margin is positive for optimization via OF 2.0. The highly negative MTC, combined with the notably low soluble boron worth suggests extreme under-moderation indicative of a neutron spectrum harder than typical LWR spectra.

Despite the high fast to thermal neutron flux ratio and low soluble boron worth, these cores probably do not present an increased fast fluence hazard to the RPV. Since the core nominal power is fixed in all cases presented herein, the fission rates of each case are roughly the

same (to first order, fission energy is the same for all fissioning isotopes present in this work). Given nearly identical fission rates and moderator fractions between PuO_2/ThO_2 and other **Thick SiC** clad fuel cases, there is no reason for fast flux leakage to be significantly altered. The differences in the ^{238}U and ^{232}Th fast neutron capture cross sections are relatively minor, with slightly higher fast neutron absorption exhibited by ^{232}Th. Thus, it is reasonable to conclude that RPV fast fluence is not significantly altered—and if it is altered it is likely reduced.

The 300K fission and neutron capture cross sections for ^{238}U and ^{232}Th are shown below in Figure 24. The green and red lines are ^{238}U capture and fission, respectively. The purple and blue lines are ^{232}Th capture and fission, respectively.

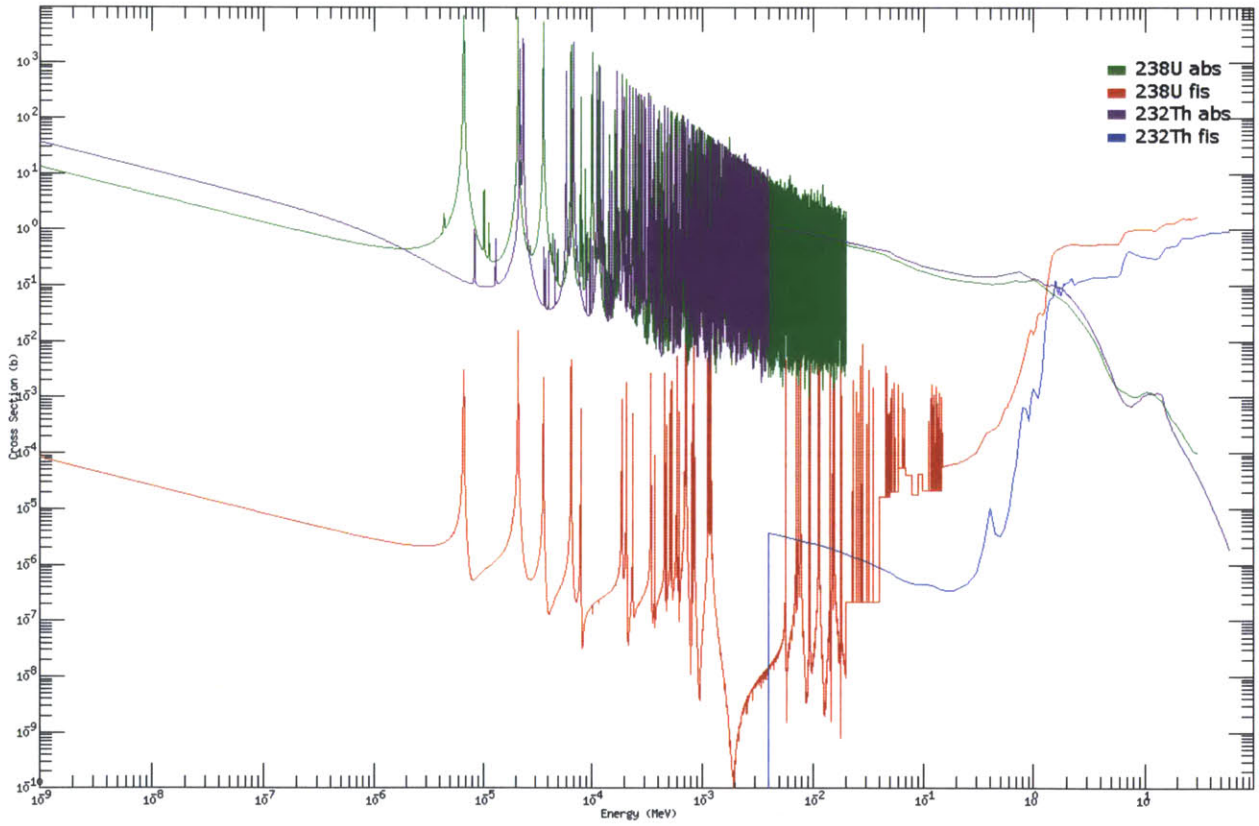

Figure 24: ^{238}U and ^{232}Th Fission and Capture Cross Sections [17]

6.2 Plutonium Content as a Function of Burnup

CASMO depletion modeling has been conducted for the above fuel and clad combination for a series of conditions defined in terms of Pu wt% of IHM. There are 11 cases, and in each case the CASMO 2D depletion is conducted at the power density specified in Section 2.8.

These plots predict the quantity of plutonium in an assembly at a given burnup. For example, given a specific Pu loading in terms of wt% IHM, the plot can be used to determine the Pu content (as wt% of IHM) at 60 MWd/kg. The difference between the initial and discharge plutonium content is the quantity of plutonium that has been consumed.

Figure 25 below shows the total and fissile plutonium content and k_∞ as a function of burnup for 11 cases relevant to this work. Each separate case is defined by its initial quantity of plutonium as read at the 0 MWd/kg intercepts.

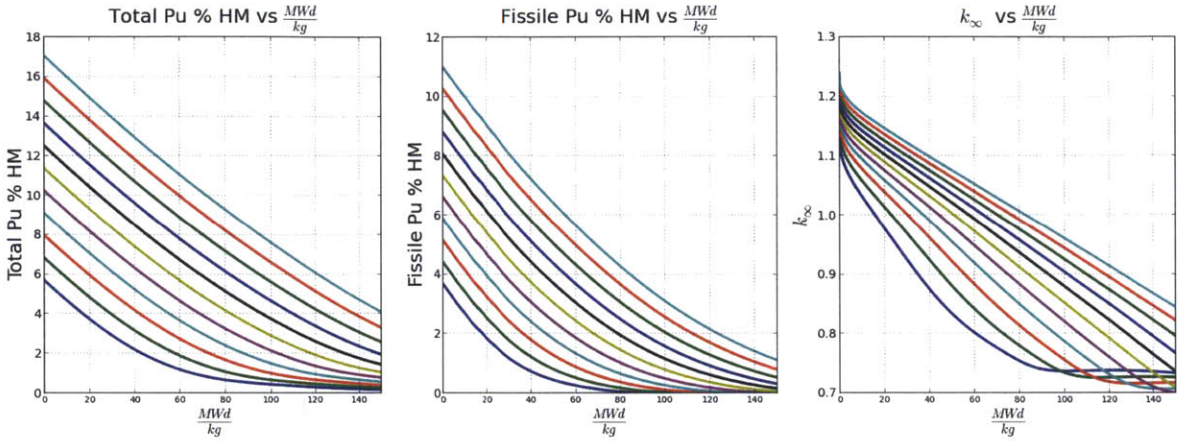

Figure 25: Pu Content and k_∞ as a Function of Burnup For Different Pu wt% IHM

Using the total Pu 12.5 wt% IHM (black) line in the above figure it can be estimated that at 60 MWd/kg the total Pu wt% will be 6.7 wt% of initial heavy metal. The fissile Pu wt% at the same burnup will be 3.5 wt%. This indicates that to a first approximation the PuO_2/ThO_2 cores designed above burn roughly 46% of total Pu and 57% of fissile Pu.

While more precise calculations derived from full-core modeling produce more specific results, the above plot serves as a general guide to plutonium consumption with depletion for assemblies of this type. A similar set of curves can be generated for any assembly type corresponding to different material, geometry, temperature, and power density conditions.

For example, if one were to decide that one wished to reduce fissile plutonium by 75%, these plots will tell you how much burnup is required for a given initial loading—or vice versa. If a 40 MWd/kg exposure was desired, then using this plutonium vector, fissile Pu at EOL will be 75% of Beginning of Life (BOL) fissile Pu for an initial fissile Pu wt% IHM of ~3.8%. Conversely, if it was desirable to consume 75% of fissile Pu when the initial fissile Pu wt% IHM was ~10%, the EOL burnup required is ~100 MWd/kg.

7 Results Reviewed Via OF

7.1 Geometry, Material Density, and Mass Summary for All Cores

The performance of annular UO_2 pellets and BeO enhanced UO_2 pellets in thick SiC cladding have been analyzed. Also, the burning of Pu in ThO_2 with thick SiC cladding has been analyzed. Table 31 summarizes the geometry, material densities, and heavy metal mass for all cores analyzed.

Table 31: Geometry, Material Density, and Mass Summary, All Cores

Fuel/Clad/Reloads	R_{co}	R_{ci}	R_{fo}	R_{fi}	ρ_f	ρ_c	H/HM	m_{HM} (kg)
Zr UO_2, 84	0.475	0.418	0.4096	0	10.47	6.55	3.35	90661
ThkSiC Ann. UO_2, 64	0.475	0.3861	0.3777	0.129	10.47	2.85	4.47	68094
ThkSiC Ann. UO_2, 84	0.475	0.3861	0.3777	0.129	10.47	2.85	4.47	68096
ThkSiC2 Ann. UO_2, 84	0.5069	0.418	0.4096	0.129	10.47	2.85	3.31	81668
ThkSiC UO_2/BeO, 84	0.475	0.3861	0.3777	0	9.71	2.85	4.38	69380
ThkSiC PuO_2/ThO_2, 84	0.475	0.3861	0.3777	0	9.35	2.85	4.34	68662

7.2 OF 0.7, All Fuel/Clad Combinations

All cores had the same total power (3587 MW_{th}). The core physics performance was optimized under constraints for peaking factors, boron concentration, MTC, peak pin burnup, and shutdown margin. Three OFs were considered for the optimization: OF 0.7, OF 1.0, and OF 2.0. Figure 26 shows the peaking factors and soluble boron letdown curves of all cases optimized using OF 0.7.

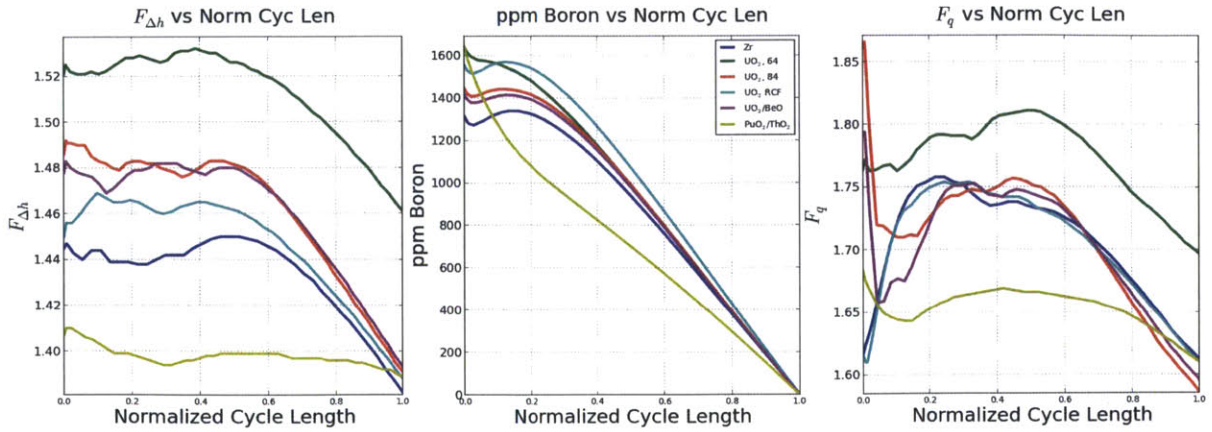

Figure 26: OF 0.7, Peaking Factors and Soluble Boron, All Cores

Figure 27 shows reactivity coefficient results for all cases optimized using OF 0.7.

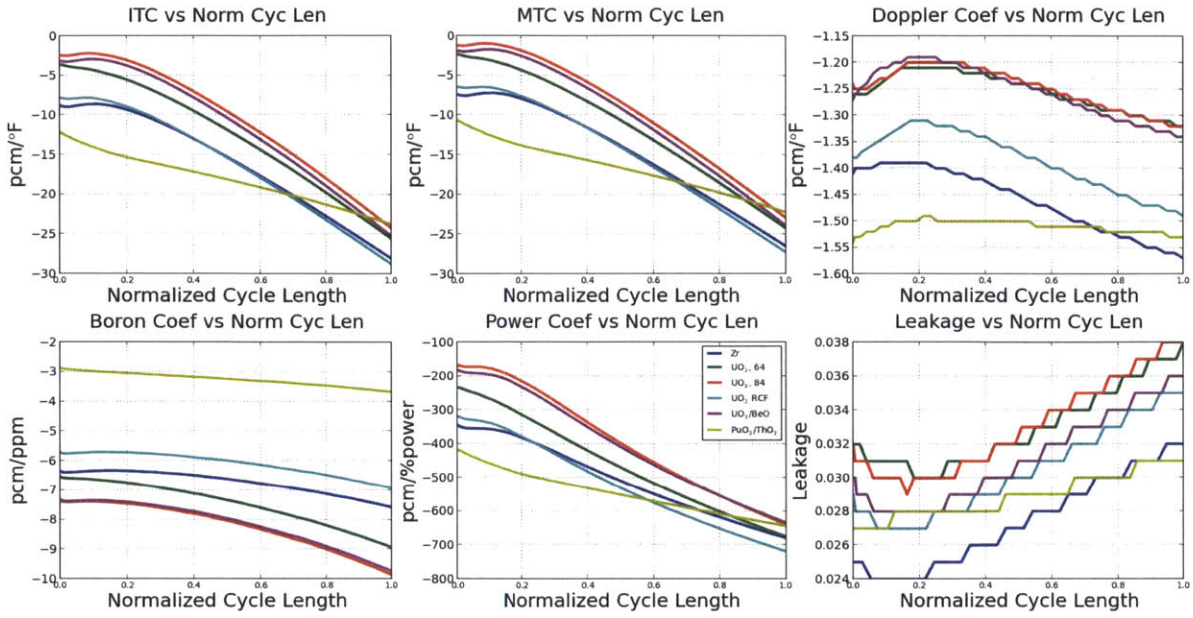

Figure 27: OF 0.7, Coefficient Calculations, All Cores

Table 32 summarizes physics performance values for all cases optimized using OF 0.7.

Table 32: OF 0.7, Physics Summary, All Cores

Fuel/Clad/Rlds	w/o	EFPD	B_c	B_d	BOR	$F_{\Delta h}$	F_q	PkExp	SDB	SDE
Zr U 64	4.29	466.5	18.46	42.78	1340	1.450	1.758	71.6	-2090	-1610
TkSiC U 64	6.59	466.3	24.57	74.06	1641	1.532	1.811	102.6	-2897	-2458
TkSiC U 84	5.43	466.3	24.56	55.65	1444	1.492	1.866	90.9	-2637	-2434
TkSiC2 U 84	4.80	465.8	20.46	45.55	1571	1.469	1.754	79.5	-2275	-1433
TkSiC UBe 84	5.32	465.9	24.09	54.53	1417	1.483	1.794	85.4	-2214	-2034
TkSiC PuTh 84	12.04	458.0	23.93	54.08	1640	1.410	1.683	101.8	-779	-209

The cores optimized using OF 0.7 were the first set of cores constructed. Their optimization was conducted before the final update of the SIMULATE temperature correlation inputs, resulting in a slight degradation of their performance. Nevertheless, this set of cores provides an example of optimization according to peaking factors alone.

Compared to the other sets of cores optimized according to the other OFs, this set has the lowest cycle lengths and some very significant BOC peaks in F_q.

The **Zr** and **Thick SiC RCF** cases meet cycle length requirements using no more than 5.0% enrichment. They have very similar characteristics: their peaking, ITC, MTC, and power coefficient plots all track together. They also have the lowest peaking of the UO_2 fueled cores (including UO_2/BeO).

Similarly, the **Thick SiC** UO_2 and UO_2/BeO cores' peaking, ITC, MTC, boron coefficient, power coefficient, and Doppler coefficient track together.

The cycle length of the OF 0.7 cores are the lowest in comparison to the cycle lengths achieved via the other OFs. Also, the OF 0.7 cores have the highest values of peak pin burnup for each fuel and cladding combination.

7.3 OF 1.0, All Fuel/Clad Combinations

Figure 28 shows the peaking factors and soluble boron letdown curves of all cases optimized using OF 1.0.

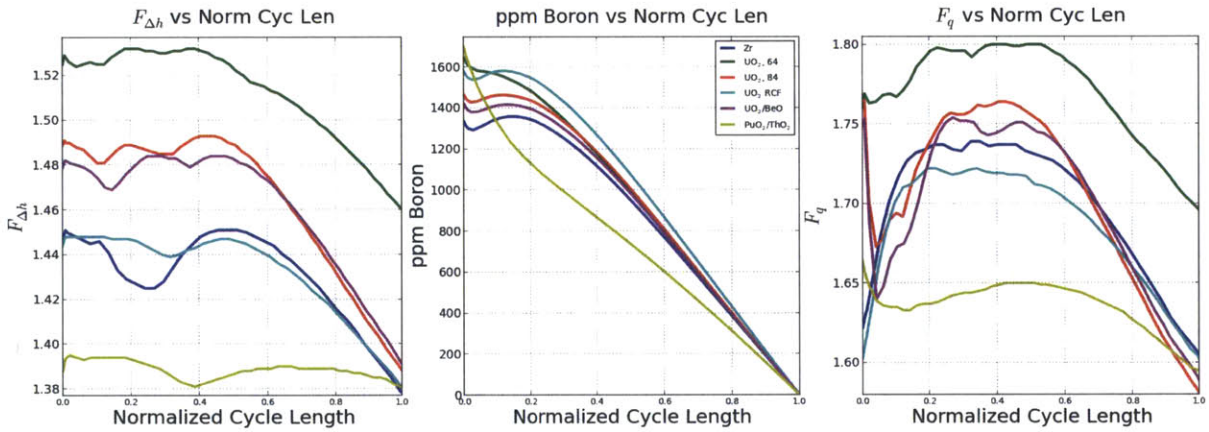

Figure 28: OF 1.0, Peaking Factors and Soluble Boron, All Cores

Figure 29 shows reactivity coefficient results for all cases optimized using OF 1.0.

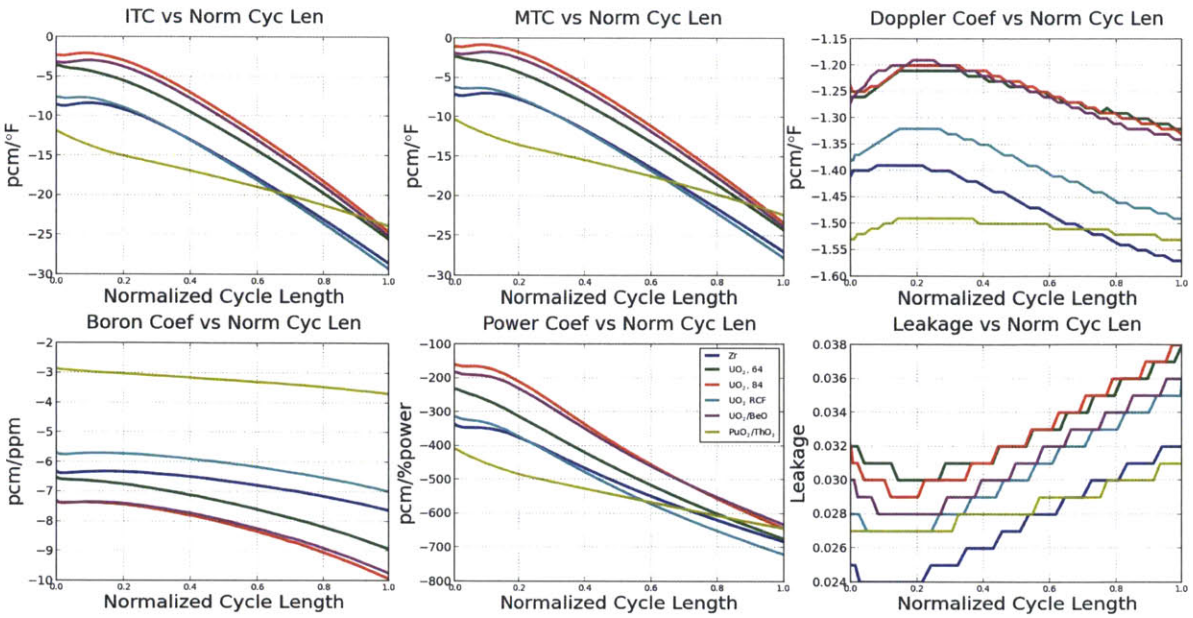

Figure 29: OF 1.0, Coefficient Calculations, All Cores

Table 33 summarizes physics performance values for all cases optimized using OF 1.0.

Table 33: OF 1.0, Physics Summary, All Cores

Fuel/Clad/Rlds	w/o	EFPD	B_c	B_d	BOR	$F_{\Delta h}$	F_q	PkExp	SDB	SDE
Zr U 64	4.29	470.8	18.63	42.21	1358	1.451	1.739	71.1	-2074	-1601
TkSiC U 64	6.59	466.5	24.57	74.07	1643	1.532	1.800	101.8	-2900	-2458
TkSiC U 84	5.43	469.3	24.72	55.35	1464	1.493	1.765	88.7	-2711	-2416
TkSiC2 U 84	4.80	468.7	20.59	45.64	1582	1.448	1.722	76.8	-2173	-1379
TkSiC UBe 84	5.32	466.6	24.12	54.31	1419	1.484	1.754	87.5	-2242	-2020
TkSiC PuTh 84	12.04	471.4	24.63	53.89	1697	1.395	1.664	102.2	-781	-235

OF 1.0 was effective in extending cycle length while simultaneously lowering peaking factors, and managed to balance BOC F_q peaks with intra-cycle F_q peaks.

The optimization algorithm would frequently extend cycle length in small increments and then make large jumps when a map with a lower product of $F_{\Delta h}$ and F_q was found. These large jumps often coincided with a shortening of cycle length. Then at the new peaking values the algorithm would again extend cycle length, often beyond the previous level.

OF 1.0 was also more active in accepting new maps than OF 0.7. The higher frequency of accepting new maps appeared to allow OF 1.0 to optimize core reload maps more quickly than OF 0.7.

The **Zr** and **Thick SiC RCF** cores again displayed similar performance. This was also true of the **Thick SiC** UO_2 and UO_2/BeO cores' performance.

Optimization via OF 1.0 increased cycle length for all fuel and clad combinations. The OF 1.1 presented in Section 4.4.2 exhibited behavior similar to OF 1.0, however optimization results from OF 1.1 are left to be included as an addendum or for future work.

7.4 OF 2.0, All Fuel/Clad Combinations

Figure 30 shows the peaking factors and soluble boron letdown curves of all cases optimized using OF 2.0.

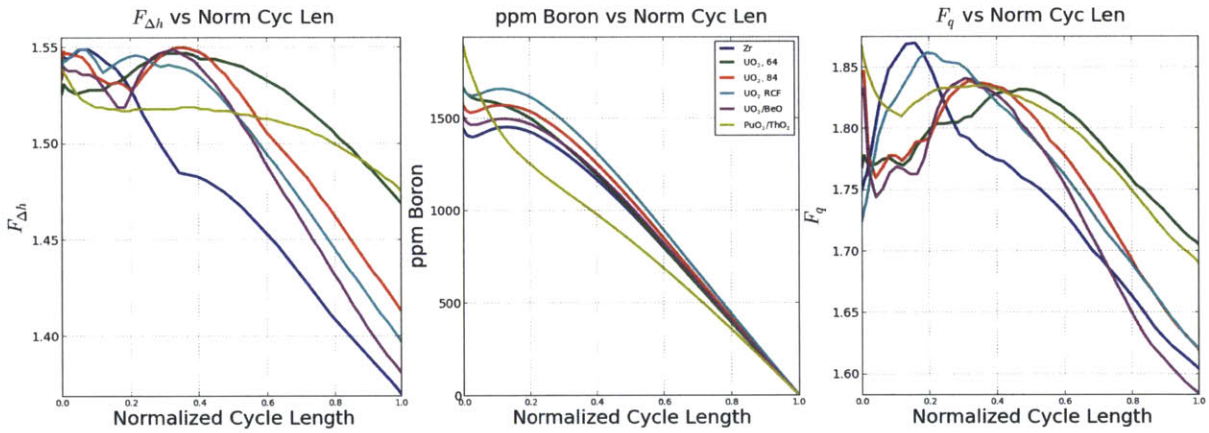

Figure 30: OF 2.0, Peaking Factors and Soluble Boron, All Cores

Figure 31 shows reactivity coefficient results for all cases optimized using OF 2.0.

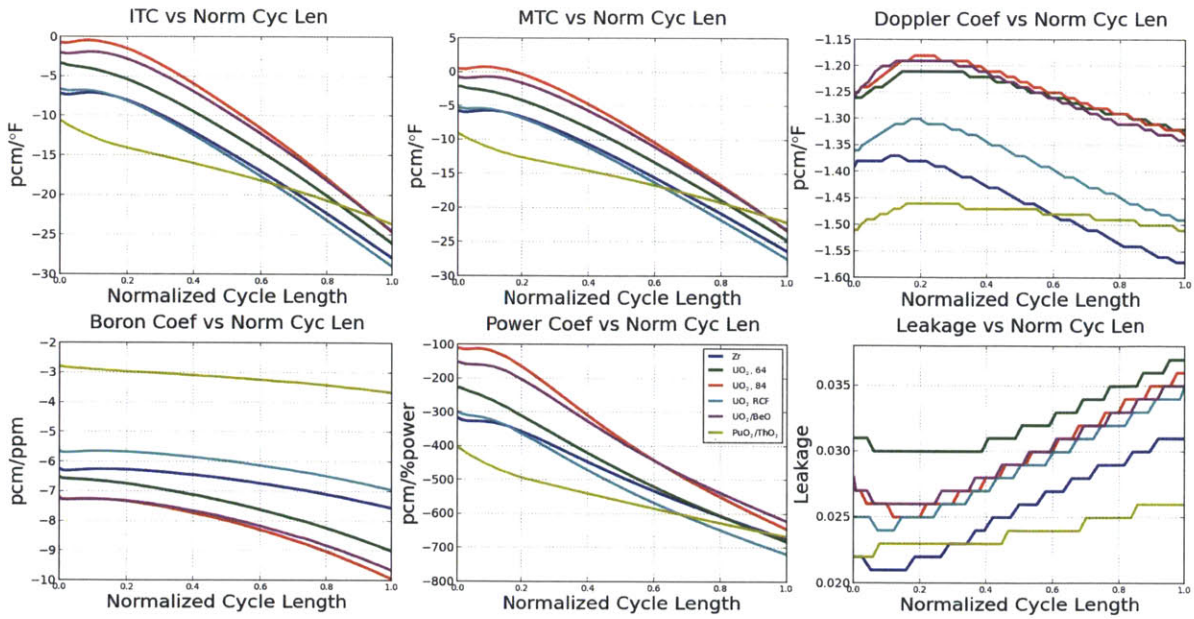

Figure 31: OF 2.0, Coefficient Calculations, All Cores

Table 34 summarizes physics performance values for all cases optimized using OF 2.0.

Table 34: OF 2.0, Physics Summary, All Cores

Fuel/Clad/Rlds	w/o	EFPD	B_c	B_d	BOR	$F_{\Delta h}$	F_q	PkExp	SDB	SDE
Zr U 64	4.29	481.3	19.04	41.68	1454	1.549	1.870	67.5	-2055	-1645
TkSiC U 64	6.59	468.0	24.65	74.20	1664	1.547	1.832	98.7	-2895	-2449
TkSiC U 84	5.43	476.7	25.11	54.69	1573	1.550	1.847	80.6	-2713	-2575
TkSiC2 U 84	4.80	474.3	20.83	45.64	1665	1.549	1.862	72.0	-2038	-1414
TkSiC UBe 84	5.32	475.0	24.56	53.62	1506	1.549	1.841	79.7	-2418	-2227
TkSiC PuTh 84	12.04	492.6	25.73	57.69	1890	1.539	1.867	97.9	-614	43

Optimization using OF 2.0 demonstrates the competitive relationship between cycle length and peaking factors. In each case, cycle length was extended beyond the values achieved by either of the other two OFs—and at the same time peaking factors were not given any weight in determining a map's value. Only cycle length was considered for any map whose peaking factors were below the limits outlined in Section 2.12.1, and the peaking factors rose to very near those limits in all cases. Leakage dropped in all cases.

The **Zr** and **Thick SiC RCF** cores again displayed similar performance, as in the cases of optimization via OF 0.7 and OF 1.0. This was also again true of the **Thick SiC** UO_2 and UO_2/BeO cores' performance.

8 Remarks on Uncertainties

8.1 Uncertainty in CASMO/SIMULATE

Validity of the core simulation codes is well established for PWRs using the current fuel materials and geometry. Predictions of PWR reactor physics made by CASMO-4 and SIMULATE-3 have been compared to measurements obtained *in situ* from operating large scale reactors. Predictions by CASMO-4 and SIMULATE-3 have been validated for: assembly power, soluble boron letdown, control rod worth, ITC, peak pin exposure, and other parameters. Results have been shown to be accurate and with low uncertainties. [18] As an industry standard tool, it has been used by utilities to perform their own Fuel Management analyses to support licensing with the NRC. It is also noted that while MIT does not have access to the most up-to-date versions of CASMO/SIMULATE, the deficiencies in the versions used in this work are expected to cancel out when comparing various designs to each other.

8.2 Depletion of Be in UO_2/BeO Fuel

CASMO-4E does not deplete beryllium present in fuel. Therefore, since beryllium does deplete via various mechanisms, it is reasonable to ask to what extent does beryllium deplete and what reactivity effect does this depletion have?

Depletion of Be was modeled in SERPENT; the depletion of Be at 60 MWd/kg in 5.5% ^{235}U enriched fuel was negligible as the difference between the SERPENT predicted eigenvalue vs. CASMO0-4E remained constant over the fuel burnup [K. Shirvan, private communication, 2013]. This validates the CASMO-4E calculations with constant presence of BeO in the UO_2/BeO fuel over the interval of interest to this work.

8.3 Plutonium and Thorium Cross Sections in ENDF-VI

There are inaccuracies associated with the ENDF-VI cross section library that is used by CASMO-4E to generate the two group cross sections used by SIMULATE in the evaluation of core physics performance.

Comparison of ENDF-VI based CASMO results with ENDF-VII based SERPENT results for PuO_2/ThO_2 cases was performed and found to be within 300 pcm [K. Shirvan, private communication, 2013].

8.4 Annularization of Fuel

Figure 32 shows CASMO 2D, assembly-level depletion simulation results for a series of fuel geometries and compositions where the initial loading of ^{235}U per fuel rod is fixed. The annular plenum radius is therefore determined as a function of enrichment or vice-versa—as more ^{238}U is removed there is less fuel volume and the fuel that remains exists as an annular fuel pellet.

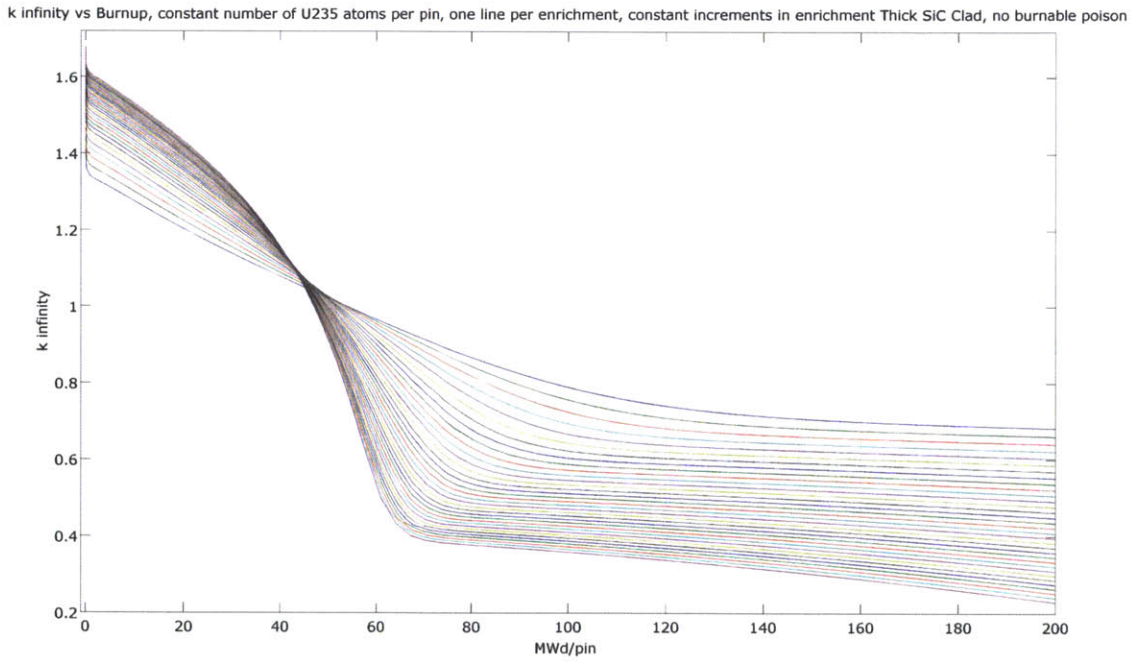

Figure 32: Effect of Increasing Annularization With Constant ^{235}U Content

It is observed via this sensitivity study that the annularization of fuel increases the slope of the reactivity curve as a function of energy released per fuel rod (or equivalently burnup per unit mass if initial ^{235}U loading, since that is the same for all cases). The smoothest curve will be that of the solid pellet, and it is reasonably expected that this will be true for all fuels.

Neutron capture in ^{238}U is when the fuel is annularized. Absorption per ^{238}U atom is increased, which competes with the effect of reduced ^{238}U content. Overall reduced rates of neutron capture in ^{238}U result in significantly higher initial reactivity and less breeding of new

fissile material throughout the cycle. These effects are the primary causes of the steepening of the reactivity curves with increasing annularization.

Steeper reactivity curves complicate core design and necessarily imply higher peaking factors, $F_{\Delta h}$ and F_q. This elevation of peaking reduces the dynamic range of performance available to core designers.

8.5 Homogeneous Fissile Oxide/BeO Mixtures

The primary motivation to add BeO to nuclear reactor fuel is to reduce the average and peak fuel temperatures. This addition also slightly improves neutron moderation and neutron multiplication in the fuel. BeO presence in the fuel introduces the following nuclear reaction:

$$^{9}_{4}\mathrm{Be}+\mathrm{n}\rightarrow 2\left(^{4}_{2}\mathrm{He}\right)+2\mathrm{n}$$

However, this reduction in fuel temperature does not come without a cost. The additional helium production, increases EOL plenum pressure and partially offsets the reduced fission gas release due to the lower fuel temperature.

Further, thermal conductivity data for UO_2/BeO is not as plentiful as for UO_2. It is certainly possible that thermal conductivity of UO_2/BeO is sensitive to manufacturing processes and burnup in ways that are not currently understood or accurately modeled. Therefore, the fuel temperature correlation used in this work may require revision and thus obscure the true performance of homogeneous UO_2/BeO mixtures.

9 Conclusion and Future Work

9.1 Conclusion

The core design and modeling work presented herein demonstrates the neutronic feasibility of annular UO_2 and UO_2/BeO fuels clad in **Thick SIC** and annular UO_2 clad in **Thick SiC RCF**. The most notable observation in this work is that the **Thick SiC RCF** cases allow for fuel enrichment of not more than 5.0%.

The **Zr** and **Thick SIC RCF** cases are very similar in the time evolution of their performance, enrichment utilization of 5.0% or less, and low peak pin burnup values.

The **Thick SiC** annular UO_2 and UO_2/BeO cases are also very similar in the time evolution of their performance. The differences in their performance is readily accounted for by the additional initial heavy metal mass of the UO_2/BeO cases.

The OF 2.0 84 assembly reload **Thick SIC** clad annular UO_2 core has a positive MTC early in life which may be overcome via the use of additional burnable poison.

The PuO_2/ThO_2 cores all have unacceptable shutdown margins, including a positive shutdown margin at EOC for the OF 2.0 **Thick SiC** clad PuO_2/ThO_2 core. Increasing control rod worth may improve the shutdown margins of the PuO_2/ThO_2 cores.

Previous work by Dobisesky shows that **Thin SiC** requires less enrichment than **Thick SiC** to achieve 492 EFPD at 3587 MW_{th}. However, the methodology developed herein may further reduce the enrichment requirements of the **Thin SiC** cases.

9.2 Recommendations for Future Work

While significant effort has been invested in the development of CSpy and the results presented in this thesis, there remains considerable additional work to be done in order to reveal a more complete picture of the potential of Thick SiC Clad fuels in a PWR environment.

9.2.1 Core Power Uprates or Longer Fuel Cycle

Increasing the core power represents a significant gain the electrical power production capacity of a nuclear power plant. Extending the fuel cycle length also increases the plant capacity factor and could lead to cheaper fuel cycle cost. Detailed core physics models of uprated or extended

cycle scenarios may provide impetus for further consideration of plant power uprates. These may involve other plant modifications which affect the lifetime average capital costs, including earlier steam generator replacement or modification, potential reduction in reactor pressure vessel life, increased rates of corrosion in piping due to off-design temperatures of operation, turbine replacement(s), pumping upgrades and other modifications requiring sophisticated engineering analyses.

9.2.2 Variation of Burnable Poison Rod Number

Variation of the number of burnable poison rods per assembly is a key feature of a truly general core physics optimization code and study. In this thesis this parameter was fixed in order to simplify the optimization search space and to simplify coding of CSpy, however expansion of CSpy to include this capability is essential to its development as a general code for optimization of PWR core physics.

In particular, three cores presented in this work may benefit from fewer burnable poison rods used in their assemblies: both 84 and 64 reload number **Thick SiC** clad annular UO_2 cores, and the **Thick SiC** clad UO_2/BeO 84 reload cores. All three cases have OF 0.7 results where BOC F_q values are in excess of a subsequent local F_q maximum at higher burnup. This indicates presence of excessive burnable poison. Correcting this should bring the OF 0.7 cycle peak F_q for all three of the above mentioned cases in line with the **Zr** clad reference cores—however the soluble boron required to hold down reactivity throughout the cycle will rise as less IFBA is used.

9.2.3 Split Enrichment Feed

The work presented in this thesis relies heavily on optimization schema to produce core designs utilizing loading only a single assembly type at each reload. However, it may be possible to achieve superior core physics performance and fuel economy by loading more than one type of assembly at each reload.

The design process would then be expanded to include the number of assembly types, and then the clad type, fuel type, enrichment, burnable poison type, and number of burnable poison rods for each assembly type to be loaded.

The first relevant case expanding upon the work of this thesis would be to develop a two-assembly **Zr** clad UO_2 reference core. Initial inquiry should start with 20 assemblies of higher enrichment than the bulk, leaving all other parameters equal.

9.2.4 Twice Burned Fuel on the Periphery

By loading twice burned fuel on the periphery of a given core, it may be possible to extend cycle length and reduce leakage. Optimization via OF 2.0 resulted in placement of more twice burned fuel on the core periphery than via the other OFs, however a heuristic requirement may another way to investigate core design and physics performance using twice burned fuel on the periphery.

Heuristic implementation requires that most twice burned fuel assemblies occupy peripheral assembly locations in the case of 84 reloads per cycle, or that most peripheral assembly locations be occupied by twice burned fuel in the case of 64 reloads per cycle.

9.2.5 Extraction of Pin Power Profiles

Axial power profiles for peak power and peak burnup fuel rods are required inputs to fuel performance codes, which currently rely on conservative assumptions that may prove too limiting in the analysis of the viability of Thick SiC clad fuels. Detailed axial power shapes as functions of burnup for all rods that are the peak power rod for any given time step during the first cycle would be valuable data for realistic simulation of fuel performance. Alternatively, one could also use peak power assemblies of each batch to construct power profiles for fuel performance simulations.

9.2.6 Further Development and Utilization of Optimization Schema

Speculation as to which OF is most appropriate for a given situation is a topic that receives much attention and is debated by experienced professionals. The true test of an OF is its efficacy in producing the desired results. As such, further investigation into optimization schema will include further development of and experimentation with new OFs.

It may also be beneficial to expand CSpy to include a Genetic Algorithm and/or a Simulated Annealing Algorithm to provide additional means by which to permute assembly burnable poison layouts and core reload map configurations.

9.2.7 Fuel Performance Oriented Optimization

I envision an iterative process in which FRAPCON fuel performance limits can be used as optimization criteria for SIMULATE core reload map optimization. When a new core reload map is found via SIMULATE optimization, the new core's peak pin power history is to be automatically extracted and input into a new FRAPCON simulation. This new FRAPCON simulation defines new fuel performance limitations which can then be used to update the optimization criteria for SIMULATE core reload map optimization.

This iterative process may find an integrated balance between fuel performance and neutronics that is superior to conventional methodologies today.

9.2.8 Definition of Outer Axial Blanket Composition as a Function of Main Length Composition

Outer axial blankets affect both core neutron leakage and axial power shape. Higher outer blanket enrichment is associated with higher leakage, and lower outer blanket enrichment is associated with greater heterogeneity of the axial power shape. Future work may consider specifying outer axial blanket enrichment as a fraction of the enrichment of the main heated length.

9.2.9 Variation of Reload Assembly Number

One additional means to reduce enrichment requirements is to use more reload assemblies. For cores using enrichments above 5.0%, it may prove valuable to find the number of reload assemblies required to keep the maximum enrichment used to no more than 5.0%. This information may better guide industry consideration of new fuels and claddings.

9.2.10 Improving the Thick SiC Clad PuO_2/ThO_2 Shutdown Margin

Shutdown margin must be improved significantly before cores using **Thick SiC** clad PuO_2/ThO_2 can be considered viable. Alternate control rod materials, increasing coolant fraction at the expense of fuel fraction, or other means may be investigated to improve the shutdown margin of **Thick SiC** clad PuO_2/ThO_2 cores.

9.2.11 Thermal Hydraulic Safety Analysis

The thermal hydraulic safety analysis must be performed for all cases presented herein. DNB margins, fretting wear, sliding wear, pressure drop, and other parameters must be modeled in anticipated and unanticipated transient scenarios.

References

[1] Kessler, G., and K. Wirtz. "From the Discovery of Nuclear-Fission to Present-Day Reactor Technology." *Atomwirtschaft-Atomtechnik* 37.12 (1992): 582-89. Print.

[2] Buchan, A. G., et al. "Simulated Transient Dynamics and Heat Transfer Characteristics of the Water Boiler Nuclear Reactor - Supo - with Cooling Coil Heat Extraction." *Annals of Nuclear Energy* 48 (2012): 68-83. Print.

[3] Aoki, M., and G. Rothwell. "A Comparative Institutional Analysis of the Fukushima Nuclear Disaster: Lessons and Policy Implications." *Energy Policy* 53 (2013): 240-47. Print.

[4] D.M. Carpenter; G. Kohse; M.S. Kazimi, "An Assessment of Silicon Carbide as a Cladding Material for Light Water Reactors," MIT-ANP-TR-132, 2010

[5] M.S. Kazimi, and N.E. Todreas, "Nuclear Systems Volume 1: Thermal Hydraulic Fundamentals," 2nd Edition, Francis and Taylor, 2012

[6] J. Dobisesky, E. Pilat and M.S. Kazimi, "Reactor Physics Considerations For Implementing Silicon Carbide Cladding Into A PWR Environment," MIT-ANP-TR-136, CANES, 2011

[7] L. L. Snead, T. Nozawa, Y. Katoh, T. Byun, S. Kondo, D.A. Petti, "Handbook of SiC Properties for Fuel Performance Modeling," Journal of Nuclear Materials 371 p. 329-377, 2007

[8] M. Rohde, "Reduction of the thermal conductivity of SIC by radiation damage," Journal of Nuclear Materials 182 (1991) 87-92

[9] P. Fenici a, A.J. Frias Rebelo a,*, R.H. Jones b, A. Kohyama c, L.L. Snead d, "Current status of SiC/SiC composites R&D," Journal of Nuclear Materials 258±263 (1998) 215±225

[10] http://www.nrc.gov/reactors/operating/licensing/power-uprates/pwr-stretch/seabrook-pu.html, retreived 3/17/2013

[11] M. Driscoll, T. Downar, and E. Pilat, "The Linear Reactivity Model for Nuclear Fuel Management," ANS, 1990

[12] NRC, "Standard Review Plan for the Review of Safety Analysis Reports for Nuclear Power Plants: LWR Edition (NUREG 0800), Chapter 4.2, 2007

[13] PWR Axial Offset Anomaly (AOA) Guidelines, Revision 1. EPRI, Final Report, June 2004.

[14] F.A. Garner, "Radiation Damage in Austenitic Steels," Comprehensive Nuclear Materials, 2012

[15] D.E. Goldberg, "Genetic Algorithms in Search, Optimization, and Machine Learning," Addison Wesley, 1989

[16] D.J. Kropaczek, P.J. Turinsky, "In-Core Nuclear Fuel Management Optimization for Pressurized Water Reactors Utilizing Simulated Annealing," Nuclear Technology, Vol. 95, 1991

[17] http://atom.kaeri.re.kr/cgi-bin/endfplot.plasdf, retrieved 4/4/2013

[18] H. Lin, S. Yaur, T. Lin, W. Kuo, J. Shiue, Y. Huang, "Qualification of the Taiwan Power Company's pressurized water reactor physics methods using CASMO-4/SIMULATE-3," Nuclear Engineering and Design 253 (2012) 71–76

[19] http://www.nrc.gov/reading-rm/doc-collections/fact-sheets/3mile-isle.html retrieved 4/27/13 10:58 PM

[20] C.R.F. Azevedo, "Selection of fuel cladding material for nuclear fission reactors," Engineering Failure Analysis 18 (2011) 1943–1962

[21] M. E. Bunker, "Early Reactors: From Fermi's Water Boiler to Novel Power Prototypes," Los Alamos Science, 1983

[22] IAEA-TECDOC-1666, Optimization of Water Chemistry to Ensure Reliable Water Reactor Fuel Performance at High Burnup and in Ageing Plant (FUWAC), IAEA, Vienna, 2011.

[23] S. Xu, "Comparison of Different Methods to Improve LWR Fuel Performance with Silicon Carbide Cladding for High Burnup", internal memo Massachusetts Institute of Technology, (2012). A summary was presented at the ICAPP meeting in Chicago, in June 2012.

[24] Nuclear Power Plants, *Westinghouse Electric Company LLC*, Retrieved November 25, 2012, from http://www.westinghousenuclear.com/ProductLines/Nuclear_Power_Plants/

[25] G. Markham et al., "Silicon Carbide Clad Thoria Plutonia Fuel for Light Water Reactors", 9 Month Progress Report, Ceramic Tubular Products, LLC, 2012.

[26] Studsvik, "*CASMO-4E: A Fuel Assembly Burnup Program User's Manual*," Studsvik SSP-09/443-U Rev 0 proprietary.

[27] Studsvik, "*Simulate-3: Advanced Three Dimensional Two Group Reactor Analysis Code*," SSP-09/447-U Rev 0, proprietary.

Appendix A: Fuel Composition and Cycle Burnup Calculations

UO2/BeO Fuel Composition

The BeO content of the proposed UO_2/BeO fuel is specified as 10% by volume. Calculations in Appendix XX provide values for use in specifying the isotopic composition of the homogeneous UO_2/BeO fuel in CAMSO. The fuel is assumed to have no ^{234}U content.

First, the molar masses of uranium and uranium dioxide must be calculated.

$$a = \frac{e}{e + \frac{M_{235_U}}{M_{238_U}}(1 - e)}$$

$$M_U = a \cdot M_{235_U} + (1 - a)M_{235_U}$$

$$M_{UO_2} = M_U + 2M_O$$

The quantity of BeO present in the fuel is specified as 10% by volume. This quantity must be converted to a BeO mass fraction of the total mass, thus specifying each oxide's mass fraction of the total fuel mass.

$$\rho_m = v\%_{BeO} \cdot \rho_{BeO} + v\%_{UO_2} \cdot \rho_{UO_2}$$

$$wt_T\%_{BeO} = \frac{v\%_{BeO} \cdot \rho_{BeO}}{\rho_m}$$

$$wt_T\%_{UO_2} = \frac{v\%_{UO_2} \cdot \rho_{UO_2}}{\rho_m}$$

Knowing the oxide mass fractions and molar masses, element mass fractions can be determined.

$$wt_T\%_{Be} = wt_T\%_{BeO} \cdot \frac{M_{Be}}{M_{BeO}}$$

$$wt_T\%_U = wt_T\%_{UO_2} \cdot \frac{M_U}{M_{UO_2}}$$

$$wt_T\%_O = 100\% - wt_T\%_U - wt_T\%_{Be}$$

Finally, using the enrichment and uranium mass fraction, the isotopic mass fractions can be determined.

$$wt_T\%_{235_U} = wt_T\%_U \cdot wt_{HM}\%_{235_U} = wt_T\%_U \cdot e$$

$$wt_T\%_{238_U} = wt_T\%_U \cdot (1 - e)$$

The isotopic mass fractions are then converted to percentages of total fuel mass which are used to specify fuel composition in CASMO.

PuO2/ThO2 Fuel Composition

Determining the weight percent of total mass for each isotope in PuO_2/ThO_2 starts by specifying the heavy metal mass fraction of plutonium. Derivation of the necessary relations begins by using mass balances.

$$m_{Pu}\frac{M_{PuO_2}}{M_{Pu}} + m_{Th}\frac{M_{ThO_2}}{M_{Th}} = m_{PuO_2} + m_{ThO_2} = m_{Total}$$

$$m_{Pu} + m_{Th} = m_{HM}$$

Using the definition of percent of heavy metal, the relation between heavy metal mass and total mass can be obtained.

$$\frac{m_{Pu}}{m_{HM}}\frac{M_{PuO_2}}{M_{Pu}} + \frac{m_{Th}}{m_{HM}}\frac{M_{ThO_2}}{M_{Th}} = wt_{HM}\%_{PuO_2}\frac{M_{PuO_2}}{M_{Pu}} + (1 - wt_{HM}\%_{PuO_2})\frac{M_{ThO_2}}{M_{Th}} = \frac{m_{Total}}{m_{HM}}$$

Multiplication by the ratio of heavy metal mass to total mass provides the necessary values to specify percent of total weight for each isotope present in the PuO_2/ThO_2 fuel.

$$wt_{HM}\%_{PuO_2} \cdot \frac{m_{HM}}{m_{Total}} = \frac{m_{Pu}}{m_{Pu} + m_{Th}} \cdot \frac{m_{Pu} + m_{Th}}{m_{PuO_2} + m_{ThO_2}} = wt_T\%_{PuO_2}$$

$$wt_{HM}\%_{ThO_2} \cdot \frac{m_{HM}}{m_{Total}} = \frac{m_{Pu}}{m_{Pu} + m_{Th}} \cdot \frac{m_{Pu} + m_{Th}}{m_{PuO_2} + m_{ThO_2}} = wt_T\%_{ThO_2}$$

Similarly, given a known plutonium percent of total mass one can determine the plutonium percent of heavy metal.

$$wt_{HM}\%_{PuO_2} = \frac{\frac{M_{ThO_2}}{M_{Th}}}{\frac{1}{wt_T\%_{PuO_2}} - \frac{M_{PuO_2}}{M_{Pu}} + \frac{M_{ThO_2}}{M_{Th}}}$$

Cycle Burnup Calculations

First, the fuel volume is calculated.

$$V_f = \#\text{rods per assy} \cdot \#\text{assys} \cdot \pi(R_{fo}^2 - R_{fi}^2)^2 \cdot L$$

In the case of annular UO_2:

$$m_{HM} = V_f \rho_f \frac{M_U}{M_{UO_2}}$$

In the case of homogeneous UO_2/BeO:

$$m_{HM} = \text{vol}\%_{UO_2} \cdot V_f \rho_f \frac{M_U}{M_{UO_2}}$$

The EFPD target is calculated as follows:

$$((30.5 \times 18) - 28) \times 0.90 = 468.9 \sim 469$$

Cycle burnup targets are calculated as follows:

$$B_c = \frac{\text{EFPD} \cdot MW_{th}}{m_{HM}}$$

The cycle burnup is recalculated for comparisons with previous work using 492 EFPD.

LRM Calculations

LRM cycle and discharge burnup calculations for 84 reload cores:

$$EOFPL = \frac{1 + \frac{193}{84}}{2} B_c$$

$$B_d = \frac{193}{84} B_c$$

LRM cycle and discharge burnup calculations for 64 reload cores:

$$EOFPL = \frac{1 + \frac{193}{64}}{2} B_c$$

$$B_d = \frac{193}{64} B_c$$

LRM prediction for required enrichment to achieve off-design cycle length:

$$\Delta\text{enrichment} \propto \Delta\left(\frac{B_c + B_d}{2}\right)$$

The ratio of $\mathbf{B_c/B_d}$ is assumed to be invariant when making LRM predictions for off-design cycle lengths.

SDM Calculations

In the following equation for Δk_1 the value of k_{eff} comes from the HFP to HZP calculation.

$$\Delta k_1 = (k_{eff} - 1) \times 10^5$$

In the following equation for Δk_2 the value of k_{eff} comes from the HFP to 30% rods in calculation.

$$\Delta k_2 = (1 - k_{eff}) \times 10^5$$

In the following equation for Δk_3 the value of k_{eff} comes from the HFP to HZP calculation.

$$\Delta k_3 = (k_{eff} - 1) \times 10^5$$

The values of Δk_4 are read directly from the SIMULATE output for the HFP to most effective rod in calculation.

Calculation of H/HM

The ratio of hydrogen to heavy metal is calculated as shown below:

$$\frac{H}{HM} = \frac{mol_H}{mol_{HM}} = \frac{2 * V_H * \rho_{H_2O}}{mm_{H_2O} * mol_{HM}}$$

Appendix B: Burnable Poison Maps

The burnable poison layout shown below in Figure 33 was used in all 156 1.0x IFBA rod assemblies. This pattern was produced via EDBS optimization. Once the fuel composition was finalized for all fuel and clad combinations, re-optimization via EDBS showed that the pattern below was either optimal or differed in peak lifetime intra-assembly peaking by 0.001. Future optimization schema may include additional parameters for the optimization of burnable poison layouts.

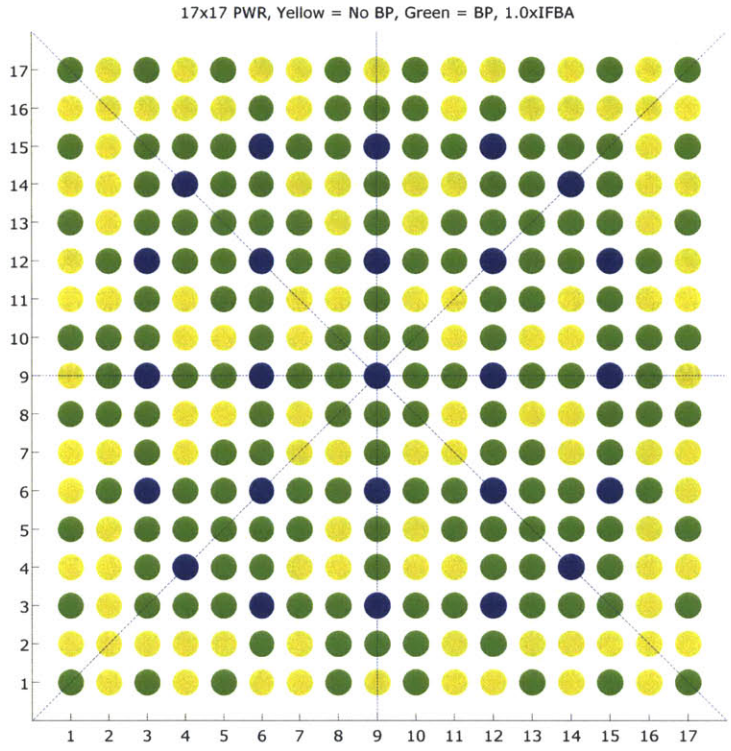

Figure 33: 156 1.0x IFBA Rod Assembly Layout

The burnable poison layout shown below in Figure 34 used in the 156 1.5x IFBA rod assemblies. Only the **Thick SiC** clad PuO_2/ThO_2 cases utilized 1.5x IFBA.

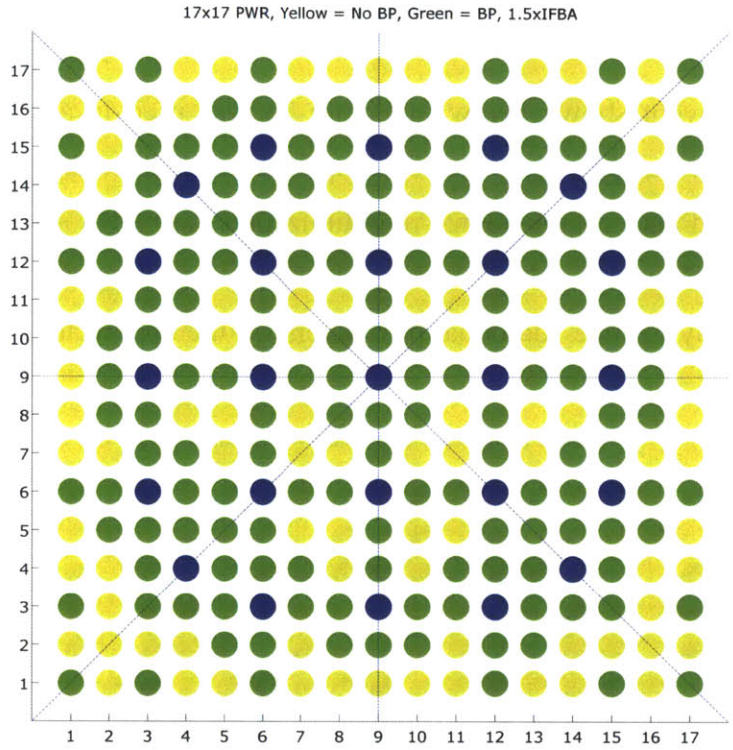

Figure 34: 156 1.5x IFBA Rod Assembly Layout

Appendix C: Example CASMO/SIMULATE Input Files

The following is a sample CASMO-4E input file.

```
TTL * K0F1R4096E0450B0P1 Python

* State Parameters
PDE 109.926
PRE 155.130
TFU 810
TMO 585
BOR 600
VOI 000

* Assembly Geometry Parameters
PWR 17.00 1.26  21.50

* Pin Geometry Parameters
PIN 1 0.4096 0.4180 0.4750 /'1' 'MI1' 'CAN'
PIN 2 0.4096 0.4180 0.4750 /'1' 'MI1' 'CAN'
PIN 3 0.5690 0.6147 /'MOD' 'BOX'
PIN 4 0.5690 0.6147 /'MOD' 'BOX'
PIN 4 0.4331 0.4369 0.4839 0.5690 0.6147
      /'AIC' 'AIR' 'CRS' 'MOD' 'BOX'
      //1 'RCC' 'ROD'

* Fuel Composition Parameters
FUE 1 10.47         / 04.50

* Material Composition Parameters
CAN 6.55 / 304=100.0
MI1 1.159E-03 / 2003=1.3E-05
SPA 10.81934 1.800E-05 ,, 8.154 / 718=84.59 347=15.41

* Pin Layout Map
LPI
3
1  1
1  1  1
4  1  1  4
1  1  1  1  1
1  1  1  1  1  4
4  1  1  4  1  1  1
1  1  1  1  1  1  1  1
1  1  1  1  1  1  1  1  1

* Depletion and Execute Statement
DEP , -100
SIM , 'K0F1R4096E0450B0P1'
S3C
STA
END
```

The following is a sample SIMULATE-3 input file.

```
'DIM.PWR' 15/
'DIM.CAL' 24 2 2/
'DIM.DEP' 'EXP' 'SAM' 'HTMO' 'HBOR' 'HTFU' 'PIN' 'EBP'/

'TIT.PRO' 'Zircaloy-4 Clad UO2 Fuel'/
'TIT.RUN' 'Solid Pellet,156 1.0xIFBA'/
'TIT.CAS' 'Cycle 01'/

'LIB' '/home/dbloore/LIB/K0F1R0P1.lib'/

'COR.SYM' 'ROT'/
```

```
'COR.DAT' 21.5 365.76 109.926 751.53/
'COR.STM' 0/

'PWR.OPT' 'ON'/
'PWR.CTP' 0 25 50 75 100/
'PWR.TIN' 557 557.4 557.8 558.2 558.6/

'REF.LIB' , 01 'K0F1REFBOT'/
          , 02 'K0F1REFRAD'/
          , 03 'K0F1REFTOP'/
'SEG.LIB' , 04 'K0F1R4096E0200B0P1'/
          , 05 'K0F1R4096E0360B0P1'/
          , 06 'K0F1R4096E0370B0P1'/
          , 07 'K0F1R4096E0380B0P1'/
          , 08 'K0F1R4096E0390B0P1'/
          , 09 'K0F1R4096E0400B0P1'/
          , 10 'K0F1R4096E0410B0P1'/
          , 11 'K0F1R4096E0420B0P1'/
          , 12 'K0F1R4096E0430B0P1'/
          , 13 'K0F1R4096E0440B0P1'/
          , 14 'K0F1R4096E0450B0P1'/
          , 15 'K0F1R4096E0200B1P1'/
          , 16 'K0F1R4096E0360B1P1'/
          , 17 'K0F1R4096E0370B1P1'/
          , 18 'K0F1R4096E0380B1P1'/
          , 19 'K0F1R4096E0390B1P1'/
          , 20 'K0F1R4096E0400B1P1'/
          , 21 'K0F1R4096E0410B1P1'/
          , 22 'K0F1R4096E0420B1P1'/
          , 23 'K0F1R4096E0430B1P1'/
          , 24 'K0F1R4096E0440B1P1'/
          , 25 'K0F1R4096E0450B1P1'/

'SEG.TFU'  0 0 347.38 -5.3799/

'FUE.ZON' , 01 1 'K0F1REFRAD' 01 0.0 02 365.76 03/
          , 02 1 'K0F1R4096E0450B1P1'  01 0.00 04 15.24 14 30.48 25 335.28 14 350.52 04 365.76 03/
          , 03 1 'K0F1R4096E0450B1P1'  01 0.00 04 15.24 14 30.48 25 335.28 14 350.52 04 365.76 03/
          , 04 1 'K0F1R4096E0450B1P1'  01 0.00 04 15.24 14 30.48 25 335.28 14 350.52 04 365.76 03/
          , 05 1 'K0F1R4096E0450B1P1'  01 0.00 04 15.24 14 30.48 25 335.28 14 350.52 04 365.76 03/
          , 06 1 'K0F1R4096E0450B1P1'  01 0.00 04 15.24 14 30.48 25 335.28 14 350.52 04 365.76 03/
'FUE.GRD' 'ON'   2.82 3.36 'INC'
                64.87 3.36 'INC'
               117.07 3.36 'INC'
               169.27 3.36 'INC'
               221.46 3.36 'INC'
               273.66 3.36 'INC'
               325.86 3.36 'INC'/
'FUE.TYP' 1
          2 2 2 2 2 2 2 2 1
          2 2 2 2 2 2 2 2 1
          2 2 2 2 2 2 2 2 1
          2 2 2 2 2 2 2 2 1
          2 2 2 2 2 2 2 1 1
          2 2 2 2 2 2 2 1 0
          2 2 2 2 2 2 1 1 0
          2 2 2 2 1 1 1 0 0
          1 1 1 1 1 0 0 0 0/

'FUE.NEW' 'TYPE01' 'A01' 16 02,,,,,20 24
       1 24*36 7 24*0.704 9 24*600/
'FUE.NEW' 'TYPE01' 'A17' 16 03,,,,,20 24
       1 24*36 7 24*0.704 9 24*600/
'FUE.NEW' 'TYPE01' 'A33' 20 04,,,,,20 24
       1 24*36 7 24*0.704 9 24*600/
'FUE.NEW' 'TYPE01' 'A53' 16 05,,,,,20 24
       1 24*36 7 24*0.704 9 24*600/
'FUE.NEW' 'TYPE01' 'A69' 16 06,,,,,20 24
       1 24*36 7 24*0.704 9 24*600/
```

```
'FUE.NEW' 'TYPE01' 'B01' 16 02,,,,,20 24
      1 24*18 7 24*0.704 9 24*600/
'FUE.NEW' 'TYPE01' 'B17' 16 03,,,,,20 24
      1 24*18 7 24*0.704 9 24*600/
'FUE.NEW' 'TYPE01' 'B33' 20 04,,,,,20 24
      1 24*18 7 24*0.704 9 24*600/
'FUE.NEW' 'TYPE01' 'B53' 16 05,,,,,20 24
      1 24*18 7 24*0.704 9 24*600/
'FUE.NEW' 'TYPE01' 'B69' 16 06,,,,,20 24
      1 24*18 7 24*0.704 9 24*600/

'FUE.NEW' 'TYPE01' 'C01' 16 02/
'FUE.NEW' 'TYPE01' 'C17' 16 03/
'FUE.NEW' 'TYPE01' 'C33' 20 04/
'FUE.NEW' 'TYPE01' 'C53' 16 05/
'FUE.NEW' 'TYPE01' 'C69' 16 06/

'FUE.SER' 4/
01 1                     B48  B52  A16  A30  B05  B08  B40
02 1           B31  B68  C32  C83  C16  C84  C39  C60  C41  B06  B59
03 1       B67  C15  C30  B49  C50  B82  C29  B76  B07  C58  C73  C07  B23
04 1       B14  C81  B32  C82  A14  C65  A29  C05  B41  B75  B24  C22  B60
05 1  B50  C51  C66  B83  B30  C31  B65  C52  B58  B73  B22  C74  B39  C24  B38
06 1  B16  C68  B15  B51  B81  A31  C48  A15  C06  A23  C23  A06  C40  C75  B42
07 1  B13  C49  B84  C13  B66  C14  B29  C67  B21  C38  B57  C57  B74  C08  A08
08 1  A26  C80  C25  A25  C47  A11  C63  A01  C59  A07  C42  A21  C21  C76  A22
09 1  A12  C12  B78  C61  B61  C43  B25  C55  B17  C02  B54  C01  B72  C34  B01
10 1  B47  C79  C45  A10  C27  A27  C10  A03  C33  A19  B69  B36  B03  C56  B04
11 1  B43  C28  B44  C78  B26  B77  B62  C37  B53  C19  B18  B71  C54  C36  B35
12 1       B64  C26  B28  B79  B46  C09  A17  C53  A02  C70  B20  C69  B02
13 1       B27  C11  C77  C62  B11  B80  C17  B70  C35  B34  C18  C03  B55
14 1           B63  B10  C46  C64  C44  C72  C04  C71  C20  B56  B19
15 1                     B45  B12  B09  A18  A04  B37  B33
 0 0

'RES' 'NEWFUEL'/

'HYD.ITE' /

'BAT.EDT' 'OFF'/

'ITE.BOR' 1500/
'ITE.SRC' 'SET' 'EOLEXP',,0.001,,,'KEF' 1.000 0.00001 'MINBOR'/

'DEP.CYC' 'CYCLE01' 0.0 01/
'DEP.STA' 'AVE' 0.0 0.15 0.25 0.5 -0.5 20/
'PRI.STA' '2EXP' '2RPF'/
'SUM' '/home/dbloore/SIMA2RL2E25P1_01.sum'/
'WRE' '/home/dbloore/SIMA2RL2E25P1_01.res' 20000/

'STA'/
'END'/

'DIM.PWR' 15/
'DIM.CAL' 24 2 2/
'DIM.DEP' 'EXP' 'SAM' 'HTMO' 'HBOR' 'HTFU' 'PIN' 'EBP'/

'TIT.CAS' 'Cycle 02'/

'FUE.NEW' 'TYPE01' 'D01' 16 02/
'FUE.NEW' 'TYPE01' 'D17' 16 03/
'FUE.NEW' 'TYPE01' 'D33' 20 04/
'FUE.NEW' 'TYPE01' 'D53' 16 05/
'FUE.NEW' 'TYPE01' 'D69' 16 06/

'FUE.SER' 4/
01 1                     C48  C52  B16  B30  C05  C08  C40
02 1           C31  C68  D32  D83  D16  D84  D39  D60  D41  C06  C59
```

```
03 1       C67  D15  D30  C49  D50  C82  D29  C76  C07  D58  D73  D07  C23
04 1       C14  D81  C32  D82  B14  D65  B29  D05  C41  C75  C24  D22  C60
05 1  C50  D51  D66  C83  C30  D31  C65  D52  C58  C73  C22  D74  C39  D24  C38
06 1  C16  D68  C15  C51  C81  B31  D48  B15  D06  B23  D23  B06  D40  D75  C42
07 1  C13  D49  C84  D13  C66  D14  C29  D67  C21  D38  C57  D57  C74  D08  B08
08 1  B26  D80  D25  B25  D47  B11  D63  B01  D59  B07  D42  B21  D21  D76  B22
09 1  B12  D12  C78  D61  C61  D43  C25  D55  C17  D02  C54  D01  C72  D34  C01
10 1  C47  D79  D45  B10  D27  B27  D10  B03  D33  B19  C69  C36  C03  D56  C04
11 1  C43  D28  C44  D78  C26  C77  C62  D37  C53  D19  C18  C71  D54  D36  C35
12 1       C64  D26  C28  C79  C46  D09  B17  D53  B02  D70  C20  D69  C02
13 1       C27  D11  D77  D62  C11  C80  D17  C70  D35  C34  D18  D03  C55
14 1            C63  C10  D46  D64  D44  D72  D04  D71  D20  C56  C19
15 1                 C45  C12  C09  B18  B04  C37  C33
 0 0

'RES' '/home/dbloore/SIMA2RL2E25P1_01.res' 20000/

'ITE.BOR' 1500/
'ITE.SRC' 'SET' 'EOLEXP',,0.001,,,'KEF' 1.000 0.00001 'MINBOR'/

'DEP.CYC' 'CYCLE02' 0.0 02/
'DEP.STA' 'AVE' 0.0 0.15 0.25 0.5 -0.5 20/
'PRI.STA' '2EXP' '2RPF'/
'SUM' '/home/dbloore/SIMA2RL2E25P1_02.sum'/
'WRE' '/home/dbloore/SIMA2RL2E25P1_02.res' 20000/

'STA'/
'END'/

'DIM.PWR' 15/
'DIM.CAL' 24 2 2/
'DIM.DEP' 'EXP' 'SAM' 'HTMO' 'HBOR' 'HTFU' 'PIN' 'EBP'/

'TIT.CAS' 'Cycle 03'/

'FUE.NEW' 'TYPE01' 'E01' 16 02/
'FUE.NEW' 'TYPE01' 'E17' 16 03/
'FUE.NEW' 'TYPE01' 'E33' 20 04/
'FUE.NEW' 'TYPE01' 'E53' 16 05/
'FUE.NEW' 'TYPE01' 'E69' 16 06/

'FUE.SER' 4/
01 1                 D48  D52  C16  C30  D05  D08  D40
02 1            D31  D68  E32  E83  E16  E84  E39  E60  E41  D06  D59
03 1       D67  E15  E30  D49  E50  D82  E29  D76  D07  E58  E73  E07  D23
04 1       D14  E81  D32  E82  C14  E65  C29  E05  D41  D75  D24  E22  D60
05 1  D50  E51  E66  D83  D30  E31  D65  E52  D58  D73  D22  E74  D39  E24  D38
06 1  D16  E68  D15  D51  D81  C31  E48  C15  E06  C23  E23  C06  E40  E75  D42
07 1  D13  E49  D84  E13  D66  E14  D29  E67  D21  E38  D57  E57  D74  E08  C08
08 1  C26  E80  E25  C25  E47  C11  E63  C01  E59  C07  E42  C21  E21  E76  C22
09 1  C12  E12  D78  E61  D61  E43  D25  E55  D17  E02  D54  E01  D72  E34  D01
10 1  D47  E79  E45  C10  E27  C27  E10  C03  E33  C19  D69  D36  D03  E56  D04
11 1  D43  E28  D44  E78  D26  D77  D62  E37  D53  E19  D18  D71  E54  E36  D35
12 1       D64  E26  D28  D79  D46  E09  C17  E53  C02  E70  D20  E69  D02
13 1       D27  E11  E77  E62  D11  D80  E17  D70  E35  D34  E18  E03  D55
14 1            D63  D10  E46  E64  E44  E72  E04  E71  E20  D56  D19
15 1                 D45  D12  D09  C18  C04  D37  D33
 0 0

'RES' '/home/dbloore/SIMA2RL2E25P1_02.res' 20000/

'ITE.BOR' 1500/
'ITE.SRC' 'SET' 'EOLEXP',,0.001,,,'KEF' 1.000 0.00001 'MINBOR'/

'DEP.CYC' 'CYCLE03' 0.0 03/
'DEP.STA' 'AVE' 0.0 0.15 0.25 0.5 -0.5 20/
'PRI.STA' '2EXP' '2RPF'/
'SUM' '/home/dbloore/SIMA2RL2E25P1_03.sum'/
'WRE' '/home/dbloore/SIMA2RL2E25P1_03.res' 20000/
```

```
'STA'/
'END'/

'DIM.PWR' 15/
'DIM.CAL' 24 2 2/
'DIM.DEP' 'EXP' 'SAM' 'HTMO' 'HBOR' 'HTFU' 'PIN' 'EBP'/

'TIT.CAS' 'Cycle 04'/

'FUE.NEW' 'TYPE01' 'F01' 16 02/
'FUE.NEW' 'TYPE01' 'F17' 16 03/
'FUE.NEW' 'TYPE01' 'F33' 20 04/
'FUE.NEW' 'TYPE01' 'F53' 16 05/
'FUE.NEW' 'TYPE01' 'F69' 16 06/

'FUE.SER' 4/
01 1                    E48  E52  D16  D30  E05  E08  E40
02 1           E31  E68  F32  F83  F16  F84  F39  F60  F41  E06  E59
03 1       E67  F15  F30  E49  F50  E82  F29  E76  E07  F58  F73  F07  E23
04 1       E14  F81  E32  F82  D14  F65  D29  F05  E41  E75  E24  F22  E60
05 1  E50  F51  F66  E83  E30  F31  E65  F52  E58  E73  E22  F74  E39  F24  E38
06 1  E16  F68  E15  E51  E81  D31  F48  D15  F06  D23  F23  D06  F40  F75  E42
07 1  E13  F49  E84  F13  E66  F14  E29  F67  E21  F38  E57  F57  E74  F08  D08
08 1  D26  F80  F25  D25  F47  D11  F63  D01  F59  D07  F42  D21  F21  F76  D22
09 1  D12  F12  E78  F61  E61  F43  E25  F55  E17  F02  E54  F01  E72  F34  E01
10 1  E47  F79  F45  D10  F27  D27  F10  D03  F33  D19  E69  E36  E03  F56  E04
11 1  E43  F28  E44  F78  E26  E77  E62  F37  E53  F19  E18  E71  F54  F36  E35
12 1       E64  F26  E28  E79  E46  F09  D17  F53  D02  F70  E20  F69  E02
13 1       E27  F11  F77  F62  E11  E80  F17  E70  F35  E34  F18  F03  E55
14 1            E63  E10  F46  F64  F44  F72  F04  F71  F20  E56  E19
15 1                 E45  E12  E09  D18  D04  E37  E33
 0 0

'RES' '/home/dbloore/SIMA2RL2E25P1_03.res' 20000/

'ITE.BOR' 1500/
'ITE.SRC' 'SET' 'EOLEXP',,0.001,,,'KEF' 1.000 0.00001 'MINBOR'/

'DEP.CYC' 'CYCLE04' 0.0 04/
'DEP.STA' 'AVE' 0.0 0.15 0.25 0.5 -0.5 20/
'PRI.STA' '2EXP' '2RPF'/
'SUM' '/home/dbloore/SIMA2RL2E25P1_04.sum'/
'WRE' '/home/dbloore/SIMA2RL2E25P1_04.res' 20000/

'STA'/
'END'/

'DIM.PWR' 15/
'DIM.CAL' 24 2 2/
'DIM.DEP' 'EXP' 'SAM' 'HTMO' 'HBOR' 'HTFU' 'PIN' 'EBP'/

'TIT.CAS' 'Cycle 05'/

'FUE.NEW' 'TYPE01' 'G01' 16 02/
'FUE.NEW' 'TYPE01' 'G17' 16 03/
'FUE.NEW' 'TYPE01' 'G33' 20 04/
'FUE.NEW' 'TYPE01' 'G53' 16 05/
'FUE.NEW' 'TYPE01' 'G69' 16 06/

'FUE.SER' 4/
01 1                    F48  F52  E16  E30  F05  F08  F40
02 1           F31  F68  G32  G83  G16  G84  G39  G60  G41  F06  F59
03 1       F67  G15  G30  F49  G50  F82  G29  F76  F07  G58  G73  G07  F23
04 1       F14  G81  F32  G82  E14  G65  E29  G05  F41  F75  F24  G22  F60
05 1  F50  G51  G66  F83  F30  G31  F65  G52  F58  F73  F22  G74  F39  G24  F38
06 1  F16  G68  F15  F51  F81  E31  G48  E15  G06  E23  G23  E06  G40  G75  F42
07 1  F13  G49  F84  G13  F66  G14  F29  G67  F21  G38  F57  G57  F74  G08  E08
08 1  E26  G80  G25  E25  G47  E11  G63  E01  G59  E07  G42  E21  G21  G76  E22
```

```
09 1  E12  G12  F78  G61  F61  G43  F25  G55  F17  G02  F54  G01  F72  G34  F01
10 1  F47  G79  G45  E10  G27  E27  G10  E03  G33  E19  F69  F36  F03  G56  F04
11 1  F43  G28  F44  G78  F26  F77  F62  G37  F53  G19  F18  F71  G54  G36  F35
12 1       F64  G26  F28  F79  F46  G09  E17  G53  E02  G70  F20  G69  F02
13 1       F27  G11  G77  G62  F11  F80  G17  F70  G35  F34  G18  G03  F55
14 1            F63  F10  G46  G64  G44  G72  G04  G71  G20  F56  F19
15 1                 F45  F12  F09  E18  E04  F37  F33
 0 0

'RES' '/home/dbloore/SIMA2RL2E25P1_04.res' 20000/

'ITE.BOR' 1500/
'ITE.SRC' 'SET' 'EOLEXP',,0.001,,,'KEF' 1.000 0.00001 'MINBOR'/

'DEP.CYC' 'CYCLE05' 0.0 05/
'DEP.STA' 'AVE' 0.0 0.15 0.25 0.5 -0.5 20/
'PRI.STA' '2EXP' '2RPF'/
'SUM' '/home/dbloore/SIMA2RL2E25P1_05.sum'/
'WRE' '/home/dbloore/SIMA2RL2E25P1_05.res' 20000/

'STA'/
'END'/

'DIM.PWR' 15/
'DIM.CAL' 24 2 2/
'DIM.DEP' 'EXP' 'SAM' 'HTMO' 'HBOR' 'HTFU' 'PIN' 'EBP'/

'TIT.CAS' 'Cycle 06'/

'FUE.NEW' 'TYPE01' 'H01' 16 02/
'FUE.NEW' 'TYPE01' 'H17' 16 03/
'FUE.NEW' 'TYPE01' 'H33' 20 04/
'FUE.NEW' 'TYPE01' 'H53' 16 05/
'FUE.NEW' 'TYPE01' 'H69' 16 06/

'FUE.SER' 4/
01 1                 G48  G52  F16  F30  G05  G08  G40
02 1            G31  G68  H32  H83  H16  H84  H39  H60  H41  G06  G59
03 1       G67  H15  H30  G49  H50  G82  H29  G76  G07  H58  H73  H07  G23
04 1       G14  H81  G32  H82  F14  H65  F29  H05  G41  G75  G24  H22  G60
05 1  G50  H51  H66  G83  G30  H31  G65  H52  G58  G73  G22  H74  G39  H24  G38
06 1  G16  H68  G15  G51  G81  F31  H48  F15  H06  F23  H23  F06  H40  H75  G42
07 1  G13  H49  G84  H13  G66  H14  G29  H67  G21  H38  G57  H57  G74  H08  F08
08 1  F26  H80  H25  F25  H47  F11  H63  F01  H59  F07  H42  F21  H21  H76  F22
09 1  F12  H12  G78  H61  G61  H43  G25  H55  G17  H02  G54  H01  G72  H34  G01
10 1  G47  H79  H45  F10  H27  F27  H10  F03  H33  F19  G69  G36  G03  H56  G04
11 1  G43  H28  G44  H78  G26  G77  G62  H37  G53  H19  G18  G71  H54  H36  G35
12 1       G64  H26  G28  G79  G46  H09  F17  H53  F02  H70  G20  H69  G02
13 1       G27  H11  H77  H62  G11  G80  H17  G70  H35  G34  H18  H03  G55
14 1            G63  G10  H46  H64  H44  H72  H04  H71  H20  G56  G19
15 1                 G45  G12  G09  F18  F04  G37  G33
 0 0

'RES' '/home/dbloore/SIMA2RL2E25P1_05.res' 20000/

'ITE.BOR' 1500/
'ITE.SRC' 'SET' 'EOLEXP',,0.001,,,'KEF' 1.000 0.00001 'MINBOR'/

'DEP.CYC' 'CYCLE06' 0.0 06/
'DEP.STA' 'AVE' 0.0 0.15 0.25 0.5 -0.5 20/
'PRI.STA' '2EXP' '2RPF'/
'SUM' '/home/dbloore/SIMA2RL2E25P1_06.sum'/
'WRE' '/home/dbloore/SIMA2RL2E25P1_06.res' 20000/

'STA'/
'END'/

'DIM.PWR' 15/
'DIM.CAL' 24 2 2/
```

```
'DIM.DEP' 'EXP' 'SAM' 'HTMO' 'HBOR' 'HTFU' 'PIN' 'EBP'/

'TIT.CAS' 'Cycle 07'/

'FUE.NEW' 'TYPE01' 'J01' 16 02/
'FUE.NEW' 'TYPE01' 'J17' 16 03/
'FUE.NEW' 'TYPE01' 'J33' 20 04/
'FUE.NEW' 'TYPE01' 'J53' 16 05/
'FUE.NEW' 'TYPE01' 'J69' 16 06/

'FUE.SER' 4/
01 1                    H48  H52  G16  G30  H05  H08  H40
02 1           H31  H68  J32  J83  J16  J84  J39  J60  J41  H06  H59
03 1      H67  J15  J30  H49  J50  H82  J29  H76  H07  J58  J73  J07  H23
04 1      H14  J81  H32  J82  G14  J65  G29  J05  H41  H75  H24  J22  H60
05 1 H50  J51  J66  H83  H30  J31  H65  J52  H58  H73  H22  J74  H39  J24  H38
06 1 H16  J68  H15  H51  H81  G31  J48  G15  J06  G23  J23  G06  J40  J75  H42
07 1 H13  J49  H84  J13  H66  J14  H29  J67  H21  J38  H57  J57  H74  J08  G08
08 1 G26  J80  J25  G25  J47  G11  J63  G01  J59  G07  J42  G21  J21  J76  G22
09 1 G12  J12  H78  J61  H61  J43  H25  J55  H17  J02  H54  J01  H72  J34  H01
10 1 H47  J79  J45  G10  J27  G27  J10  G03  J33  G19  H69  H36  H03  J56  H04
11 1 H43  J28  H44  J78  H26  H77  H62  J37  H53  J19  H18  H71  J54  J36  H35
12 1      H64  J26  H28  H79  H46  J09  G17  J53  G02  J70  H20  J69  H02
13 1      H27  J11  J77  J62  H11  H80  J17  H70  J35  H34  J18  J03  H55
14 1           H63  H10  J46  J64  J44  J72  J04  J71  J20  H56  H19
15 1                    H45  H12  H09  G18  G04  H37  H33
 0 0

'RES' '/home/dbloore/SIMA2RL2E25P1_06.res' 20000/

'ITE.BOR' 1500/
'ITE.SRC' 'SET' 'EOLEXP',,0.001,,,'KEF' 1.000 0.00001 'MINBOR'/

'DEP.CYC' 'CYCLE07' 0.0 07/
'DEP.STA' 'AVE' 0.0 0.15 0.25 0.5 -0.5 20/
'PRI.STA' '2EXP' '2RPF'/
'SUM' '/home/dbloore/SIMA2RL2E25P1_07.sum'/
'WRE' '/home/dbloore/SIMA2RL2E25P1_07.res' 20000/

'STA'/
'END'/

'DIM.PWR' 15/
'DIM.CAL' 24 2 2/
'DIM.DEP' 'EXP' 'SAM' 'HTMO' 'HBOR' 'HTFU' 'PIN' 'EBP'/

'TIT.CAS' 'Cycle 08'/

'FUE.NEW' 'TYPE01' 'K01' 16 02/
'FUE.NEW' 'TYPE01' 'K17' 16 03/
'FUE.NEW' 'TYPE01' 'K33' 20 04/
'FUE.NEW' 'TYPE01' 'K53' 16 05/
'FUE.NEW' 'TYPE01' 'K69' 16 06/

'FUE.SER' 4/
01 1                    J48  J52  H16  H30  J05  J08  J40
02 1           J31  J68  K32  K83  K16  K84  K39  K60  K41  J06  J59
03 1      J67  K15  K30  J49  K50  J82  K29  J76  J07  K58  K73  K07  J23
04 1      J14  K81  J32  K82  H14  K65  H29  K05  J41  J75  J24  K22  J60
05 1 J50  K51  K66  J83  J30  K31  J65  K52  J58  J73  J22  K74  J39  K24  J38
06 1 J16  K68  J15  J51  J81  H31  K48  H15  K06  H23  K23  H06  K40  K75  J42
07 1 J13  K49  J84  K13  J66  K14  J29  K67  J21  K38  J57  K57  J74  K08  H08
08 1 H26  K80  K25  H25  K47  H11  K63  H01  K59  H07  K42  H21  K21  K76  H22
09 1 H12  K12  J78  K61  J61  K43  J25  K55  J17  K02  J54  K01  J72  K34  J01
10 1 J47  K79  K45  H10  K27  H27  K10  H03  K33  H19  J69  J36  J03  K56  J04
11 1 J43  K28  J44  K78  J26  J77  J62  K37  J53  K19  J18  J71  K54  K36  J35
12 1      J64  K26  J28  J79  J46  K09  H17  K53  H02  K70  J20  K69  J02
13 1      J27  K11  K77  K62  J11  J80  K17  J70  K35  J34  K18  K03  J55
14 1           J63  J10  K46  K64  K44  K72  K04  K71  K20  J56  J19
```

```
15 1                     J45  J12  J09  H18  H04  J37  J33
 0 0

'RES' '/home/dbloore/SIMA2RL2E25P1_07.res' 20000/

'ITE.BOR' 1500/
'ITE.SRC' 'SET' 'EOLEXP',,0.001,,,'KEF' 1.000 0.00001 'MINBOR'/

'DEP.CYC' 'CYCLE08' 0.0 08/
'DEP.STA' 'AVE' 0.0 0.15 0.25 0.5 -0.5 20/
'PRI.STA' '2EXP' '2RPF'/
'SUM' '/home/dbloore/SIMA2RL2E25P1_08.sum'/
'WRE' '/home/dbloore/SIMA2RL2E25P1_08.res' 20000/

'STA'/
'END'/

'DIM.PWR' 15/
'DIM.CAL' 24 2 2/
'DIM.DEP' 'EXP' 'SAM' 'HTMO' 'HBOR' 'HTFU' 'PIN' 'EBP'/

'TIT.CAS' 'Cycle 09'/

'FUE.NEW' 'TYPE01' 'L01' 16 02/
'FUE.NEW' 'TYPE01' 'L17' 16 03/
'FUE.NEW' 'TYPE01' 'L33' 20 04/
'FUE.NEW' 'TYPE01' 'L53' 16 05/
'FUE.NEW' 'TYPE01' 'L69' 16 06/

'FUE.SER' 4/
01 1                     K48  K52  J16  J30  K05  K08  K40
02 1           K31  K68  L32  L83  L16  L84  L39  L60  L41  K06  K59
03 1      K67  L15  L30  K49  L50  K82  L29  K76  K07  L58  L73  L07  K23
04 1      K14  L81  K32  L82  J14  L65  J29  L05  K41  K75  K24  L22  K60
05 1 K50  L51  L66  K83  K30  L31  K65  L52  K58  K73  K22  L74  K39  L24  K38
06 1 K16  L68  K15  K51  K81  J31  L48  J15  L06  J23  L23  J06  L40  L75  K42
07 1 K13  L49  K84  L13  K66  L14  K29  L67  K21  L38  K57  L57  K74  L08  J08
08 1 J26  L80  L25  J25  L47  J11  L63  J01  L59  J07  L42  J21  L21  L76  J22
09 1 J12  L12  K78  L61  K61  L43  K25  L55  K17  L02  K54  L01  K72  L34  K01
10 1 K47  L79  L45  J10  L27  J27  L10  J03  L33  J19  K69  K36  K03  L56  K04
11 1 K43  L28  K44  L78  K26  K77  K62  L37  K53  L19  K18  K71  L54  L36  K35
12 1      K64  L26  K28  K79  K46  L09  J17  L53  J02  L70  K20  L69  K02
13 1      K27  L11  L77  L62  K11  K80  L17  K70  L35  K34  L18  L03  K55
14 1           K63  K10  L46  L64  L44  L72  L04  L71  L20  K56  K19
15 1                K45  K12  K09  J18  J04  K37  K33
 0 0

'RES' '/home/dbloore/SIMA2RL2E25P1_08.res' 20000/

'ITE.BOR' 1500/
'ITE.SRC' 'SET' 'EOLEXP',,0.001,,,'KEF' 1.000 0.00001 'MINBOR'/

'DEP.CYC' 'CYCLE09' 0.0 09/
'DEP.STA' 'AVE' 0.0 0.15 0.25 0.5 -0.5 20/
'PRI.STA' '2EXP' '2RPF'/
'SUM' '/home/dbloore/SIMA2RL2E25P1_09.sum'/
'WRE' '/home/dbloore/SIMA2RL2E25P1_09.res' 20000/

'STA'/
'END'/

'DIM.PWR' 15/
'DIM.CAL' 24 2 2/
'DIM.DEP' 'EXP' 'SAM' 'HTMO' 'HBOR' 'HTFU' 'PIN' 'EBP'/

'TIT.CAS' 'Cycle 10'/

'FUE.NEW' 'TYPE01' 'M01' 16 02/
'FUE.NEW' 'TYPE01' 'M17' 16 03/
```

```
'FUE.NEW' 'TYPE01' 'M33' 20 04/
'FUE.NEW' 'TYPE01' 'M53' 16 05/
'FUE.NEW' 'TYPE01' 'M69' 16 06/

'FUE.SER' 4/
01 1                        L48  L52  K16  K30  L05  L08  L40
02 1             L31  L68  M32  M83  M16  M84  M39  M60  M41  L06  L59
03 1        L67  M15  M30  L49  M50  L82  M29  L76  L07  M58  M73  M07  L23
04 1        L14  M81  L32  M82  K14  M65  K29  M05  L41  L75  L24  M22  L60
05 1  L50  M51  M66  L83  L30  M31  L65  M52  L58  L73  L22  M74  L39  M24  L38
06 1  L16  M68  L15  L51  L81  K31  M48  K15  M06  K23  M23  K06  M40  M75  L42
07 1  L13  M49  L84  M13  L66  M14  L29  M67  L21  M38  L57  M57  L74  M08  K08
08 1  K26  M80  M25  K25  M47  K11  M63  K01  M59  K07  M42  K21  M21  M76  K22
09 1  K12  M12  L78  M61  L61  M43  L25  M55  L17  M02  L54  M01  L72  M34  L01
10 1  L47  M79  M45  K10  M27  K27  M10  K03  M33  K19  L69  L36  L03  M56  L04
11 1  L43  M28  L44  M78  L26  L77  L62  M37  L53  M19  L18  L71  M54  M36  L35
12 1        L64  M26  L28  L79  L46  M09  K17  M53  K02  M70  L20  M69  L02
13 1        L27  M11  M77  M62  L11  L80  M17  L70  M35  L34  M18  M03  L55
14 1             L63  L10  M46  M64  M44  M72  M04  M71  M20  L56  L19
15 1                       L45  L12  L09  K18  K04  L37  L33
 0 0

'RES' '/home/dbloore/SIMA2RL2E25P1_09.res' 20000/

'ITE.BOR' 1500/
'ITE.SRC' 'SET' 'EOLEXP',,0.001,,,'KEF' 1.000 0.00001 'MINBOR'/

'DEP.CYC' 'CYCLE10' 0.0 10/
'DEP.STA' 'AVE' 0.0 0.15 0.25 0.5 -0.5 20/
'PRI.STA' '2EXP' '2RPF'/
'SUM' '/home/dbloore/SIMA2RL2E25P1_10.sum'/
'WRE' '/home/dbloore/SIMA2RL2E25P1_10.res' 20000/

'PIN.FIL' 'ON' /
'PIN.EDT' 'ON' 'SUMM' '2PIN'/
'BAT.EDT' 'ON' 'QPIN' 'QXPO' /

'FUE.BAT' 1,
 1 3 1 3 1 3 3 1
 3 2 3 2 3 2 3 2
 1 3 1 2 2 2 3 2
 3 2 3 2 2 3 3 2
 1 3 1 3 2 3 2 0
 3 2 3 2 3 3 2 0
 3 3 3 3 2 2 0 0
 1 1 2 2 0 0 0 0/
'STA'/
'END'/
```